17TH INTERNATIONAL CONFERENCE on Communications, Electromagnetics and Medical Applications (CEMA'23)

Athens, Greece
3rd November, 2023

Organized by:
Faculty of Telecommunications of TU-Sofia, Bulgaria

NATIONAL TECHNICAL UNIVERSITY OF ATHENS, GREECE

SCHOOL OF ELECTRICAL AND COMPUTER ENGINEERING

PROCEEDINGS

OF 17TH INTERNATIONAL CONFERENCE ON COMMUNICATIONS, ELECTROMAGNETICS AND MEDICAL APPLICATIONS (CEMA'23)

Organized by:

FACULTY OF TELECOMMUNICATIONS
TECHNICAL UNIVERSITY OF SOFIA, BULGARIA

NATIONAL TECHNICAL UNIVERSITY OF ATHENS, GREECE,
SCHOOL OF ELECTRICAL AND COMPUTER ENGINEERING

NATIONAL TECHNICAL UNIVERSITY OF ATHENS, GREECE

SCHOOL OF ELECTRICAL AND COMPUTER ENGINEERING

Athens, Greece
3rd November, 2023

KING 2001, Sofia

Edited by Prof. Dr. Eng. **Dimiter Tz. Dimitrov**

ISSN: 1314-2100

SCOPUS Indexing
http://suggestor.step.scopus.com/progressTracker, ID: 6B4F77263D276412.

Printed in Bulgaria
KING 2001, Sofia

D. Dimitrov

P. Frangos

K. Dimitrov

Dear Colleagues,

It is our privilege to thank all of you for your contributions submitted at 17th regular International Conference on 'Communication, Electromagnetic and Medical Applications' CEMA'23. This is a conference which should help future collaboration in the area of engineering, especially in the area of communication technologies and medical applications. This is an important scientific event not only in Balkan region, but in Europe, also. The International Conference on Communication, Electromagnetism and Medical Applications CEMA'23 is dedicated to all essential aspects of the development of global information and communication technologies, and their impact in medicine, as well. The objective of Conference is to bring together lecturers, researchers and practitioners from different countries, working on the field of communication, electromagnetism, medical applications and computer simulation of electromagnetic field, in order to exchange information and bring new contribution to this important field of engineering design and application in medicine. The Conference will bring you the latest ideas and development of the tools for the above mentioned scientific areas directly from their inventors. The objective of the Conference is also to bring together the academic community, researchers and practitioners working in the field of Communication, Electromagnetic and Medical Applications, not only from all over Europe, but also from America and Asia, in order to exchange information and present new scientific and technical contributions.

Many well known scientists took part in conference preparation as members of International Scientific Committee or/and as reviewers of submitted papers. We would like to thank all of them for their efforts, for their suggestions and advices.

On behalf of the International Scientific Committee, we would like to wish you successful presentations of your papers, successful discussions and new collaborations for your future scientific investigations.

Engineering and medicine should provide high level of living for all people.

P. Frangos
Conference Chairman

D. Dimitrov
Conference Vice Chairman

K. Dimitrov
Conference Vice Chairman

INTERNATIONAL SCIENTIFIC COMMITTEE

Chairman:

P. FRANGOS, National Technical University of Athens, Greece

Vice Chairmen:

D. TZ. DIMITROV, Technical University of Sofia, Bulgaria
K. L. DIMITROV, Technical University of Sofia, Bulgaria

Members

N. AMPILOVA,	University of Petersburg, Russia
T. AVOYAGI,	Tokyo Institute of Technology, Japan
A. BEKJARSKY,	Technical University of Sofia, Bulgaria
E. BOEMO,	University Authonoma, Barcelona, Spain
R. BRUZGIENE,	Kaunas University of Technology, Lithuania
N. DIB,	Jordan University of Science and Technology, Aman, Jordan
V. DUMBRAVA,	Kaunas University of Technology, Litvania
N. ESCUDEIRO,	ISEP, Porto, Portugal
E. GAGO-RIBAS,	University of Oviedo, Spain
V. GEORGIEVA,	Technical University of Sofia, Bulgaria
G. GOUSSETIS,	Heriot - Watt University, United Kingdom
S. V.HOEYE,	University of Oviedo, Spain
I. ILIEV,	Technical University of Sofia, Bulgaria
F. KLETT,	Franhofer Institute, Ilmenau, Germany
G. KLIROS,	Hellenic Air-Force Academy, Athens, Greece
V. KUKENSKA,	Technical University of Gabrovo, Bulgaria
L. LUBIH,	Technical University of Sofia, Bulgaria
G. MALLET,	University "Sophia Antipolis", Nice, France
G. MATSOPOULOS,	National Technical University of Athens, Greece
M. MARTINS,	Academia Militar da Amadora, DCEE, Portugal
M.– J. MORALES-GONZALES,	University of Valladolid, Spain
L. NARBUTAITE,	Kaunas University of Technology, Lithuania
K. NIKITA,	National Technical University of Athens, Greece
M. NIKOLOVA,	High Naval School, Varna, Bulgaria
A. PANAGOPOULOS,	National Technical University of Athens, Greece
J. PETROVSKA,	Medical University of Sofia, Bulgaria
H. ROTH,	University of Siegen, Germany
S. SAUTBEKOV,	Euroasian University, Astana, Kazakhstan
A. SAVOV,	Medical University of Sofia, Bulgaria
S. SAVOV,	Technical University of Varna, Bulgaria
H.-P. SCHADE,	Technical University of Ilmenau, Germany
I. SOLOVIEV,	University of St. Petersburg, Russia
L. SONG,	Technical University of Harbin, China
G. STAMATAKOS,	National Technical University of Athens, Greece
A. USHEVA,	University of Boston, USA
R. VERDONE,	University of Bologna, Italy

REVIEWERS

BALZANO, Q.	University of Maryland, USA
BEHARI, J.	Jawaharlal Nehru University ,New Delhi, India
BOEMO, E.	Technical University of Madrid, Spain
DIMITROV, D.	Technical University of Sofia, Bulgaria
DONTSCHEWA, M.	University of Applied Sciences, Dorbirn, Austria
GOUSSETIS, G.	Heriot - Watt University, United Kingdom
MALLET, G.	University "Sophia Antipolis", Nice, France
PETROVSKA, J.	Medical University of Sofia, Bulgaria
PRATO, F.	University of Western Ontario, Canada
ROTH, H.	University of Siegen, Germany
SAVOV, A.	Medical University of Sofia, Bulgaria
SCHADE, H-P.	Technical University of Ilmenau, Germany
SONG, L.	Technical University of Harbin, China
USHEVA, A.	University of Boston, USA

REGISTRATION

November, 3rd, 2023, 09h 30min – 16h

The conference registration desk will be on-line at
National Technical University of Athens

CONFERENCE PROGRAM

November, 3rd 2023, Friday

OPENING CEREMONY

11h – 11h 30min
The Opening Ceremony will be on-line

SCIENTIFIC PROGRAM

FIRST SESSION

11h 30min – 13h 30min

On-line presentation and discussions

Chairman: Prof. P. Frangos, *School of Electrical and Computing Engineering, National Technical University of Athens, Greece*

---

1. **AN ASSESSMENT OF EARLY MUCOSA HEALING AT THE SITE OF EXTRACTED THIRD MOLAR ACCORDING TO ITS POSITION AND PATIENT'S GENDER AND AGE**

   Anna Nenova-Nogalcheva*, Medical University - Varna, Bulgaria*
   Desislava Konstantinova*, Medical University - Varna, Bulgaria*
   Mariya Nikolova*, Nikola Vaptsarov Naval Academy, Varna, Bulgaria*
   Emiliya Koleva*, Nikola Vaptsarov Naval Academy, Varna, Bulgaria*

2. **THE IMPACT OF 0.20% CHLORHEXIDINE GEL ON THE EXTRACTION WOUND OF THIRD MOLARS BY A PRIMARY HEALING PROCESS**

   Anna Nenova-Nogalcheva*, Medical University - Varna, Bulgaria*
   Desislava Konstantinova*, Medical University - Varna, Bulgaria*
   Mariya Nikolova*, Nikola Vaptsarov Naval Academy, Varna, Bulgaria*
   Emiliya Koleva*, Nikola Vaptsarov Naval Academy, Varna, Bulgaria*

3. **EVALUATION OF THE MOBILE PHONE ANTENNA ELECTROMAGNETIC FIELD THERMAL EFFECTS FOR THE NONHOMOGENEOUS CHILD MODEL BY USING COMPUTER SIMULATION**

   Tamar Nozadze*, Ivane Javakhishvili Tbilisi State University, Department of Electric and Electronic Engineering, Laboratory of Applied Electrodynamics and Radio Engineering*

4. **DESIGN AND DEVELOPMENT OF A WEB-BASED SYSTEM FOR PROCESSING OF RESEARCH MEDICAL DATA**

   Edem Topuzov*, St. Petersburg State University, Russia*

5. **REVIEW OF MULTIMODAL MEDICAL IMAGE FUSION TECHNIQUES AND THEIR APPLICATION IN PROSTATE CANCER DIAGNOSIS**

Diana S. Tsvetkova, *Faculty of German Engineering Education and Industrial Management, Technical University of Sofia, Bulgaria*

Veska Georgieva, *Faculty of Telecommunications, Technical University of Sofia, Bulgaria*

Valeria Hadzhiyska, *Aleksandrovska University Hospital, Bulgaria*

Yavor Gramatikov, *Aleksandrovska University Hospital, Bulgaria*

6. **DIFFERENTIATION IMAGES OF MEDICAL PREPARATION CRYSTALS FROM PLACEBO BY USING METHODS OF FRACTAL ANALYSIS**

N. Ampilova, *Saint-Petersburg State University, Russia*

V. Lyamin, *Saint-Petersburg State University, Russia*

T. Novosadiyk, *POLEVET clinic, Russia*

I. Soloviev, *Saint-Petersburg State University, Russia*

i

BREAK

13h 30min – 14h 30min

SECOND SESSION

14h 30min – 16h 30min

Chairman: *Assoc.Prof. Mariya Nikolova, N. Y. Vaptsarov, NAVAL ACADEMY, Bulgaria*

---

1. **METHODOLOGY FOR COUNTING PENGUINS DURING THEIR NESTING PERIOD BASED ON UAV-IMAGES USING DEEP LEARNING TECHNIQUES**

Diana S. Tsvetkova, *Faculty of German Engineering Education and Industrial Management, Technical University of Sofia, Bulgaria*

Oleg Vassilev, *29 Javorov district, 1504 Sofia, Bulgaria*

Atilla Markov, *26 "Pop Hariton" Str, 5000 Veliko Tarnovo, Bulgaria*

Boris P. Nikolov, *Institute of Biodiversity and Ecosystem Research, Bulgarian Academy of Sciences, Bulgaria*

2. **ARCHITECTURAL DESIGN OF A SMART HOME: IMPROVING COMFORT, SAFETY AND ENERGY EFFICIENCY FOR PEOPLE WITH DISABILITIES**

Grebnev Y.V., *St. Petersburg State University, Russia,*

Soloviev I.P., *St. Petersburg State University, Russia*

3. **AN UNCERTAINTY AND MUTUAL INFORMATION OF ACOUSTIC SIGNALS WITH HIGH DYNAMICS**

I. Simeonov, *Vasil Levski National Military University, Veliko Tarnovo, Bulgaria*

4. **ON THE APPLICATION OF THE GRASSBERGER-PROCACCIA ALGORITHM TO CLASSIFICATION OF QUADCOPTER SOUNDS**

Andrei Kadomskii*, St. Petersburg State University, Russia*

5. **AN APPROACH TO COMPUTING THE GRADIENTS IN FPGA BASED EDGE DETECTION FOCUSED ON ULTIMATE EXECUTION SPEED AND EXACTNESS OF DETECTED CONTOURS**

Dimitre Kromichev*, Department of Marketing and International Economic Relations, University of Plovdiv, Bulgaria*

6. **GRADIENT BASED EDGE DETECTION: INVESTIGATING THE PROBLEM OF FALSE NEGATIVES IN TERMS OF EDGE THINNING**

Dimitre Kromichev*, Department of Marketing and International Economic Relations, University of Plovdiv, Bulgaria*

CLOSING CONFERENCE

16h 30min – 17h

CONTACT US:

http://rcvt.tu-sofia.bg/CEMA/eth.html

Prof. Dr. Dimiter Dimitrov

Faculty of Telecommunication
Technical University of Sofia
8, Kliment Ohridsky str.
1756 Sofia, Bulgaria
Phone:++359 2 9652278
Fax: ++359 2 9652278
E-mail: dcd@tu-sofia.bg

Prof. P. Frangos

National Technical University of Athens
School of Electrical and Computer Engineering
9, Iroon Polytechniou Str. ,
157 73 Zografou, Athens, Greece
Phone : 00 30 210 772 3694
Fax : 00 30 210 772 2281
E-mail : pfrangos@central.ntua.gr

TABLE OF CONTENTS

AN ASSESSMENT OF EARLY MUCOSA HEALING AT THE SITE OF EXTRACTED THIRD MOLAR ACCORDING TO ITS POSITION AND PATIENT'S GENDER AND AGE

Anna Nenova-Nogalcheva, Desislava Konstantinova

Medical University - Varna, Bulgaria
Varna 9002, 55 Marin Drinov str.
E-mail: anenova@yahoo.com; dr.konstantinova@gmail.com

Mariya Nikolova, Emiliya Koleva

Nikola Vaptsarov Naval Academy - Varna, Bulgaria
Varna 9026, 73 V. Drumev str.
E-mail: mpn@abv.bg; e.koleva@nvna.eu

Abstract

It was investigated the influence of 0.2% Chlorhexidine gel on the wound size 96 hours after extaction of third molars in upper and lower jaw according to the location of the extracted teeth, gender and age of the patients. A statistical analysis was made that proved the influence of the gender and age of the patients.

Because of the lack of clinical data on early mucosa repair at the extraction site of a third molar, the mode of treatment of this entity remains a dilemma. There is a need for a detailed analysis of the influence of bone, age and gender on the expectations of the healing process.

Our results confirmed that factors such as gender, age and location of the extraction wound influence the healing primary process, especially the wound size, pronounced after 96 hours.

1. INTRODUCTION

The process of bone healing after tooth extraction has been well studied and documented. The investigation of the effects of factors like age, gender, and position in the upper or lower jaw started in the middle of 20th century [1,2]. The traumatic operative damage to soft tissues, bone structures, significant hematomas, and postoperative edema; the individual immunity and concomitant illnesses; and patient's compliance with prescribed behaviour are also factor [3]. Treatment of the wound with substances may include the use of antiseptics, disinfectants or antibiotics. These substances help to destroy or slow down the reproduction of bacteria and other pathogenic microorganisms that can cause infection. In addition, they can stimulate tissue healing. Chlorhexidine (CHX) gel or CHX mouthrinse is extremely popular and available in Bulgaria. This is due to its affect: antimicrobial, anti-inflammatory, stimulation of cell proliferation and tissue regeneration and due to the ability to remain active on the surface of the wound for a long period of time [4]. Unfortunately, there is emerging situation of antimicrobial resistances caused by antimicrobial abuse, especially from systemic antibiotic use. To overcome this problem, topical antimicrobials in wound therapy are increasing in use [5, 6, 7]. For the treatment of an extraction wound, a concentration of 0.12% CHX is usually used to prevent infection and for standart personal oral hygiene. The higher concentration of 0.20% CHX is usually used for more intensive management of complicated cases like third molar's extraction [8] . Applying CHX to wounds is according to a doctor or health professional's guidelines for dosage, frequency of application and duration of treatment to achieve the best results and to avoid possible adverse effects.

Purpose: Because of the lack of clinical data on early mucosa repair at the extraction site of a third molar, the mode of treatment of this entity remains a dilemma. In the present study, the degree of early mucosa healing at the site of extracted maxilar or mandibular third molars is assessed.

2. MATERIAL AND METHODS

This study included 55 persons randomly selected from healthy patients referred to the Oral Surgery Praxis in Varna for extraction of upper or lower third molars. Because smoking has been linked to delayed healing, wound infection, and dehiscence, it

was decided to exclude smokers from the current study [9, 10].

2.1. Sample size

After detailed explanations about the purpose of the study 55 participants were selected. The patients were assigned to two groups: A study group (SG) - comprised 10 male and 17 female patients, with a 1:1.7 ratio; the control group (CG) included 9 male and 19 female patients, with a 1:2.11 ratio. The average age was 42.8 ± 6.0 and 29.1 ± 4.4 years in the SG and CG, respectively. All postoperative wounds were sutured to allow a primary healing process to occur. The patients were separate into two groups: the first (control) group, which included 28 people, received standard instructions for at-home care of the extraction wound, while the second (clinical) group (27 people) also received a tube of 0.20% CHX gel from the company "KIN" for applying a pea-sized amount of gel to the wound surface three times a day after brushing their teeth.

It had been depended on the participants' willingness and diligence to follow instructions after the manipulation to ensure compliance.

The study group included 16 patients with an extracted third molar on the upper jaw (maxilla), and 11 on the lower jaw (mandibula) and in the control group resp. 16 on the upper jaw and 12 lower jaw. The general characteristics of the patients are described in table 1.

Table 1. Baseline characteristics of patients

Characteristics	Study group (n=27)	Control group (n=28)
Age (years)	42.8 ± 6.0	29.1 ± 4.4
Gender:		
Male	10	9
Female	17	19
Extraction:		
UJ	16	16
LJ	11	12

UJ: Upper jaw; LJ: Lower jaw

All participants were invited for a check-up after 24 hours, after 48 hours and after 96 hours. Instrumentally, the size of the area of post-extraction hyperemia and edema was determined in millimeters using an electronic caliper, with an accuracy of 1 mm. The borders of the examined area were defined by the site of the incision and the most peripheral mucosal post-extraction changes.

2.2. Statistical analysis

Statistical analysis is the collection and interpretation of data in order to uncover patterns and trends. Descriptive statistics summarize the basic features of a dataset found in a given study. It simply makes the complex data easy to read and understand.

Inferential statistical techniques are used to analyze the sample's behavior. These include the models used for regression analysis and hypothesis testing. The variables included in the analysis are: age, gender, postoperative wound, measured in mm at 24 h, 48 h and 96 h after surgery extraction. Microsoft Excel 365 [17] and Matlab [18] were used for data processing and statistical analysis, respectively.

3. RESULTS

Different types of data analyses were performed to investigate the influence of age, gender and site of extracted maxillary or mandibular third molars.

3.1. The effect of the extraction (Upper or Lower jaw) on wound healing in patients.

The average size of the area of post-extraction hyperemia in mm depending on the extracted third molar for both groups is shown in Fig.1 and Fig.2.

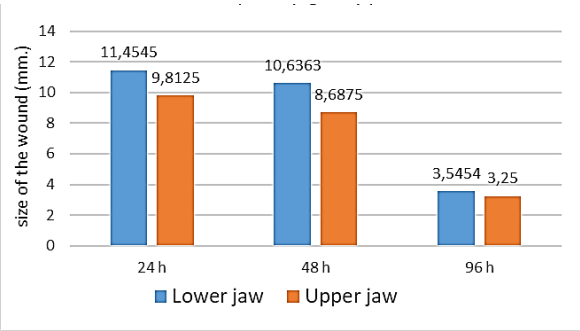

Figure 1. Average size of the wound (SG)

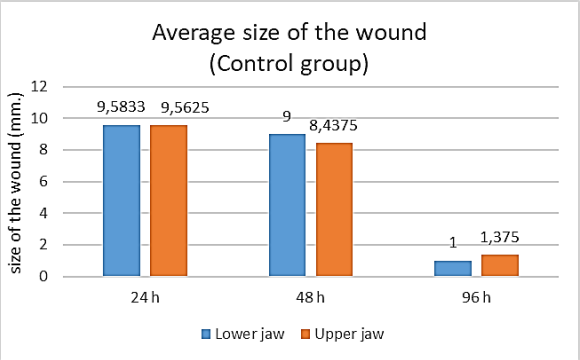

Figure 2. Average size of the wound (CG)

The mean values regarding extraction wound of mandibular wisdom teeth underline that the healing

process after 96 hours without gel is on average 3 times faster compared to one with gel. About the maxilla, after 96 hours data show 2.36 times speed up the healing. In our previous study, it was found that the use of the gel had no effect on the healing process of the wound after 96 hours. Table 2 presents mean age and mean wound size in mm for maxilla and mandible after 96 hours.

Table 2. Mean age and mean wound size at 96 hours for LJ and UJ for both groups

		Study group		Control group	
	Extractio	Age	Wound size at 96h [mm]	Age	Wound size at 96h [mm]
Mean	LJ	47.10	3.55	31.40	1.00
	UJ	39.80	3.25	27.40	1.38

Examining the data in table 2, a stastistical difference in the average age of the patients in the two groups is noticeable. This raises the following research question: "Does age affect wound size after the 96th hour?" The answer is discussed in 3.3.

3.2. The effect of gender on wound healing in patients

The average size of the wound after 96 hours by female without gel is 1.05 mm, and in male - 1.56 mm.

The statistical analyses emphasize that there are five female totally recovered on the check up after 96 hours and only one male (Table 3).

Table 3. Summary information splited by gender

wound size at 96 hours	Control group		Study group	
	women	men	women	men
0 mm	5	1	-	-
1 mm	8	4	2	1
2 mm	6	2	5	2
≥3 mm	2	-	10	7

3.3. The effect of age on wound healing in patients

By all observed patients (55 patients) incl. the control and clinical groups, an effect of age on the size of the wound after 96 hours of tooth extraction was obvious. Because of the non-normal data a Spearman's correlation coefficient ρ is used to check for correlation between age and wound size at 96 hours for both groups. The test result (ρ = 0,611, p-value<0.001) shows that there is a significant positive correlation between them.

A larger wound corresponds to a greater mean age (Table 4). An exception is the mean age for two patients in the control group for a wound ≥ 3 mm.

Table 4. Relation between age and wound size

wound size at 96 hours	Average age	
	CG	SG
0 mm	23.8	
1 mm	26.5	28.7
2 mm	39	36.9
≥3 mm	21	47.7

After the construction and subsequent examination of a scatter diagrams (fig. 3 and fig. 4) for both groups, a relation between the two quantities (age and wound size) is drawn for the SG.

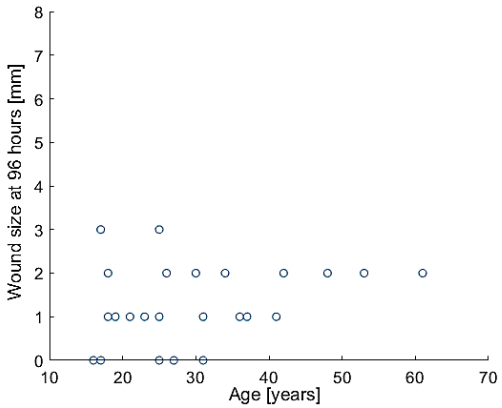

Figure 3. Wound size at 96 hours for CG

It's obvious that there is no relation between age and wound size at 96 hours (ρ= *0.2585, p-value = 0.1841 > 0.05*) for the Control group.

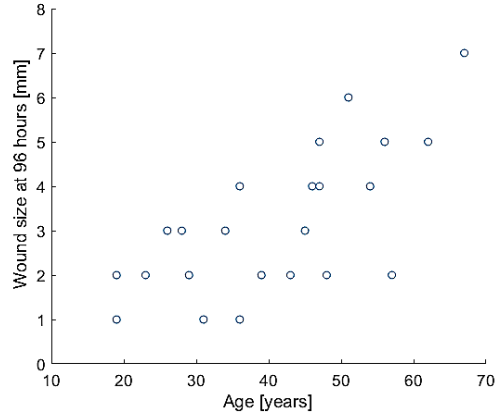

Figure 4. Wound size at 96 hours for SG

The scatterplot (fig. 4) suggests a definite relation between age and wound size, with larger values of wound size tending to be associated with larger values of age. There appears to be a positive strong correlation between the two variables.

(ρ= 0.6911; p-value = 0.0000657 < 0.05).

4. DISCUSSION

The impact of chlorhexidine on the extraction wound is essential in revealing the effectiveness and benefit of its use in preventing infections, in accelerating healing and in supporting the growth of new cells and tissues. Studying its action after tooth extraction can give us information about how quickly and effectively healing occurs when using CHX gel, can enable us to improve the post-procedure care protocol. For instance, the ideal outcome can be achieved by choosing the right chlorhexidine dose and/or frequency of treatment [11].

Alveolar crests undergo significant quantitative and qualitative changes in size after extraction [11, 12]. The most significant are the changes in width, the quantitative dimensions of which are directly dependent on the bone morphotype, the characteristics of the extraction wound and the degree of trauma [13,14,15].

5. CONCLUSION

Our study confirmed that factors such as gender, age and location influence the healing primary process, especially pronounced after 96 hours. The specific bone structure of maxilla and mandibula, the different access to the upper and lower jaw wound may impact the healing process by equal conditions. In general, female's results after third molar extraction, have a better prognosis than male's. In older patients, the wound after 96 hours is larger in the clinical group, but in the control group there is no relation between age and wound size. Maybe it is difficult to applicate the gel by older patients.

References

[1] M. Amler, "The time sequence of tissue regeneration in human extraction wounds", Oral Surg Oral Med Oral Pathol, 27(3), 1969, https://doi.org/10.1016/0030-4220(69)90357-0

[2] M. Amler, "The age factor in human extraction wound healing", J Oral Surg, 35(3), 1977, pp. 193-197

[3] E. Couso-Queiruga, S. Stuhr, M. Tattan, L. Chambrone and G. Avila-Ortiz, "Post-extraction dimensional changes: A systematic review and meta-analysis", Journal of Clinical Periodontology, 48(1), 2021, pp. 127-145, https://doi.org/10.1111/jcpe.13390

[4] A. Amaliya, R. Ramadhanti, I. Hadikrishna and T. Maulina, "The effectiveness of 0.2% chlorhexidine gel on early wound healing after tooth extraction: a randomized controlled trial", European Journal of Dentistry, 16(03), 2022, pp. 688-694, https://doi.org/10.1055/s-0041-1739544

[5] D. Fry, "Topical antimicrobials and the open surgical wound", Surg Infect (Larchmt), 17(5), 2016, https://doi.org/ 10.1089/sur.2016.107.

[6] S. Sarabahi, "Recent advances in topical wound care", Indian J Plast Surg, 45(02), 2012, pp. 379-387, https://doi.org/ 10.4103/0970-0358.101321

[7] R. Cooper, "A review of the evidence for the use of topical antimicrobial agents in wound care", World Wide Wounds, 2004, pp. 1:1-8

[8] J. Zhou, B. Hu, Y. Liu, Z. Yang and J. Song, "The efficacy of intra-alveolar 0.2% chlorhexidine gel on alveolar osteitis: a meta-analysis", Oral Dis., 23(5), 2017, pp. 598-608. https://doi.org/10.1111/odi.12553

[9] L. Sørensen, "Wound healing and infection in surgery: the pathophysiological impact of smoking, smoking cessation, and nicotine replacement therapy: a systematic review", Ann Surg., 255(06), 2012, pp.1069-1079, https://doi.org/ 10.1097/SLA.0b013e31824f632d

[10] J. Kean, "The effects of smoking on the wound healing process", J Wound Care, 19(01), 2010, pp. 5–8, https://doi.org/ 10.12968/jowc.2010.19.1.46092

[11] L. Fiorillo, "Chlorhexidine gel use in the oral district: a systematic review", Oral Surgery, Oral Medicine, Gels, 5(2), 2019, https://doi.org/10.3390/gels5020031

[12] K. Sinjab, O. Kripfgans, A. Ou and H. Chan, "Ultrasonographic evaluation of edentulous crestal bone topography: A proof-of-principle retrospective study", Oral Surg Oral Med Oral Pathol Oral Radiol., 133(1), 2022, pp. 110-117, https://doi.org/10.1016/j.oooo.2021.07.006

[13] C. Hämmerle and D. Tarnow, "The etiology of hard- and soft-tissue deficiencies at dental implants: A narrative review", J Clin Periodontol., 45 Suppl 20:S267-S277, 2018, https://doi.org/10.1111/jcpe.12955

[14] S. Lee, S. Jung, S. Song, I. Lee, J. Choi, H. Zadeh, D. Lee, S. Pi and H. You, "miRNA-Based Early Healing Mechanism of Extraction Sockets: miR190a-5p, a Potential Enhancer of Bone Healing", Biomed Res Int., 2022, https://doi.org/10.1155/2022/7194640

[15] G. Juodzbalys, A. Stumbras, S. Goyushov, O. Duruel and T. Tözüm, "Morphological Classification of Extraction Sockets and Clinical Decision Tree for Socket Preservation/Augmentation after Tooth Extraction: a Systematic Review", J Oral Maxillofac Res., 10(3), 2019, https://doi.org/10.5037/jomr.2019.10303

[16] G. Avila-Ortiz, L. Chambrone and F. Vignoletti, "Effect of alveolar ridge preservation interventions following tooth extraction: A systematic review and meta-analysis", J Clin Periodontol., 46 Suppl 21, 2019, pp.195-223, https://doi.org/10.1111/jcpe.13057

[17] H. Guerrero, "Analysis of Quantitative Data. In: Excel Data Analysis". Springer, Cham., 2019, https://doi.org/10.1007/978-3-030-01279-3_3

[18] A. King, R. Eckersley, "Statistics for Biomedical Engineers and Scientists: How to Visualize and Analize Data", ISBN 978-0-08-102939-8, Elseiver Ltd., 2019, pp. 1– 52, 77–113, 132-167, https://doi.org/10.1016/C2018-0-02241-0

THE IMPACT OF 0.20% CHLORHEXIDINE GEL ON THE EXTRACTION WOUND OF THIRD MOLARS BY A PRIMARY HEALING PROCESS

Anna Nenova-Nogalcheva, Desislava Konstantinova,

Medical University - Varna, Bulgaria
Varna 9002, 55 Marin Drinov str.
E-mail: anenova@yahoo.com; dr.konstantinova@gmail.com

Mariya Nikolova, Emiliya Koleva

Nikola Vaptsarov Naval Academy - Varna, Bulgaria
Varna 9026, 73 V. Drumev str.
E-mail: mpn@abv.bg; e.koleva@nvna.eu

Abstract

The extraction wound is treated with substances to prevent infection, speed healing, and reduce pain and inflammation. Chlorhexidine is an antiseptic widely used in medicine and dentistry for the prevention and treatment of infections. We study how 0.20% chlorhexidine gel affects a wound after the extraction of third molar by a primary healing process.

The study was conducted in specialized surgical dental practices. All the patients have had an extraction of third molar. The wound were followed up in 24, 48 and 96 hours postoperatively. The data on the size of the wound after 24 and 96 hours of extraction with the application of the gel on (Study Group) and without the gel (Control Group) were statistically analyzed.

Our research shows that the use of 0.20% chlorhexidine does not speed up the healing process after extraction of third molars by healthy patients. Patients who require chlorhexidine after tooth extraction are those who are at increased risk of infection or have difficult wound healing, according to science data.

1. INTRODUCTION

Tooth extraction is a procedure to remove it from the oral cavity. After the extraction of the tooth, the patient may feel slight pain and unpleasant sensations in the area of the wound.

The extraction wound can heal through a primary or secondary healing process - per primam or per secundam intentionem. The secondary one is characterized by the presence of a tissue defect (an open bone wound remains after the extraction of the root from the alveolus) in contrast to the primary healing process, in which there is no tissue defect. The primary healing process is characteristic of impacted teeth after suturing the soft tissues or after extraction and suturing of the alveolus [1, 2].

It has been established that various factors influence the healing process after tooth extraction and whether it will proceed normally or be complicated [3, 4]. These are: the type of pathological process that is the reason for the extraction; presence of an inflammatory process before, during and after tooth extraction; traumatic extraction [5]. Under unfavorable conditions, the healing process is complicated [6, 7].

The extraction wound is treated with substances to prevent infection, speed healing, and reduce pain and inflammation.

Chlorhexidine is an antiseptic widely used in medicine and dentistry for the prevention and treatment of infections [8].

Different concentrations of chlorhexidine (CHX) are used in practice – 0.06%, 0.12%, 0.20% [9,10]. It is important to note that the concentration of chlorhexidine to be used on a wound is a matter of professional judgment based on the nature and extent of the wound.

Objective: To investigate how 0.20% chlorhexidine gel affects a wound after the extraction of both a mandibular and a maxillary third molar by a primary healing process.

2. MATERIAL AND METHODS

The study was conducted in specialized surgical dental practices in the city of Varna, Bulgaria, in the

period from November 2021 to April 2022. The selection of volunteers was based on the need for third molar extraction. Only healthy patients, without chronical diseases and drug therapy, non-smokers and non-users of narcotics were selected for inclusion in the study.

2.1. Sample size

After detailed explanations about the purpose of the study, 55 participants were selected and took an informed part. The general characteristics of the patients are described in table 1.

The units of observation were 55 extraction wounds of third molars located in the maxilla and mandible.

The patients were divided into two groups - the first (control) group, consisting of 28 people, received standard instructions for home control after surgical treatment of the extraction wound, and the second (clinical) group of patients additionally received a tube of 0.20% gel of the company " KIN" and instructions to apply a pea-sized amount of gel to the wound surface three times a day after brushing the teeth.

Table 1. Baseline characteristics of patients

Characteristics	Study group (n=27)	Control group (n=28)
Age (years)	42.8 ± 6.0	29.1 ± 4.4
Gender:		
Male	10	9
Female	17	19
Extraction:		
UJ	16	16
LJ	11	12

UJ: Upper jaw; LJ: Lower jaw

For compliance with the given instructions after the manipulation, we relied on the voluntary and conscientious attitude of the participants.

All participants were invited for a follow-up examination after 24 hours, after 48 hours and after 96 hours. Instrumentally, the size of the area of post-extraction hyperemia and edema was determined in millimeters using an electronic caliper, with an accuracy of 1 mm. The boundaries of the examined area were defined by the site of the incision and the most peripheral mucosal post-extraction changes.

2.2. Statistical analysis

Descriptive statistics show and summarize the basic features of a dataset found in a given study. It helps to understand the data better. Inferential statistical analyses included parametric Student's *t*-Test for independent samples and the χ^2- test and/or Fisher's exact test. They are used in the study to decide whether the data at hand sufficiently support a particular hypothesis. A p-value of less than 0.05 was considered significant. Microsoft Excel 365 [13] and Matlab [14] were used for data processing and statistical analysis, respectively. The variables included in the analysis are: Age, gender, postoperative wound, measured in mm at 24 h, 48 h and 96 h after surgery extraction.

3. RESULTS

Descriptive analysis, including the mean and standard deviation for Control Group (CG) and Study Group (SG) is made.

For both groups, the mean, median and mode are similar after 24 hours and 48 hours, but there is a difference at the 96th hour (see Table 1 and 2)

The standard deviations indicate the extent to which the scores lie apart.

Table 2. Descriptive statistic for CG

	Control group		
	24 hours	*48 hours*	*96 hours*
Mean	9,571428571	8,678571	1,214286
Median	9	9	1
Mode	9	8	1
Std. Deviation	0,878912267	1,020297	0,875897
Variance	0,772486772	1,041005	0,767196
Count	28	28	28

Table 3. Descriptive statistic for SG

	Study group		
	24 hours	*48 hours*	*96 hours*
Mean	10,48148	9,481481	3,37037037
Median	10	9	3
Mode	10	8	2
Std. Deviation	1,718013	2,343081	1,6904289
Variance	2,951567	5,490028	2,85754986
Count	27	27	27

The Paired Samples t-test is used to compare the means of two measurements (the size of the wound after 24 hours and 96 hours) for each group of people. The test assumes that the differences between the pairs should be approximately normally distrib-

uted. The difference (96h-24h) for CG and SG is normally distributed (p-value=0,96>0,05 for CG; p-value=0,33>0,05 for SG).

The research question is: *Is there a statistically significant difference between the means?*

For both groups the null hypothesis that there is no difference between means is rejected.

SG: $t_{stat}(22.74) > t_{critical\ 2\text{-}tail}(2.05)$

CG: $t_{stat}(43.10) > t_{critical\ 2\text{-}tail}(2.05)$

As a result, in both groups, there was a statistically significant difference between the mean wound size after 24 hours and 96 hours. The Pearson correlation coefficient for SG $(r = 0.5454, n = 27, p < 0.01)$ said to be a medium correlation between the size of the gel treated wound at the 24th and at the 96th hour.

The results $(r = 0.3162, n = 28, p < 0.01)$ for the CG shows that there is a weak correlation in the size of wounds not treated with gel.

Fig. 1 shows the mean size of the area of post-extraction hyperemia in mm for both groups.

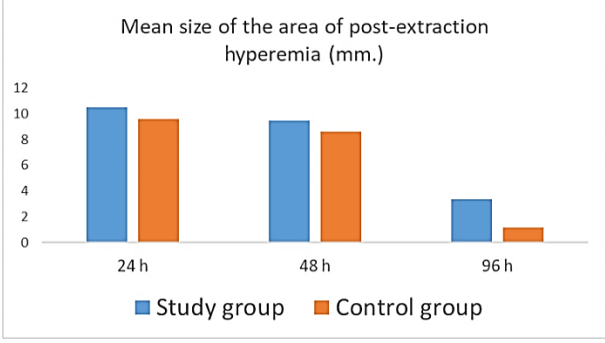

Figure 1. Wound recovery in the postoperative period

It is noted that there is a difference in the mean values, which leads to the following research question: Is there a statistically significant difference between the size of the wound after 96 hours depending on whether the wound is treated with gel or not? Since both groups had a sample size $n < 30$ a χ^2- test for normality was applied. The result of the check showed that for CG and SG data on the size of the wound after 96 hours correspond to the normal law of distribution, respectively

$p\text{ - }value(0.94) > 0.05$ for CG and

$p\text{ - }value(0.79) > 0.05$ for SG.

Therefore a two - sample student's t-Test for two independent groups (SG and CG) with unequal variances can be applied to check the hypothesis that the mean values of the groups are statistically different.

Due to the results, there was a statistically significant difference between the size of the sore after 96 hours with and without gel treatment. This is because $p < 0.05$ ($p = 0.00000070$). On average, results with use of gel were higher than these without use of gel ($t = 5.9$), which proves that primary healing wounds recover more slowly with gel.

Table 4. t-Test

t-Test: Two-Sample Assuming Unequal Variances

	Study group	*Control group*
Mean	3,37037037	1,214285714
Variance	2,857549858	0,767195767
Observations	27	28
Hypothesized Mean Difference	0	
df	39	
t Stat	5,906858929	
P(T<=t) one-tail	3,48821E-07	
t Critical one-tail	1,684875122	
P(T<=t) two-tail	6,98E-07	
t Critical two-tail	2,02269092	

Another interesting fact observed from the data shows that in the control group, 21.42% of the patients had a wound size of 0 mm after 96 hours. Among the patients who used the gel, none had a completely affected by the medicament wound.

4. DISCUSSION

The process of bone healing after tooth extraction has been well studied and documented [11]. Patients who require chlorhexidine after tooth extraction are those who are at increased risk of infection or have difficult wound healing [12]. This may include patients with diabetes, compromised immunitya, cardiovascular diseases, poor oral hygiene, or other factors that increase the risk of infection. In the present study, the degree of mucosa recovery with, resp. without use of 0,20% CHX gel at the site of extracted third molars is assessed. Our research shows that the use of 0.20% chlorhexidine in the study group does not speed up the healing process after extraction of third molars by healthy patients on 96 hour check up. The reason behind these results may be traumatic appliance of the gel on the sutured wound.

5. CONCLUSION

The study shows that the use of 0.20% chlorhexidine does not affect the healing process of tooth extraction wound in primary healing process after 96 hour and therefore the good effect is probably a placebo effect.

Research in this area is essential to establish evidence-based recommendations for the use of chlorhexidine after tooth extraction and to improve patient care and their expectations.

References

[1] R. Farina, L. Trombelli, "Wound healing of extraction sockets", Endodontic Topics, 25(1), 2011, pp. 16-43, https://doi.org/10.1111/etp.12016

[2] A. Sjuhada Oki, N. Amalia and Tantiana, "Wound healing acceleration in inflammation phase of post-tooth extraction after aerobic and anaerobic exercise", Science &Sports, 35(3), 2020, pp. 168.e1-168.e6, https://doi.org/10.1016/j.scispo.2019.06.001

[3] N. Greaves, K. Ashcroft, M. Baguneid and A. Bayat, "Current understanding of molecular and cellular mechanisms in fibroplasia and angiogenesis during acute wound healing", J Dermatol Sci, 72(3), 2013, pp. 206-217, https://doi.org/10.1016/j.jdermsci.2013.07.008

[4] T. Velnar, T. Bailey and V. Smrkolj, "The wound healing process: an overview of the cellular and molecular mechanisms", Journal of International Medical Research, 37(5), 2009, pp. 1528-1542, https://doi.org/10.1177/147323000903700531

[5] H. Wilkinson and M. Hardman, "Wound healing: Cellular mechanisms and pathological outcomes", Open biology, 10(9), 2020, https://doi.org/10.1098/rsob.200223

[6] S. Dayoub, H. Devlin and P. Sloan, "Evidence for the formation of metaplastic bone from pericytes in calcifying fibroblastic granuloma", Journal of oral pathology & medicine, 32(4), 2003, pp. 232-236, https://doi.org/10.1034/j.1600-0714.2003.00030.x

[7] K. Morjaria, R. Wilson and R. Palmer, "Bone healing after tooth extraction with or without an intervention: a systematic review of randomized controlled trials", Clinical implant dentistry and related research,, 16(1), 2014, pp. 1-20, https://doi.org/10.1111/j.1708-8208.2012.00450.x

[8] E. Couso-Queiruga, S. Stuhr, M. Tattan, L. Chambrone and G. Avila-Ortiz, "Post-extraction dimensional changes: A systematic review and meta-analysis", Journal of Clinical Periodontology, 48(1), 2021, pp. 127-145. https://doi.org/10.1111/jcpe.13390

[9] A. Amaliya, R. Ramadhanti, I. Hadikrishna and T. Maulina, "The effectiveness of 0.2% chlorhexidine gel on early wound healing after tooth extraction: a randomized controlled trial", European Journal of Dentistry, 16(03), 2022, pp. 688-694, https://doi.org/10.1055/s-0041-1739544

[10] D. Halabi, J. Escobar, C. Alvarado, N. Martinez and C. Muñoz, "Chlorhexidine for prevention of alveolar osteitis: a randomised clinical trial", J Appl Oral Sci., 2018, 26:e20170245, https://doi.org/10.1590/1678-7757-2017-0245

[11] Y. Marmary, L. Brayer, A. Tzukert and L. Feller, "Alveolar bone repair following extraction of impacted mandibular third molars" Oral Surgery, Oral Medicine, Oral Pathology, 61(4), 1986, pp. 324-326,

[12] F. Van der Weijden, F. Dell'Acqua and D. Slot, "Alveolar bone dimensional changes of post-extraction sockets in humans: a systematic review", J Clin Periodontol, 36(12), 2009, pp. 1048–1058, https://doi.org/10.1111/j.1600-051X.2009.01482.x

[13] H. Guerrero, "Analysis of Quantitative Data. In: Excel Data Analysis". Springer, Cham., 2019, https://doi.org/10.1007/978-3-030-01279-3_3

[14] A. King, R. Eckersley, "Statistics for Biomedical Engineers and Scientists: How to Visualize and Analize Data", ISBN 978-0-08-102939-8, Elseiver Ltd., 2019, pp. 1– 52, 77–113, 132-167, https://doi.org/10.1016/C2018-0-02241-0

EVALUATION OF THE MOBILE PHONE ANTENNA ELECTROMAGNETIC FIELD THERMAL EFFECTS FOR THE NONHOMOGENEOUS CHILD MODEL BY USING COMPUTER SIMULATION

Tamar Nozadze

Ivane Javakhishvili Tbilisi State University, Department of Electric and Electronic Engineering,
Laboratory of Applied Electrodynamics and Radio Engineering,
3, Chavchavadze Ave. 0176, Tbilisi, Georgia
E-mail: tamar.nozadze@tsu.ge

Abstract

The thermal effects caused by exposure to the electromagnetic (EM) field emitted by the mobile phone antenna have been investigated in the presented paper. A novelty is to study matching of the mobile phone dipole antenna to the free space for the case of a non-homogenous child model with different hand positions and different distances (1mm, 10mm, 20mm) of the mobile phone (with and without hand) from the child's head model; Through computer modeling (using the Finite-Difference Time-Domain (FDTD) method) have been evaluated the EM field energy absorption power by the child model considering the hand influence (holding the mobile phone) and have been conducted a comparative analysis for hand free cases. Because the hand holding the phone absorbs most of the radiation energy emitted by the mobile phone antenna. Studied the dependence of SAR (specific absorption rate SAR-W/kg) on the conditions of matching of the mobile phone antenna with the free space. Developed recommendations for the correct use of a mobile phone to reduce the reactive field near the child head in order to reduce head SAR values. The results of the study are presented below.

1. INTRODUCTION

The influence of electromagnetic fields (EM) emitted by mobile phone antennas on human, has been studied for many years before and especially after widespread introduction and use of cellular communications technology. Since exposure to EMF increases with reduced distance between the emitting antennas and the user the efforts to minimize exposure while increasing the radiated power are one of the most important tasks to enable efficient communication systems that are at the same time complaint with international safety standard on human exposure to EM field [1]-[3].

SAR is used for evaluating the RF radiation characteristics of mobile phones to determine if they meet Federal Communications Commission (FCC) safety requirements [4]. Current safety standards, guidelines set maximum radiation levels based on the amount of energy absorbed by the human body emitted by cell phones during communication. There are concerns that exposure to EM fields emitted by cell phones can cause cancer and other potential health problems. In 2011, the World Health Organization [5] and the International Agency for Research on Cancer [6] reviewed several scientific studies and based on the results of the studies, they classified mobile phones as a possible human carcinogen, putting them in the same category as lead, gasoline engine exhaust and chloroform.

The energy absorption in the human head caused by the exposure of human to the EM field of a mobile phone antenna depends on many factors. The distance from the antenna, the power and frequency of the radiated source and the position of the hand are also very important [7]-[10]. In addition, the type of antenna, the shape and material of the mobile "case", the location of the phone, the anatomy of the human head and the dielectric properties of the tissue significantly affect the absorption of field energy. Existing safety standards, which have not been updated in recent decades, determine the level of radiation for cases that pose a threat to human health. On the other hand, there may be some biological effects, but they are not considered dangerous for humans [11]. Harmful effects on children are very important. They are exposed to radio-frequency radiation from an early age. Main target for radiation is their brain, the skull is much thinner than adults, and therefore the possible negative impact on children can be more serious [11].

Mobile phone antennas are designed by mobile phone manufacturers so to have as low losses as possible and radiate most of the power delivered to the antenna. In this case, the antenna is well matched with free space. A quantitative characteristic is the S11 reflection coefficient, or S11 parameter. Relative positions of the user's head, hand and fingers influence on the values of the S11 parameter. Manufacturers do not consider this important factor in the process of manufacturing/testing mobile phones.

During mobile telephone communication, the antenna, the user's hand and head are mainly involved in the formation of radiation. A reactive EM field is often created near the human head. Therefore, the aim of the presented research is to study in detail how different hand configuration and different distances between the child head and the phone affect the mobile phone antenna parameter value (S11 coefficient).

The goal of the study is to determine the correlation between the matching parameter of the phone antenna (S11) and the EM field energy (SAR) absorbed by human tissues for 2100 MHz frequency, considering that smartphones automatically increase the radiation power to achieve a reliable connection in case of weak signal to the base station.

2. MATERIALS AND METHOD

Research was conducted through computer modeling. The numerical simulations were carried out using the FDTDLab software package developed at TSU [7]-[10]. The FDTDLab program is based on the Finite-Difference Time-Domain (FDTD) method, which is a discretization of Maxwell's equations. A discrete grid, each cell of which is 1 mm, is considered for the calculation area. A three-dimensional inhomogeneous discrete model of the child (Thelonious) from the "virtual population" (IT'IS Foundation) [12] with 1mm discretization was used for numerical calculations Figure 1, Figure 2.

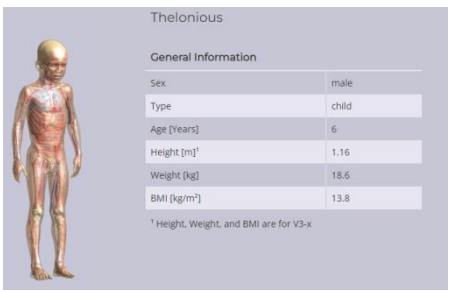

a)

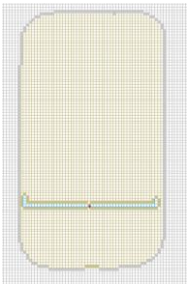

b)

Figure 1. a) Physical data of the child model (Thelonious). b) mobile phone discrete model with dipole antenna.

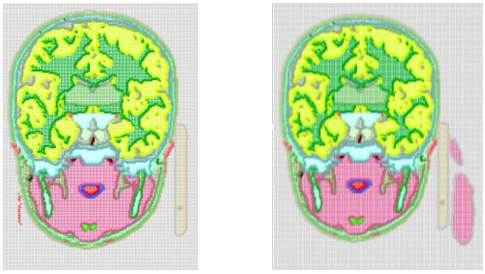

a) b)

Figure 2. Child discrete head models with the mobile phone: a) without hand, b) with hand.

Frequency-dependent tissue parameters were used from the known database [13], a sinusoidal waveform of 2100 MHz frequency will be used for simulations.

The dipole length for the selected frequency (2100 MHz) was selected so the S11 coefficient to be the lowest as possible. In this case, the best antenna matching to open space was obtained. The length of the dipole antenna was 0.52 mm.

One hand position was prepared for the child's model (because the child's hand is approximately the size of a mobile phone). The mobile phone and the hand were placed at distances of 1mm, 10mm and 20mm from the child head model.

3. RESULTS AND DISCUSSIONS

On Figure 3 is shown frequency characteristics for a considered mobile phone dipole antenna for the selected frequency.

As the numerical experiments show, the values of the S11 coefficient increase due to the influence of the hand. In some cases, the head, hand reduce the S11 coefficient, this means that the antenna is well matched to the free space, not at the considered frequency, but at shifted frequencies. It also depends on the modeling scenarios.

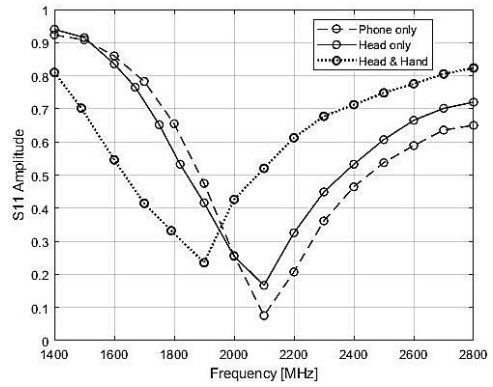

Figure 3. Mobile phone dipole antenna frequency characteristics

Peak SAR location is observed inside the hand when the antenna is covered by the hand. Child hand absorbs a big part of the EM field energy and therefore, SAR peak values in the head tissues are reduced. It can be well seen from Figure 4 and Figure 5.

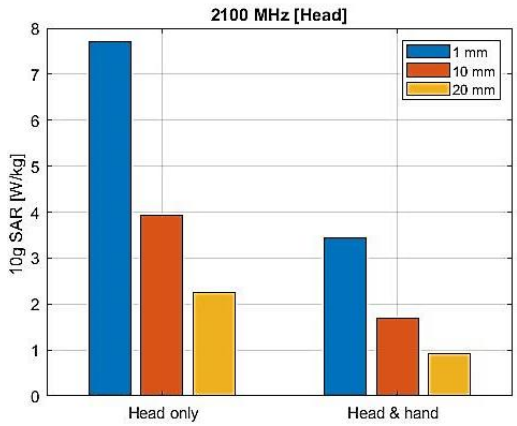

Figure 4. 10g SAR peak values for the child head model at 2100 MHz frequency

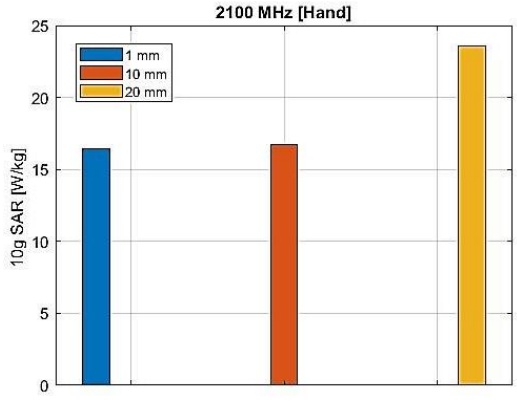

Figure 5. 10g SAR peak values for the child hand model at 2100 MHz frequency

Due to the inverse dependence of the EM field on the square of the distance, the 10g SAR values are also inversely proportional to the distance between the mobile phone and child head. The 10g SAR value decreases when the distance between the child head model and the mobile phone is big. The peak SAR values in head tissues are reduced when the presence of the hand is taken into account.

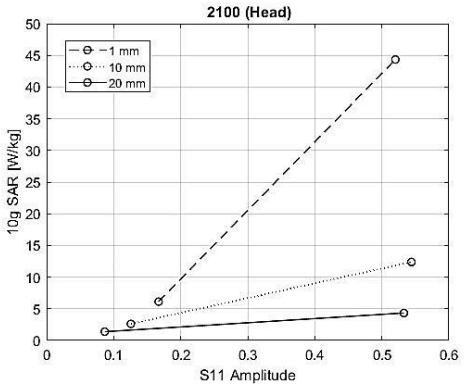

Figure 6. 10g SAR dependencies on S11 parameters for the child head model at 2100 MHz frequency

On Figure 6 dependence of SAR peak values on the matching conditions (S11 coefficient) is presented. SAR values are normalized to the value of the phone's EM field in free space. The first point on each graph corresponds to the value of SAR on the head without the hand, the second - with the hand.

From the obtained results we can assume that bad matching is the reason for the increasing in peak SAR values in the child head and hand models. The hand, which holds the communication device, absorbs part of the radiated energy; therefore, to restore a good connection with the base station the total radiated power of the mobile phone increases. As a result, we obtain increased peak SAR values in the child head model.

4. CONCLUSION

The influence of a child's hand holding a mobile phone on the process of EM exposure was investigated in this paper. The research results showed that the presence of a hand changed the peak SAR values in the child's head model. The SAR values in the head model including the hand are lower than without the hand. Also, resultant SAR values reduce by increasing distance from the EM source to the child head.

It is clear that the selection of a model parameters affects the obtained results. The hand with which we hold the communication device absorbs part of the radiated energy; Therefore, to establish a good connection with the base station, as already mentioned, the total radiated power of the mobile phone

increases. As a result, the SAR peak increased values in the child head model are obtained.

It should be noted that all people are unique and different from each other, so it is difficult to draw general conclusions. For this reason, these problems are still relevant today and require further research.

References

[1] [Online]. Available: IEEE Std (IEEE)., "Standard for Safety Level with Respect to Human Exposure to Radiofrequency Electromagnetic Fields, 3KHz to 300GHz,"2005.

[2] [Online]. Available: ICNIRP, "Guidelines for limiting exposure to time varying electric, magnetic and electromagnetic fields (up to 300 GHz),". Health Physics, vol. 74, pp. 494-522, April 1998.

[3] [Online]. Available: https://www.icnirp.org/en/activities/news/news-article/rf-guidelines-2020-published.html

[4] [Online]. Available: https://www.fcc.gov

[5] [Online]. Available: http://www.who.int/peh-emf/en/

[6] [Online]. Available:https://www.iarc.who.int/

[7] T. Nozadze, K. Henke, M. Kurtsikidze, V. Jeladze, G. Ghvedashvili, R. Zaridze. "Study How the Hand Affects on the MobileDipole Antenna Matching Conditions to the Free Space at 3700 MHz Frequency", 2022 IEEE 2nd Ukrainian Microwave Week, November 14th – 18th, 2022. DOI: 10.1109/UkrMW58013.2022.10037056

[8] V. Jeladze, T. Nozadze, I. Petoev-Darsavelidze & B. Partsvania, "Mobile phone antenna-matching study with different finger positions on an inhomogeneous human model", Electromagnetic Biology and Medicine, Volume 38, 2019 - Issue 4. 2019. DOI: 10.1080/15368378.2019.1641721

[9] T. Nozadze, V. Jeladze, R. Zaridze, 'Mobile Antenna Matching Study Considering Different Holding Positions at 2100 MHz Frequency', XXVIth International Seminar/Workshop on Direct and Inverse Problems of Electromagnetic and Acoustic Wave Theory DIPED-2020, Tbilisi, Georgia, September 15-18, 2020. DOI: 10.1109/DIPED49797.2020.9273363

[10] T. Nozadze, V. Jeladze, M. Tsverava, V. Tabatadze, M. Prishvin, R. Zaridze, "EM Exposure Study on an Inhomogeneous Child Model Considering Hand Effect", 2017 IEEE First Ukraine Conference on Electrical and Computer Engineering (UKRCON), Kyiv, Ukraine, May 29 -June 2, pp. 51, 2017. DOI: 10.1109/UKRCON.2017.8100484

[11] M. Abdul-Al, A. S. I. Amar, I. Elfergani, R. Littlehales, N. Ojaroudi Parchin, Y. Al-Yasir, Ch. Hwang See, D. Zhou, Z. Zainal Abidin, M. Alibakhshikenari, Ch. Zebiri, F. Elmegri, M. Abusitta, A. Ullah, F. M. A. Abdussalam, J. Rodriguez, N. J. McEwan, J. M. Noras, R. Hodgetts, R. A. Abd-Alhameed, "Wireless Electromagnetic Radiation Assessment Based on the Specific Absorption Rate (SAR): A Review Case Study", *Electronics 11(4), 511,* 2022

[12] [Online]. Available: [Online]. https://itis.swiss/virtual-population/virtual-population/overview/

[13] [Online]. Available: https://itis.swiss/virtualpopulation/tissueproperties/database/database-summary/)

DESIGN AND DEVELOPMENT OF A WEB-BASED SYSTEM FOR PROCESSING OF RESEARCH MEDICAL DATA

Edem Topuzov

St. Petersburg State University,
7-9 Universitetskayay Embankment, Saint Petersburg, 199034, Russia
E. edem.topuzov@gmail.com

Abstract

The challenges related to the processing of large amount of medical data are discussed. The limitations of using existing medical information systems in individual research are noted. To simplify medical research processes, we developed the web-based system. The system introduces such features as research design, collaboration, data input, access control, audit of database changes, regular backup, data analysis, and exporting data to Excel. The designed system was deployed to production and received positive feedback from users. Due to new requirements, the system is currently undergoing further development to enhance scalability and introduce new features.

1. INTRODUCTION

Technological advancements in medicine combined with new capabilities in processing large amounts of information in the healthcare field, open up prospects for development, but also generate associated problems [1, 2]. Modern evidence-based medicine requires extensive randomized studies, during which a multitude of indicators are collected and the results are subjected to statistical processing [3].

Amounts of modern medical data are enormous, and the process of extracting useful information is quite labor-intensive [4]. Medical information systems are used to address such tasks. However, at present, they are typically aimed at solving a narrow range of clinical problems [5].

A review of research in this area shows that up to date there is not a single system intended for individual research purposes. The majority of software solutions related to processing the results of medical research either involve the creating electronic medical records or basing on clinical and laboratory data suggest a possible diagnosis.

As a rule, such approach means the design of medical information systems [6].

Any medical research requires the implementation of a study design with a specific set of indicators such as grouping, sorting by patients and collecting data, and subsequent statistical processing as well. The mentioned above medical information systems do not provide such opportunities.

As a result, physician-researchers have to perform tedious technical work of creating multiple Excel tables and manual copying data between them, which is labor-intensive and inconvenient.

2. SOLVING OF THE DESCRIBED ISSUE

To simplify described processes, we have developed a web-based system that can be used at various stages of any medical research, from entering patient data to automatic analysis (including statistical) of indicators and providing prognostic data.

2.1. System advantages

The advantages of such a system are:

- Simplicity: Both the architecture and the user interface contain only the necessary components to accomplish the given task;
- Optimization: Medical research processes are streamlined by reducing the time required for data entry and standardization of collected data.
- Convenience: Creation and use of databases are made easy through the development of an intuitive interface for managing medical research data;
- Flexibility: The system allows for the creation of individualized designs for medical research by adding necessary patient groups, indicators, and data;
- Collaborative Remote Access: The system enables remote access for reading, updating,

analysing, and processing information, ensuring data protection through the implementtation of backup functionality.

By utilizing this system, we aim to enhance the efficiency and effectiveness of medical research, providing a comprehensive platform for data management, analysis, and collaboration.

3. DEVELOPMENT OF THE SYSTEM

The first step of the development is the determination of a technological stack.

Table 1. The technological stack of the system

Parameter	Value
Web framework	Ruby on Rails
Database management system (DBMS)	PostgreSQL, MongoDB
Authentication	Devise
Authorization	ActionPolicy, RoleModel
Database changes audit	PaperTrail
Statistics	ruby-statistics
Export to Excel	RubyXL
Containerization	Docker
Web server	Puma
Reverse proxy server	Nginx
Tests	RSpec, Simplecov
Linter	Rubocop
Vulnerability tracking	Bundle Audit
Frontend bundler	Webpack
Template engine	Slim
Version control system (remote repository)	Git (GitHub)

Ruby on Rails was chosen as the development framework, PostgreSQL and MongoDB as the database management systems. Puma was selected as the web server, and Nginx as the reverse proxy server. Containerization with Docker was implemented.

The application was developed and deployed on a virtual dedicated server.

3.1. System features

The system incorporates the following functionalities:

- Designing medical research studies;
- Data input, due to study design;
- Encoding data entered into the system
- Providing different access levels to the system;
- Database changes audit by the lead researcher;
- Regular database backup;
- Conducting analysis of the database contents;
- Exporting entered data to Excel;
- Grouping data and exporting them to Excel spreads heets for statistical processing based on specific grouping indicators (both single and multiple);
- Performing statistical analysis.

The developed system is covered by tests (coverage is more than 90%).

3.2. Further development of the system

The web-based system for processing medical research data has been tested and implemented in operation at a medical research centre. Over the course of a year, the product has been used by four research groups consisting of 10 individuals, with approximately 16,000 research indicators entered. During its operation, the system has demonstrated smooth performance, and positive feedback has been received from users.

Taking into account newly identified requirements during operation, related to the need for expanding the system functionality, we changed the architecture of the system.

Initially, a minimum viable product (MVP) based on Ruby on Rails was developed. However, the number and level of support for libraries responsible for statistical processing and graphing in the Ruby language are lower compared to Python [7].

Therefore, for further system development, the possibility of adding a separate microservice responsible for statistical data processing using Python as the primary language was considered.

The transition process is currently underway. A separate microservice has already been containerized, network interaction using JSON API has been established using the Flask library, and appropriate Python libraries and methods that meet the defined tasks have been selected.

4. CONCLUSION

The developed and implemented web-based system for processing medical research data has proven to be successful in operation.

During real scientific research, the system was used by researchers who requested an extension of functionality, including new methods of statistical processing, including the ability to drawgraphs. To address this requirement, a separate microservice was designed, and its development is currently ongoing.

The process of adding this microservice will make the system even more functional.

References

[1] T. Magrupov, S. Yusupov, Y. Talatov, et al., "Intelligent Medical System of Designing Medical Technics and Technology", 2020 International Conference on Information Science and Communications Technologies (ICISCT), IEEE, 2020, pp. 1-4.

[2] K. Moutselos, et al., "Trustworthy data processing for health analytics tasks", 2018 IEEE International Conference on Big Data (Big Data), IEEE, 2018, pp. 3774-3779.

[3] G. Guyatt, J. Cairns, D. Churchill, et al., "Evidence-based medicine: a new approach to teaching the practice of medicine", Jama, 268(17), 1992, pp. 2420-2425.

[4] C. Auffray, R. Balling, I. Barroso, et al., "Making sense of big data in health research: towards an EU action plan", Genome medicine, 8(1), 2016, pp. 1-13.

[5] D. Singh, S. Verma, J. Singla, "A comprehensive review of intelligent medical diagnostic systems", 2020 4th International Conference on Trends in Electronics and Informatics (ICOEI)(48184), IEEE, 2020, pp. 977-981.

[6] O. Karpov, A. Nikulichev, O. Penzin, et al., "Architecture of next-generation health information systems", Bulletin of Pirogov National Medical and Surgical Center, 14(3), 2019, pp. 126-134 (in Russian).

[7] S. Chandran, K. Abraham. "A Correlative Scrutiny on two Programming Dialects: RUBY Vs PYTHON", International Journal of Engineering and Advanced Technology (IJEAT), 9(3), 2020, pp. 4395-4404.

REVIEW OF MULTIMODAL MEDICAL IMAGE FUSION TECHNIQUES AND THEIR APPLICATION IN PROSTATE CANCER

Diana S. Tsvetkova

Faculty of German Engineering Education and Industrial Management,
Technical University of Sofia, Bulgaria
1000 Sofia, "Kl. Ohridsky" str.8
diana.tsvetkova@fdiba.tu-sofia.bg

Veska Georgieva

Faculty of Telecommunications, Technical University of Sofia, Bulgaria
1000 Sofia, "Kl. Ohridsky" str.8
T. (+359 2) 965-3293; E-mail: vesg@tu-sofia.bg

Valeria Hadzhiyska

Aleksandrovska University Hospital, Bulgaria
1431 Sofia, "Georgi Sofiiski" str.1
E-mail: v.h.hadzhiyska@gmail.com

Yavor Gramatikov

Aleksandrovska University Hospital, Bulgaria
1431 Sofia, "Georgi Sofiiski" str.1
E-mail: yavorgramatikov@abv.bg

Abstract

The Medical imaging is crucial for diagnosing and treating diseases, with a major challenge being accurate detection and effective treatment. Multimodal medical image fusion combines different images from various imaging methods into a single, comprehensive image. The fusion enhances the interpretability of medical images, leading to a better understanding during evaluation and diagnosis.

Prostate cancer ranks among the primary factors contributing to male death rate worldwide. Utilizing advanced image fusion techniques in prostate imaging can greatly aid in detecting and treating prostate cancer. This paper offers a review of multimodal medical image fusion techniques and their application in prostate cancer imaging and diagnostics. The primary goal is to contribute to the advancement of medical imaging methods, particularly those that improve the diagnosis of prostate diseases

1. INTRODUCTION

Detecting Prostate cancer (PCa) in its early stages is essential to improve survival rates and facilitate timely intervention. The role of imaging is becoming increasingly significant in the early identification and management of the disease. In 1989, Hodge et al. [1] achieved a significant milestone with the introduction of grayscale B-mode ultrasound (US) imaging to assist in guiding transrectal prostate biopsies. This advancement quickly replaced the conventional method of physically conducting a digital rectal examination (DRE) as the preferred approach for guiding needle biopsies in the diagnosis of prostate cancer. Today, over a quarter-century later, imaging is regarded as essential for managing PCa [2].

Recent advancements in imaging technologies have led to significant progress in the field of image processing and data fusion techniques, aimed at improving data acquisition [3]. Image fusion is a technique for combining relevant information from a series of images depicting the same scene into one output image that describes the scene better, while retaining valuable information from the source images. Additionally, the fused image provides improved spatial and spectral resolution. As a result, image fusion is extensively applied across various domains, including the medical field [4,5].

2. MULTIMODAL MEDICAL IMAGE FUSION

Image fusion typically starts with image registration, which is the procedure of aligning medical image data from different multimodal sources onto a common coordinate system. Following this step, image segmentation occurs, where relevant objects within 2D and/or 3D visual data are identified and characterized. Predefined fusion rules are then employed

to combine the source images. As a result, image fusion generates a single, improved, and enhanced output image that contains all the pertinent information from the source images. Therefore, the main goal of image fusion is to generate informative and classifiable images that can be employed for a broad array of beneficial applications.

2.1. Image Fusion Techniques

Extensive research has been conducted in the field of image fusion techniques. A categorization of multimodal medical image fusion techniques can be seen on Fig.1 along with some examples from each category [6].

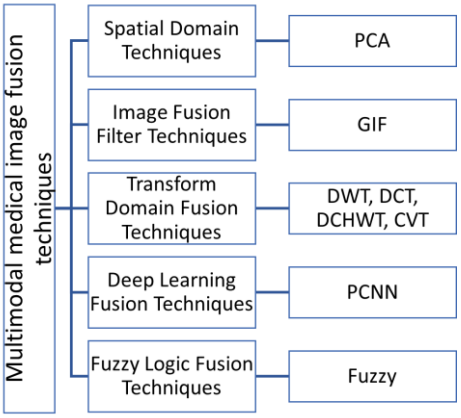

Figure 1. Categorization graph of multimodal medical image fusion techniques [6]

Spatial domain techniques are relatively uncomplicated but excel at producing highly focused fused images with substantial spatial details. It is possible for techniques in this category to produce blurring effect and spectral degradation. An example for a Spatial domain technique is the Principal Component Analysis (PCA). This technique utilizes multiple bands, making it widely favoured. It stores shared information from all the bands in the first principal component, often referred to as PC1, which contains high variances, providing greater detail about the panchromatic image. PC1 is then replaced by a high-resolution component adjusted to match PC1's variance. An inverse PCA process is applied to create the final high-resolution multispectral image.

When discussing Image fusion filter techniques – guided image filters (GIF), weighted least squares and bilateral filters are used for smoothing the images while preserving its edges. The guided image filter (GIF) stands out due to its superior results and faster execution time in fusion processes. This filter relies on a local linear approach, making it applicable not only to the image fusion process, but also to various image processing tasks like image matting, up-sampling, and colorization. The guided image filter uses a multi-level representation and combines the base and feature layers of multi-modal medical images through a weighted average fusion technique.

Transform domain fusion techniques are categorized with the fact that all fusion operations are performed in the contourlet-, shearlet- or wavelet-domains. The input images are decomposed to the chosen domain and then all following processing is done in this domain. The last step of developing fused image is to perform an inverse transform that makes it possible to visualize the fused image. Examples of such techniques are the Discrete Wavelet Transform (DWT) [7,8], Discrete cosine harmonic wavelet transform (DCHWT), Curvelet Transform Techniques (CVT).

Deep learning image fusion techniques are a recently popular method for image fusion, applicable in various domains. The ability of deep learning to perceive the problems with case-based reasoning techniques is used to improve the outcome of the resulting image. There are many interpretations of using Deep Learning as an image fusion technique. One example involves using a Pulse Coupled Neural Network (PCNN). Its feedback network consists of receptive field, modulation field, and pulse generator. Each neuron in the network corresponds to an image The matching of the pixel's intensity is used as an external input to the Pulse Coupled Neural Network.

Fuzzy logic fusion techniques involve utilizing fuzzy sets to process images. These techniques consist of three main steps: fuzzification, modification of membership values using fuzzy rules, and defuzzification to obtain actual results. Fuzzy techniques play a crucial role in coding and decoding image data, with the modification of membership values being a key aspect. These techniques adjust membership values after transforming the medical image data from grey-level to membership planes, often relying on fuzzy integration and rules based on fuzzy clustering. Ultimately, the process results in a fused multimodality medical image.

3. PROSTATE CANCER IMAGING AND DIAGNOSIS

As males grow older, the prostate gland has the potential to increase in size, which can result in potential problems related to urinary and reproductive health.. As mentioned earlier, imaging has now become the predominant method for detecting prostate cancer (PCa). Presently, the key modalities for guiding PCa diagnosis include ultrasound-based imaging, multi-parametric MRI (mpMRI) and PET imaging. The selection of the imaging method depends on the specific characteristics of the tumour's biological behaviour. As indicated by reference [2] within Table 1, you can find a comprehensive presentation of various imaging techniques, emphasizing their main clinical uses, along with their respective advantages and disadvantages.

4. APPLICATION OF MULTIMODAL MEDICAL IMAGE FUSION IN PROSTATE CANCER DIAGNOSIS

Within the field of medical imaging, image fusion has firmly established itself as a clinically valuable tool for disease classification and initial diagnostic purposes [4]. This section will delve into various image fusion techniques within the context of diagnosing prostate cancer.

Table 1. Main imaging modalities for prostate cancer detection

Image Modality	Clinical Usage	Advantages	Disadvantages
Ultrasound-based	Early identification and evaluation.	Office-based, cost-effective, provides real-time results.	Restricted tissue differentiation between cancerous and non-cancerous tissue.
mpMRI-based	Early diagnosis and recurrence, continuous monitoring, progression assessment, metastatic involvement.	Superior tissue differentiation that aids in identifying clinically significant prostate cancer.	Costly because of the extended in-bore time, absence of immediate imaging, requires advanced training
PET-based	Staging, recurrence, metastatic spread.	Provides additional data for the staging, characterization, and assessment of metastatic presence in tumors.	Costly, technological difficulties (attenuation correction), clinical obstacles (radiation exposure).

4.1. MRI/US fusion

In MRI/US fusion-guided procedures, biopsies are conducted using live B-mode ultrasound (US) in an outpatient setting, maintaining cost-efficiency and procedure duration. Before the procedure, a pelvic mpMRI examination identifies abnormal areas, which are then overlaid onto US images through image fusion techniques. While expert uroradiologists can perform subjective visual or cognitive image fusion, more widely adopted are regulatory-cleared MRI/US fusion devices, offering operator-independent fusion. Reference [9] provides a summary of such regulatory-approved MRI/US Fusion Platforms and their fundamental specifications, which can be found in Table 2.

4.2. MRI/PET fusion

MRI/PET imaging, a hybrid technology that offers both biological and morphological data for oncological diagnosis, holds great promise for prostate cancer patients.

Table 2. Summary of regulatory-cleared MRI/US Fusion Platforms and their basic specifications

Fusion System		Principle Investigator Location	MRI Device	Ultrasound image Acquisition	Method of image Registration
Trade Name	Manufacturer				
UroNav	In Vivo/Philips	Bethesda, USA	3T Philips	Manual US 2D sweep. Freehand manipulation of US probe.	Rigid
Artemis	Eigen	Los Angeles, USA	3T Siemens	Manual rotation along a fixed axis (US probe on a tracking arm)	Elastic
Urostation	Koelis	Paris, France Oslo, Norway Grenoble, France	1.5T Siemens, 1.5 Siemens, 3T Philips	Automatic US probe rotation, 3 different volumes elastically registered	Elastic
BiopSee	PiMedical/MedCom	Heidelberg, Germany	3T Siemens	Custom-made biplane Transrectal US probe mounted on a stepper	Rigid
Virtual Navigator	Esaote	Paris, France Lille, France	1.5T Siemens 1.5T Philips	Manual US sweep. Freehand rotation of US probe.	Rigid
HI RVS/Real-Time Virtual Sonography	Hitachi	Chiba, Japan	1.5T Philips	Real-time biplanar TRUS	Rigid

Since MRI/PET systems are only found in a very limited number of clinical centres worldwide, there is a need for good enough software to merge the separate PET and MRI images acquired from the same patient within a short period of time. This integration will produce functional images of the

detected lesion along with the essential anatomical information required for conducting the fusion prostate biopsy.

A study by Guberina et al. [10] in September 2019, involving 93 patients, compared Ga PSMA PET-MRI with Ga PSMA PET-CT for men with recurrent prostate cancer. The findings indicated that Ga PSMA PET-MRI outperformed Ga PSMA PET-CT, particularly in improving the sensitivity of identifying the index lesion when using fused Ga PSMA PET-MRI. [11]

Additionally, Liu et al. [12] shares the perspective that MRI/PET is well-suited for evaluating local and regional disease, whether it's for the initial staging or reevaluating the staging process.

4.3. MRI/CT fusion

In a study by Hentschel et al. [13], it was found that CT scans tend to overestimate prostate volume by 35% compared to MRI. However, using MRI/CT image fusion for treatment planning in prostate cancer patients allows for more accurate staging prediction and precise identification of the target volume.

Kagawa et al. [14] concluded that MRI localization of the prostate is more accurate than CT, with MRI indicating a distance of 15 mm from the cone to the apex. The MRI/CT image fusion technique provides valuable supplementary information to CT for more precise targeting in prostate cancer radiation therapy.

However, comparison of prostate cancer detection methods was conducted by Khoo et al. [15] They found no overall difference in the detection of clinically significant prostate cancer between visual estimation (cognitive registration) and image fusion (software registration) during targeted transperineal prostate biopsy. Nonetheless, image fusion could offer benefits when utilized by skilled professionals.

4.4. Alternative fusion methods

Researchers do not constrain themselves to the utilization of MRI-US, MRI-PET, and MRI-CT fusion techniques, as a multitude of scholarly articles underscore the adoption of alternative fusion methods. In ths section, we will highlight some examples.

In study [16] the use of interventional MRI (iMRI) for guiding radiofrequency thermal ablation as a minimally invasive treatment for prostate cancer is explored. While nuclear medicine can identify tumours in the prostate that may not be visible on MRI, the aim is to combine the advantages of functional nuclear medicine SPECT images with iMRI-guided treatments. This involves registering low-resolution SPECT with high-resolution MRI and then mapping the functional and anatomical data to live-time iMRI images for enhanced tumour targeting. The study tested this concept using data from patients and volunteers, achieving a registration accuracy of 0.4 mm to 0.2 mm, making it feasible to integrate SPECT and high-resolution MRI into iMRI-guided procedures.

Wachter et.al. [17] assessed the value of combining CT and MRI with AC PET imaging to detect hidden prostate cancer recurrences. The combination of Image fusion techniques (CT-PET, MRI-PET) enhanced lesion characterization and precise localization, impacting patient management. The retrospective fusion of AC PET with CT/MRI proved crucial, particularly for patients with prostate region AC uptake.

Paper [18] presents an automated fusion method using a U-Net, which generates weight distribution through neural network learning based on image feature information and multifocus training targets. This approach fuses a pair of MRI images for prostate cancer (axial T2-weighted and ADC map) using local similarity and Gaussian pyramid transformation. Experimental results show that the method enhances the visualization of prostate cancer in terms of both visual quality and objective evaluation.

5. CONCLUSION

In conclusion, image fusion plays a vital role in improving the diagnosis and treatment of prostate cancer, offering a range of techniques and modalities to enhance accuracy and efficiency in clinical practice. This review underscores the multimodal medical image fusion techniques and their relevance in the context of prostate cancer diagnosis.

6. ACKNOWLEDGMENTS

The authors would like to thank the Research and Development Sector at the Technical University of Sofia for the financial support.

References

[1] K. Hodge, J. McNeal, T. Stamey. "Ultrasound guided transrectal core biopsies of the palpably abnormal prostate". J Urol. 1989 Jul;142(1):66-70. doi: 10.1016/s0022-5347(17)38663-9. PMID: 2659826.

[2] S. Sarkar, S. Das. "A Review of Imaging Methods for Prostate Cancer Detection", Biomed Eng Comput Biol. 2016 Mar 2;7(Suppl 1):1-15. doi: 10.4137/BECB.S34255. PMID: 26966397; PMCID: PMC4777886.

[3] J.K. Aggarwal, editor (2013) "Multisensor fusion for computer vision", Springer Science & Business Media 99

[4] S.P. Yadav, S. Yadav, "Image fusion using hybrid methods in multimodality medical images", Med Biol Eng Comput. 2020 Apr;58(4):669-687. doi: 10.1007/s11517-020-02136-6. Epub 2020 Jan 28. PMID: 31993885.

[5] A.P. James, B.V. Dasarathy, "Medical Image Fusion: A survey of the state of the art", Information Fusion, 2014

[6] B. Rajalingam, R.Priya, "Multimodal medical image fusion using various hybrid fusion techniques for clinical treatment analysis", Smart Construction Research, Vol. 2, Issue :2, pp.1-2018.

[7] D. Tsvetkova, V. Georgieva, "GUI for image fusion in medical images of brain", in Journal of Applied Electromagnetism, ISSN: 1109-1606, Proceedings of 15th International Conference on Communications, Electromagnetism and Medical Applications (CEMA'21), pp. 43-47, 2021.

[8] V. M. Georgieva, P. P. Petrov, D. S. Tsvetkova and L. B. Laskov, "MRI/SPECT Image Fusion of Brain Based on Multi-Scale Wavelet Decomposition, "56th International Scientific Conference on Information, Communication and Energy Systems and Technologies (ICEST), pp. 85-88, 2021.

[9] J.K. Logan, S. Rais-Bahrami, B. Turkbey, A. Gomella, H. Amalou, P.L. Choyke, B.J. Wood, P.A. Pinto. "Current status of magnetic resonance imaging (MRI) and ultrasonography fusion software platforms for guidance of prostate biopsies", BJU Int. 2014 Nov;114(5):641-52. doi: 10.1111/bju.12593. Epub 2014 May 22. PMID: 24298917; PMCID: PMC4568118.

[10] N Guberina, P Hetkamp, H Ruebben, W Fendler, J Grueneisen, S Suntharalingam, J Kirchner, L Puellen, N Harke, JP Radtke, L Umutlu, BA Hadaschik, K Herrmann, M Forsting, "A Wetter. Whole-Body Integrated [68Ga]PSMA-11-PET/MR Imaging in Patients with Recurrent Prostate Cancer: Comparison with Whole-Body PET/CT as the Standard of Reference", Mol Imaging Biol. 2020 Jun;22(3):788-796. doi: 10.1007/s11307-019-01424-4. PMID: 31482413.

[11] A Arslan, E Karaarslan, AL Güner, Y Sağlıcan, MB Tuna, O Özışık, AR Kural, "Comparison of MRI, PSMA PET/CT, and Fusion PSMA PET/MRI for Detection of Clinically Significant Prostate Cancer", J Comput Assist Tomogr. 2021 Mar-Apr 01;45(2):210-217.

[12] FY Liu, TW Sheng, JR Tseng, KJ Yu, KH Tsui, ST Pang, LJ Wang, G Lin, "Prostate-specific membrane antigen (PSMA) fusion imaging in prostate cancer: PET-CT vs PET-MRI", Br J Radiol. 2022 Mar 1;95(1131):20210728. doi: 10.1259/bjr.20210728. Epub 2021 Dec 21. PMID: 34767482; PMCID: PMC8978229.

[13] B Hentschel, W Oehler, D Strauss, A Ulrich, A Malich, "Definition of the CTV prostate in CT and MRI by using CT-MRI image fusion in IMRT planning for prostate cancer", Strahlenther Onkol. 2011 Mar;187(3):183-90. doi: 10.1007/s00066-010-2179-1. Epub 2011 Feb 24. PMID: 21347638.

[14] K. Kagawa, W.R. Lee, T.E. Schultheiss, M.A. Hunt, A.H. Shaer, G.E. Hanks, "Initial clinical assessment of CT-MRI image fusion software in localization of the prostate for 3D conformal radiation therapy" , International Journal of Radiation Oncology*Biology*Physics, Volume 38, Issue 2, 1997, Pages 319-325, ISSN 0360-3016, https://doi.org/10.1016/S0360-3016(96)00620-7.

[15] J Urol 2021 Apr 01;205(4)1075-1081, CC Khoo, D Eldred-Evans, M Peters, M van Son, PSN van Rossum, MJ Connor, F Hosking-Jervis, MB Tanaka, D Reddy, E Bass, L Powell, S Ahmad, E Pegers, S Joshi, D Sri, K Wong, H Tam, D Hrouda, H Qazi, S Gordon, S McCracken, M Winkler, HU Ahmed, "A Comparison of Prostate Cancer Detection Between Visual Estimation (Cognitive Registration) and Image Fusion (Software Registration) Targeted Transperineal Prostate Biopsy", The Journal of Urology

[16] Baowei Fei et al., "Registration and fusion of SPECT, high-resolution MRI, and interventional MRI for thermal ablation of prostate cancer," in IEEE Transactions on Nuclear Science, vol. 51, no. 1, pp. 177-183, Feb. 2004, doi: 10.1109/TNS.2003.823027.

[17] S Wachter, S Tomek, A Kurtaran, N Wachter-Gerstner, B Djavan, A Becherer, M Mitterhauser, G Dobrozemsky, S Li, R Pötter, R Dudczak, K Kletter, "11C-acetate positron emission tomography imaging and image fusion with computed tomography and magnetic resonance imaging in patients with recurrent prostate cancer", J Clin Oncol. 2006 Jun 1;24(16):2513-9. doi: 10.1200/JCO.2005.03.5279.

[18] X. Huang et al., "Application of U-Net Based Multiparameter Magnetic Resonance Image Fusion in the Diagnosis of Prostate Cancer," in IEEE Access, vol. 9, pp. 33756-33768, 2021, doi: 10.1109/ACCESS.2021.3061078.

[19] H. Elhoseny O.Faragallah E.El-Rabaie F.El-Samie, "Medical Image Fusion: A Literature Review Present Solutions and Future Directions" , July 2017

[20] YY Zhang, B Hu, L Chen. "Imaging fusion in the diagnosis of prostate cancer", Zhonghua Nan Ke Xue. 2015 Jan;21(1):78-81. Chinese. PMID: 25707146.

DIFFERENTIATION IMAGES OF MEDICAL PREPARATION CRYSTALS FROM PLACEBO BY USING METHODS OF FRACTAL ANALYSIS

N. Ampilova

Saint-Petersburg State University
n.ampilova@spbu.ru

V. Lyamin

Saint-Petersburg State University
lyaminva@yandex.ru

T. Novosadiyk

POLEVET clinic
vethom@mail.ru

I. Soloviev

Saint-Petersburg State University
i.soloviev@spbu.ru

Abstract

To analyze digital images having complex structure one should apply suitable processing methods. To localize peculiarities of the image one need to use an appropriate representation depending on the type of images. The choice of the presentation is the essential part of the study. In the paper we consider the application of fractal and multifractal methods to compare crystals of medical preparations with a control image which does not contain a preparation.

The images under study were transformed to grayscale palette. It was shown that the choice of a filtration method depends on the image type. For several classes containing 5-6 images the applied methods demonstrated the separation of obtained characteristics, which means the difference in structures of medical preparations and placebo.

1. INTRODUCTION

In many cases digital images may be interpreted as phase portraits of complex processes in different moments of time. The analysis of these representations by mathematical methods gives a possibility to describe the properties of observed processes by using various characteristics (features) of the images.

As the distribution of pixel intensities is the main information about a digital image, specifications of the image are formulated in these terms. As a rule, mathematical methods of analysis use a normed distribution on the cells of a given size, which is a probabilistic measure defined on the image. The norming (the choice of a measure) may be performed by different ways depending on a problem. The simplest way takes the ratio of sum of pixel intensities in a cell to the common sum of intensities for the image. Such a method results in an average of intensities, and sometimes smooths out the difference between parts of the image. The more preferable way is to choose the ratio of the sum of intensities from a given interval (for a cell) to the sum of intensities from such an interval for the image.

The experience of many researchers confirms that for images having complex structure the choice of appropriate methods is not just a technique, but an art. We should perform a preliminary processing to improve an image, but not destroy its specific structure.

At the same time a preparing the image to the application of mathematical methods is an equally important and very significant part of the study. One need find the area of interest and transform the image to a standard presentation convenient for problems of a certain class. This work may be performed both with the help of graphic editors and specially devised algorithms.

Methods of image preprocessing are used both for filtration and improving the quality of an image. They help to highlight and emphasize certain properties of images and to facilitate their visual perception by an expert. In medical applications this approach helps an expert to clarify the diagnosis. The combining filtration with following morphological analysis demonstrate reliable results in operating with radiograph and ultrasound images [3, 4].

Mathematical methods result in obtaining characteristic which may be used for further image classification. So, Haralick's texture methods describe the image structure in terms brightness ratio for neighboring pixels [5]. Morphological methods reveal specific patterns, for example contours of various forms.

Methods of fractal analysis describe the image by using fractal dimensions. As one numerical value cannot characterize the image structure, we should apply some modifications to obtain vector characteristics. In this sense, the "blanket technics" is very productive. It is applied to calculate the Minkovsky dimension for gray level images [2]. An image is represented as a surface in 3-dimension space, where two coordinates indicate the position of a pixel, and the third one is the pixel intensity. There is one-to-one correspondence between the surface and the given image. The surface is given by the gray level function, which is defined for integer values and then extends to real numbers. Such a definition corresponds to an approximation of the surface by unit squares parallel to the image plane.

Then we construct upper and bottom "blankets" for the surface by a definite rule, such that every next iteration is on the distance 1 from the previous one.

Actually, this procedure means a sequential smoothing of the surface. On every step we calculate the volume of the body between upper and bottom blankets and then calculate an approximate value of the surface area and as a result the Minkovsky dimension of the surface. However, the most informative characteristic is not this dimension, but the ratio logarithm of the area on the next step to the step number. For a given set of steps we obtain a vector value (called the next characteristic vector). These vectors are different for images of different classes.

Blanket technics was successfully applied for study of biomedical preparations [1] and SAR images as well [7, 8].

Multifractal methods are useful if analyzed images may be interpreted as a union of several fractal subsets. In this case we can obtain the set of fractal dimensions of the subsets (multifractal spectrum) or Renyi spectra measuring changes of the initial distribution of pixel intensities at its sequential renormalizations.

Our experience when analyzing biomedical images allows proposing a combined application fractal and multifractal methods to obtain reliable results [9].

In this work we developed a technology for differentiation crystals of medical preparations obtained by the thesiography method from the image of control pattern which does not contain the preparation. It should be noted that getting the images and their preprocessing for the following application of mathematical methods is voluminous and quite time-consuming part of the study. When preparing images we used combined methods of preprocessing. Mathematical methods used in this paper are calculation of characteristic vector (blanket technics) and Renyi spectra. Experiments were performed for 3 classes of medical preparation images. All results demonstrated the separation of calculated features.

The paper has the following structure. The first section contains material and methods for obtaining images. In section 2 the description of the preliminary image processing for the application of mathematical methods is given. The next part is devoted to the fractal and multifractal methods. The results of experiments are demonstrated in section 4.

2. MATERIALS AND METHODS

2.1. Materials

The images were obtained by the light microscope MIKMED – 6, which consists of eyepiece LOMO WF 10X/22, objectives Plan 4/0,1 Plan 10/0,25 Plan 40/0,65, and video-camera MC – 6,3 (USB-3,0).

The samples were prepared on laboratory slides. Medical preparations of plant, animal and mineral origin in dilution from 1 to 1000 CH by C. Haneman were manufactured in Homeopathic center of St. Petersburg (sugar nibs), and in pharmacy POLE-VET (oil). Sterile brine solution (NaCl – 0.9%) was used.

2.2. Method of study

The research of the crystallization of biosubstrates was conducted by thesiograthy method. At first the

preparation under study was dynamized (by the method of "shaking"). Brine solution (from 1 to 3 drop depending on the substrate quantity) was dripped on a slide. Then 1 nib (or drop) of the substrate was set in the drop of brine solution. The result of crystallization was fixed after 24 hours.

Sugar nibs, oil and brine solution were taken as placebo, and their images as control ones. In this work we take the image of brine solution as placebo. The obtained crystals of biosubstrates were compared with the control image.

3. IMAGE EDITING

3.1. Transforming images to a standard form

To apply methods of image analysis we should convert the images to some appropriate form. For this purpose we cut out the part of the image which contains crystal. The cutting is produced so that there was a "little" space between crystal and the image boundary. One may use graphic editors such as Gravit Designer, Photo Pos Pro, Paint. It is important to do it so the center of the crystal coincide with the center of the image. Then, following the formula below, we perform a rotation of the image so that the sides of the crystal faces become parallel to the sides of the image.

$$x_1 = x_0 + (x - \mathrm{w}/2)\cos\varphi - (y - \mathrm{h}/2)sin\varphi$$
$$y_1 = x_0 + (x - \mathrm{w}/2)\sin\varphi - (y - \mathrm{h}/2)cos\varphi$$

where (x_1, y_1) — new coordinates, (x,y) — old coordinates, (x_0, y_0) the center of rotation, and $\boldsymbol{\phi}$ — the angle of rotation, and (w,h) define the size of the new image. This transformation is performed by the C# program. After the processing of initial images by the described way we choose the image of minimal size and cut all the others by this size. Then all the images are transformed to grayscale palette. The example illustrating this processing is given below.

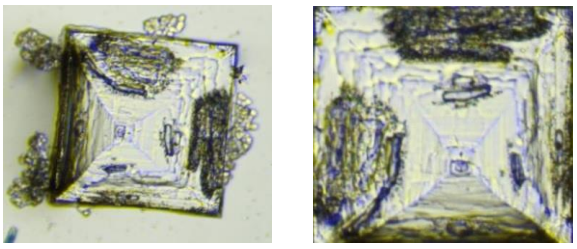

a) b)

c)

Figure 1. a) a crystal, b) after rotation and cutting, c) grayscale image

3.2. Image preprocessing

To choose an appropriate methods of image preliminary processing we perform several experiments. We considered global and local equalization, the Laplace operator, linear and nonlinear filtering, unsharp masking. Different ways to combine spatial enhancement methods were applied as well.. Experiment show that the choice of an adequate method is a complex problem. For the images studied in this work global equalization practically did not change an image, and local equalization lead to unexpected results. Summarizing our experiments, we settled on the following methods: the Laplace operator and unsharp masking. The Laplace operator is isotropic, i.e. invariant under rotation, and unsharp masking allows flexible parametric adjustment.

4. MATHEMATICAL METHODS

4.1. Blanket construction

A detailed description of this method can be found in [2, 10], so we will provide here only the information necessary to describe the algorithm for its implementation.

Let $\mathrm{G} = \{\mathrm{X_{ij}}, \mathrm{i} = 0,1, \ldots, \mathrm{K}, \mathrm{j} = 0,1, \ldots, \mathrm{L}\}$ be a gray-scale image and X_{ij} be the gray level of the (i, j)-th pixel. This is a gray-level surface for the image, which can be viewed as a fractal for a certain measure range.

Consider $F \subset \mathbb{R}^n$. Then δ-parallel body F_δ is a set of points being at a distance from F of no more than δ. i.e

$$F_\delta = \{x \in \mathbb{R}^n : |x - y| \leq \delta, \mathrm{y} \in F\}.$$

We denote by $Vol(F_\delta)$ n-dimensional volume of F_δ. If for some constant s at $\delta \to 0$ the limit $Vol(F_\delta)/\delta^{n-D}$ is positive and bounded, then the

number D is called the Minkovski dimension of the set F.

We build blankets u_δ, b_δ for a gray level surface as follows

$$u_\delta(i,j) = max\{u_{\delta-1}(i,j)+1, max_{|(m,n)-(i,j)|\le 1} u_{\delta-1}(m,n)\}$$

$$b_\delta(i,j) = min\{b_{\delta-1}(i,j)-1, min_{|(m,n)-(i,j)|\le 1} u_{\delta-1}(m,n)\}$$

$$u_0(i,j) = b_0(i,j) = X_{ij}$$

A point $F(x,y)$ is included in a δ-parallel body if $b_\delta(i,j) < F(x,y) < u_\delta(i,j)$. The definition of a blanket is based on the fact that the blanket for a surface of radius δ includes all the points of the blanket for a surface of radius $\delta-1$ together with the points that are at the distance of 1 from this blanket.

The volume of a δ-parallel body is calculated by u_δ and b_δ:

$$Vol(F_{\delta)} = \sum_{i,j}(u_\delta(i,j) - b_\delta(i,j)).$$

The surface area may be calculated using one of two formulas

$$A_\delta = \frac{Vol_\delta}{2\delta}$$

$$A_\delta = \frac{Vol_\delta - Vol_{\delta-1}}{2}.$$

Minkovsky dimension is defined as

$$D \approx 2 - {}^{ln\, A_\delta}/_{ln\, \delta}$$

To obtain the image characteristics, we use a vector $((\ln\delta, \ln A_\delta))$, the size of which is determined by the number of different values of δ.

4.2. Renyi spectra

The detailed information about multifractal and Renyi spectra may be found in [6]. Consider the set $M \subset R^n$, and its partition into $N(\varepsilon)$ cells with side (or volume) ε. We define the probability measure $p(\varepsilon) = \{p_i(\varepsilon)\}$,
$i = 1, \dots, N(\varepsilon)$, $\sum_{i=1}^{N(\varepsilon)} p_i(\varepsilon) = 1$.

Also consider the generalized statistical sum (or the sum of the moments of the measure)

$$S(q,\varepsilon) = \sum_{i=1}^{N(\varepsilon)} p_i^q\ (\varepsilon)$$

As usual we assume that for the measure and statistical sum the power law holds:

$$p_i(\varepsilon) \sim \varepsilon^{\alpha_i}\ ,\ \ S(q,\varepsilon) \sim \varepsilon^{\tau(q)}$$

where $\tau(q)$ is a function of class C^1. The symbol "~" is understood as follows:

$$\alpha_i = \lim_{\varepsilon\to 0} \frac{\ln\ p_i(\varepsilon)}{\ln\varepsilon}, \tau(q) = \lim_{\varepsilon\to 0} \frac{\ln\ S(q,\varepsilon)}{\ln\varepsilon}.$$

Under these assumptions, the set of generalized Renyi dimensions is

$$D_q = \lim_{\varepsilon\to 0} \frac{1}{q-1} \frac{\ln S(q,\varepsilon)}{\ln\varepsilon}$$

These values describe the changing of initial measure $\{p_i(\varepsilon)\}$ for a range of q.

For q=0 we obtain capacity dimension, and for q=1 by applying the Lopital rule we obtain the so called information dimension (or the dimension of a measure support)

$$D_1 = \lim_{\varepsilon\to 0} \frac{\sum_i p_i(\varepsilon) ln p_i(\varepsilon)}{\ln\varepsilon}.$$

5. RESULTS OF EXPERIMENTS

In all the illustrations we use following denotations.

Preparation	Denotation
Placebo (brine solution)	Sample 0
Conium 1000 CH	Sample 1
Acidum phosphoricum 30 CH	Sample 2
Lac defloratum 1000 CH	Sample 3

Next we compare the samples with placebo.

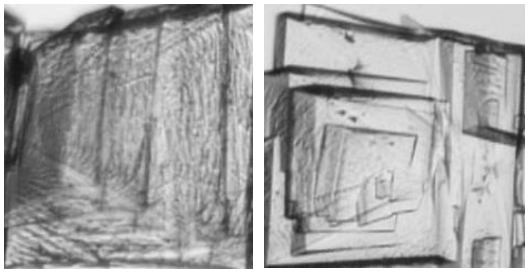

a) b)

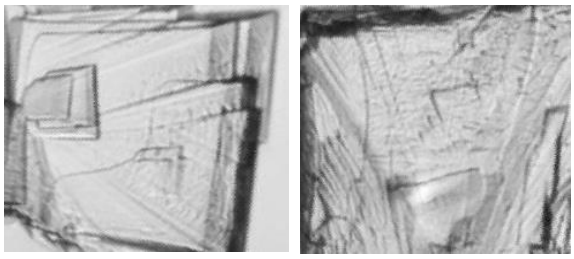

c) d)

Figure 2. a) Sample 0, b) Sample 1, c) Sample 2, d) Sample 3

The picture shows images of crystals of biosubstrates and placebo. On Fig.3 graphs of characteristic vectors and Renyi spectra for Sample 1 and Sample 0 are given. Graphs are separated. The point of intersection in Renyi spectra means that all the images have close value of capacity dimension.

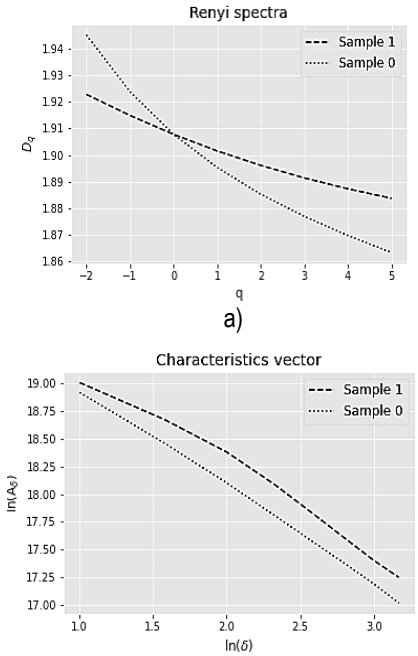

a)

b)

Figure 3. Comparing results for Conium 1000 CH and Placebo: a) Renyi spectra and b) characteristic vectors

The following graphs demonstrate the difference between the structure of the crystal of *Acidum* phosphoricum 30 CH and placebo.

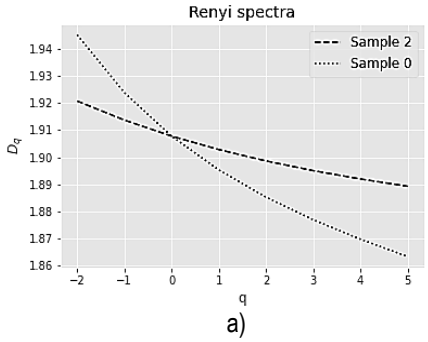

a)

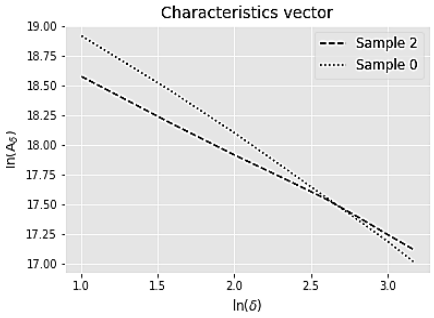

b)

Figure 4. Comparing results for *Acidum* phosphoricum 30 CH and placebo: a) Renyi spectra and b) characteristic vectors

In this case Renyi spectra give a better result than characteristic vectors. Analogical graphs results for the crystal of Lac defloratum 1000 CH and placebo are given in Fig. 5.

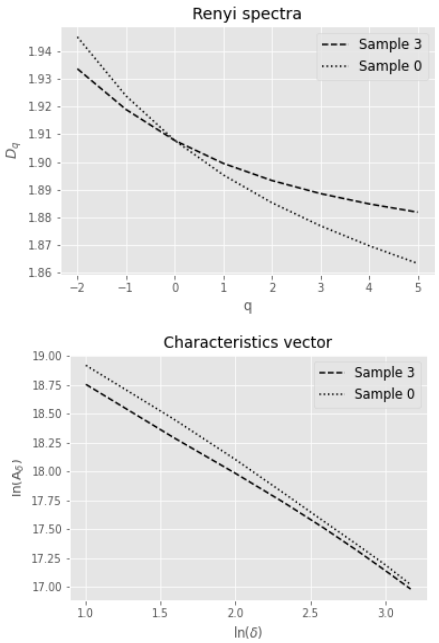

Figure.5. Comparing results for Lac defloratum 1000 CH and placebo

6. CONCLUSION

Our experiments show that the combining of image preprocessing and methods of fractal analysis allows obtaining graphs that are separated.

The fact that Renyi spectra have a point of intersection near q=0 means that all the images studied have close values of capacity dimension. This circumstance once again confirms that only capacity dimension cannot be used as a classifying sign in image analysis. In this case one consider spectra for q>0 and q<0 separately.

References

[1] **N. Ampilova, I. Soloviev , J.-G. Barth.** Application of fractal analysis methods to images obtained by crystallization modified by an additive. Journal of Measurements in Engineering, Vol. 7, Issue 2, 2019, p. 48-57. https://doi.org/10.21595/jme.2019.20436

[2] K. J. Falconer, "Fractal geometry", Chichester: Wiley, 1990.

[3] V.Georgieva, S. Vassilev. Kidney segmentation in ultrasound images via active countours, Proc. 11 Int. Conf. CEMA16, 13-15 Oct. 2016, Sofia, Bulgaria. p.43-46

[4] V. Geogieva, P.Petrov, B.Iantovics. X-ray image processing for tissue involvent-based caries detection, Proc. 14 Int. Conf. CEMA19, 17-19 Oct. 2017, Sofia, Bulgaria. p.22-26.

[5] Haralick R. M. Textural Features for Image Classification / R. M. Haralick, K. Shanmugan, I. Dinstein. //IEEE Transactions on systems, man and cybernetics, volume SMC-3. - IEEE, 1979. - №6. - P. 610-621. - ISSN 00189472.

[6] S.P. Kuznetsov, "Dynamical chaos", M, Izd.fiz-mat lit.,2001 (in Russian)

[7] A.Malamou,C.Pandis,P.Frangos and P.Stefaness. SAR image terrain classification using the modified fractal signature (MFS) method, Proc. 9 Int. Conf. CEMA14, 16-18 Oct. 2014, Sofia, Bulgaria. p.8-11.

[8] G. Pouraimis, A. Kotopoulis, N. Ampilova, I. Soloviev,E. Kalitsis and P. Frangos, Sea state determination using normalized one-dimensional radar signatures at X-band and fractal techiques, Proc. 14 Int. Conf. CEMA19, 17-19 Oct. 2019, Sofia, Bulgaria, p. 27-31.

[9] I. Soloviev, Application of multifractal methods for the analysis of crystal structures JAE 2022 JAE-Journal of Applied Electromagnetism (ntua.gr), 24(2),19-30.

[10] Y. Y. Tang, C. Y. Suen, "Modified fractal signature (MFS): a new approach to document analysis for automatic knowledge acquisition", IEEE Transactions on Knowledge and Data Engineering,1997, 9, № 5,p. 747-762.

METHODOLOGY FOR COUNTING PENGUINS DURING THEIR NESTING PERIOD BASED ON UAV-IMAGES USING DEEP LEARNING TECHNIQUES

Diana S. Tsvetkova

Faculty of German Engineering Education and Industrial Management;
Technical University of Sofia, Bulgaria;
8 "Kl. Ohridsky" Str, 1000 Sofia;
E-mail: diana.tsvetkova@fdiba.tu-sofia.bg

Oleg Vassilev

29 Javorov district, 1504 Sofia, Bulgaria;
E-mail: ovassilev@gmail.com

Atilla Markov

26 "Pop Hariton" Str, 5000 Veliko Tarnovo, Bulgaria;
E-mail: atilla.markovv@gmail.com ;
T.(+359) 89-620-1879

Boris P. Nikolov

Institute of Biodiversity and Écosystème Research,
Bulgarian Academy of Sciences ;
1 "Tsar Osvoboditel" Blvd., 1000 Sofia, Bulgaria ;
E-mail: lanius.bg@gmail.com

Abstract

Observing penguin populations in Antarctica holds significant importance because they serve as key markers for detecting environmental shifts in these delicate ecosystems. Conventional monitoring techniques are not only expensive but also stressful to the animals. This paper presents an alternative, non-intrusive method using unmanned aerial vehicles (UAVs) and a unique 3D mesh-level algorithm for counting penguins based on UAV imagery. Our methodology, applied to data from the 30th and 31st Bulgarian Antarctic Expeditions, has shown promising results, achieving 97% accuracy in penguin detection. This novel approach holds wider implications for biodiversity research and has the potential to propel advancements in both the field of deep learning and ecological studies.

1. INTRODUCTION

Due to the high sensitivity of Antarctic ecosystems, relatively small impacts have significant negative consequences. Penguins are an integral part of this biome. Therefore, the alteration in the population size of penguins can indicate fluctuations in environmental factors, which can be used as a predictor for possible environmental changes in the future [1][2]. Monitoring of colonially breeding penguins is of great importance and should be done at regular intervals and with high accuracy [3].

Many of the traditional monitoring methods (manual counting, direct field data collection, manned flights, satellite data) have been used with varying degrees of success because of their different accuracy, high time and financial costs and stressful effects on animals. In recent years, unmanned aerial vehicles (UAV) have been increasingly used as an alternative to conventional methods for monitoring various elements of biodiversity. They offer resource efficiency and minimal negative impact on the environment [4][5][6].

Most articles on wildlife counting using deep neural networks tend to prefer deep convolutional neural networks (CNNs) due to their remarkable precision and accuracy [7][8]. Models such as RetinaNet [9] and ResNet [10] have shown promising results, although they come with the drawback of extended processing times and complex implementation [11] [12][13]. Torney et al. [14] introduced a dependable model for automatically counting wild animals in UAV imagery, utilizing a single-pass deep CNN called YOLOv3(abbreviation from "You Only Look Once", real-time object detection system) one-stage

method, contrasting with the two-pass-deep CNNs. In [15] YOLOv7 achieves an accuracy of 94.6% in penguin detection, demonstrating significant promise. Notable, the development of YOLO algorithms has been advancing rapidly and effectively, with the recent introduction of YOLOv8 in January 2023, which is expected to significantly enhance research in this field [16][17][18].

This paper introduces an innovative algorithm for non-invasive penguin colony counting using UAV-captured images. It employs a 3D mesh-level algorithm for orthomosaic generation and deep learning techniques for penguin counting, with a focus on accuracy and efficiency. The chosen deep neural network architecture is YOLOv8, known for its speed and precision.

2. MAIN STAGES OF PROPOSED APPROACH

The chosen YOLOv8 architecture is gaining rapid popularity due to its exceptional speed and accuracy in tasks such as object detection, image classification, and segmentation. A notable advantage of YOLO models is their ability to be trained on a single graphics processing unit (GPU), which sets them apart from other image object detection algorithms.

To train YOLOv8 for recognizing and counting penguins in footage captured during the 30th and 31st Bulgarian Antarctic Expedition with drones DJI Phantom 4 Pro PKK and DJI Air 2S, the following steps were executed (*See Figure 1).*

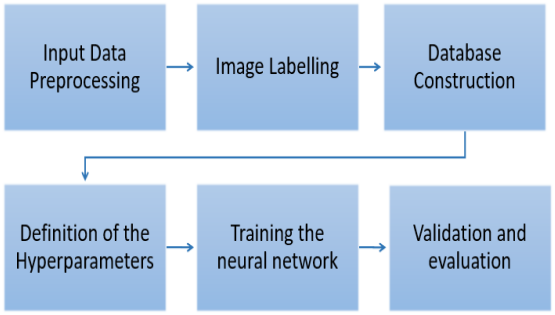

Figure 1. Main steps in proposed approach

2.1. Input Data Processing

During the training of a neural network, selecting the appropriate input data is crucial. The input data is captured on Hannah Point during the 30th and 31st Bulgarian Antarctic Expedition (BAE). Hannah Point is situated on the southern coastline of Livingston Island within the South Shetland Islands, Antarctica. There we can identify tightly clustered breeding colonies of Antarctic Penguins *(Pygoscelis antarcticus)*, making them suitable for drone-based monitoring. In December, they enter the incubation period. The beginning of the nesting period is the optimal time for monitoring these species. Images from this typically exhibit higher contrast due to the reduced presence of guano around the penguins and less blurriness, as penguins tend to be less active during this stage. These factors enable better differentiation of each penguin from the background *(See Figure 2).*

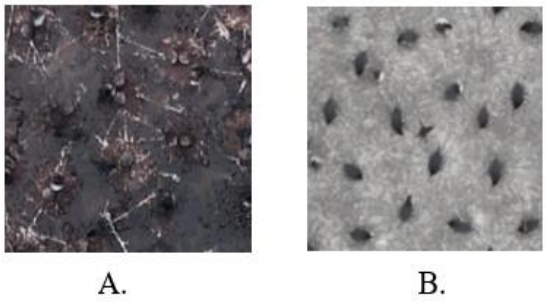

Figure 2. Antarctic Penguin subcolony at Hannah Point, Livingston Island. (A) Image from the early stages of the breeding season (12.12.2022); (B) Image from the advanced stages of breeding season (14.01.2022).

For this study's objectives, the most suitable approach involves training the neural network with images. Given that the available content is in video format, two methods were employed to extract data from the videos.

Direct extraction of single frames from the video material

For this purpose, VLC-software was used, which extracts frames in JPEG format with dimensions of 3840 x 2160 pixels.

Creation of orthomosaic from the provided video recordings

The acquired video recordings undergo photogrammetric processing until an orthomosaic created. The orthomosaics are generated using PIX4D mapper version 4.8.4. The size of each orthomosaic can vary based on the specific terrain covered during the filming.

To ensure optimal performance during the training of the neural network, it's essential that all images are either identical in size or very closely matched. To achieve this, the orthomosaic images are subdivided into smaller sections (referred to as "tiles") to align their sizes closely with the frames extracted from the videos.

2.2. Image Labelling

Following the data processing, we have acquired 587 penguin images with high informativeness and 230 background images that do not feature penguins but are crucial for the training process. All of these extracted images undergo the "Labeling" procedure, which aims to mark and identify each penguin within every image. This task is executed using "LabelImg", which is an image annotation tool designed for labeling bounding boxes around objects in images.

Labeling penguins in the images is a process that demands careful attention, as inaccuracies or omissions in the labels can adversely affect the accuracy of subsequent penguin recognition within the images.

Upon completing this step, the "LabelImg" tool generates a text file for each labeled image. Each text file contains the class of the designated objects (in our case, they belong to the "penguin" class) along with the coordinates defining the rectangular area covering each penguin's location.

2.3. Database Construction

The labeled images need to be split into two distinct sets: a *training set* and a *validation set*. This division is a precautionary measure to prevent "Overfitting," which occurs when the neural network becomes overly specialized in the training data but struggles to accurately generalize to new data.

The training set plays a crucial role during the network's training phase. It allows the algorithm to study and adapt from the data, continuously adjusting and optimizing the neural network's parameters.

On the other hand, the validation set is employed to assess the trained neural network's performance when presented with new data. It serves as a means to measure the final accuracy of the trained algorithm.

The ratio between the training set and validation set data often varies. Given our data volume, the recommended split ratio is 80:20. This implies that 80% of the labeled images are allocated to the training data, while the remaining 20% constitute the validation data. By dividing the input data in this manner, we construct the database as shown in the accompanying Figure 3.

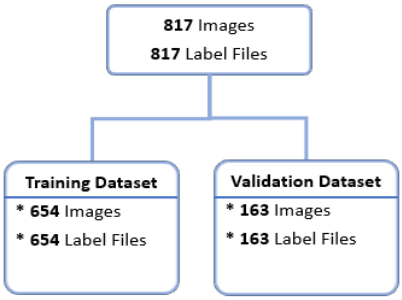

Figure 3. Database structure

2.4. Definition of the Hyperparameters

Before initiating the network training, it's crucial to ensure that the network parameters are appropriately configured to align with both the input data and the computing hardware employed for this procedure. This alignment is essential to enhance the model's performance, speed, and accuracy when identifying penguins in images.

Following a series of experiments, the subsequent training parameters were selected to augment the precision of automatic penguin recognition in images (refer Table 1 for details).

YOLOv8 provides a range of pre-trained models tailored for various tasks and performance requirements, simplifying the selection of the most suitable model for your specific use case. After conducting numerous experiments, the model that achieved the highest accuracy is "YoloV8m-P2." This model builds upon the base YoloV8m by adding a secondary head, "P2," to enhance the detection of small objects, which closely resemble penguins in UAV images

Table 1. Training Hyperparameters

Parameter	Value
Model	YoloV8m-P2
Epochs	100
Optimizer	Adam
Image size	2160
Batch Size	1
Initial learning rate	0,001
Final learning rate	0.0005

The term **"Epoch"** refers to the number of times the entire dataset passes through the neural network during training. Too few epochs result in underfitting because the network hasn't learned adequately. Conversely, an excessive number of epochs can lead to overfitting, where the model excels at pre-

dicting existing data but struggles with new, unseen images. The ideal number of epochs depends on the database size, and in this case, it is set at 100 for optimal results.

The **optimizer** plays a pivotal role in modifying the learning rate and neural network weights to minimize the loss function. Selecting the right optimizer is crucial for achieving the highest possible accuracy or minimum loss. Among the eight available optimizers (SGD, Adam, Adamax, AdamW, NAdam, RAdam, RMSProp), "Adam" best suits our requirements.

The **size of input images** significantly impacts the process. Mismatching input image size with network requirements can result in image quality deterioration, leading to reduced recognition accuracy and training success. Conversely, opting for excessively large image sizes may cause slow learning and potential memory issues. To address this, the "batch size" parameter can be adjusted to balance image quality and processing speed.

Another crucial hyperparameter is the **learning rate**, controlling the model's step size in achieving minimum loss and maximum accuracy. A higher learning rate accelerates learning but risks overfitting, while a lower rate increases the likelihood of proper network training. To strike a balance, a lower learning rate can be compensated by a larger number of epochs.

2.5. Training the neural network

A Windows 11-powered machine was employed to conduct the network training. The experiments utilized an NVIDIA GeForce RTX 3060 Ti graphics card with an 8 GB memory capacity. Details of the training configuration and settings are outlined in the provided table. Considering these factors, the training process concluded in 6 hours and 27 minutes.

Following the training process, several graphs are generated to depict the training's progress and its effectiveness. Among these graphs is the F1-confidence curve (See Figure 4), which is a machine learning evaluation metric used to assess a model's accuracy. It combines precision and recall scores to provide an overall measure of a model's performance, ranging from 0 to 1, where 1 signifies optimal performance. The mathematical formula for calculating the F1 score is given below (See Equation (1)).

$$F1\ score = 2 * \frac{Precision * Recall}{Precision + Recall} \quad (1)$$

,where

$$\text{Precision} = \frac{TP}{TP + FP}$$

$$\text{Recall} = \frac{TP}{TP + FN}$$

The trend in Figure 4 indicates that the F1-curve has consistently improved throughout the training process, affirming that the training has been effective, ultimately resulting in the model achieving a 97% accuracy on the provided dataset.

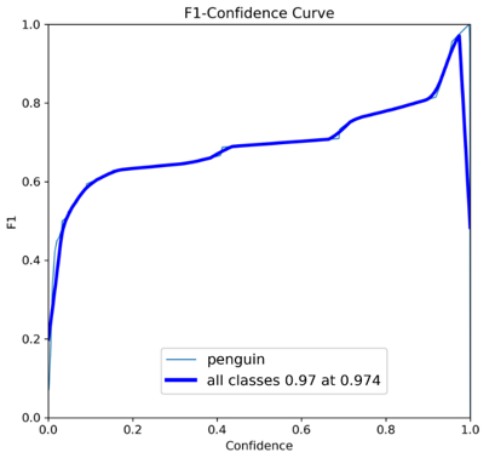

Figure 4. F1-Confidence score during training

2.6. Validation and evaluation

Validation phase takes place after the neural network has completed its training. During this stage the model is assessed using a predefined validation set to gauge its accuracy and overall performance. This mode is frequently employed to fine-tune the model's hyperparameters for performance enhancement.

During the research process, several key challenges were identified:

- distinguishing stones from penguins in the images;
- difficulty in recognizing nearby penguins within a colony;
- limited accuracy in detecting penguins across the entire orthomosaic;

Following a series of experiments and the establishment of optimal network training parameters, the following outcomes were achieved:

- a high penguin detection accuracy in images, reaching up to 97%;
- improved ability to differentiate between rocks and penguins;
- enhanced recognition of nearby penguins within the images;

Examples of output from the trained neural network, proving that main key challenges are overcome are shown at Fig.5 and Fig.6.

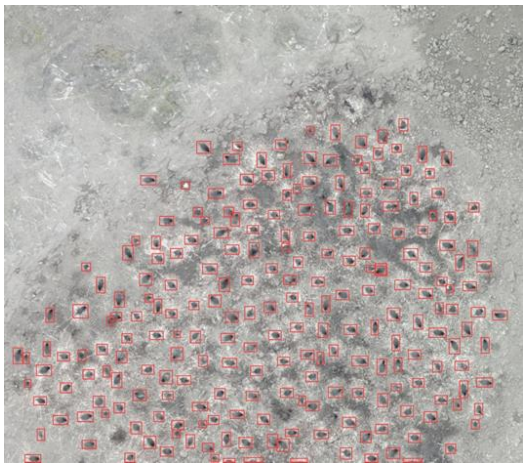

Figure 5. Outlined in red penguins are detected and differentiated from the surrounding terrain

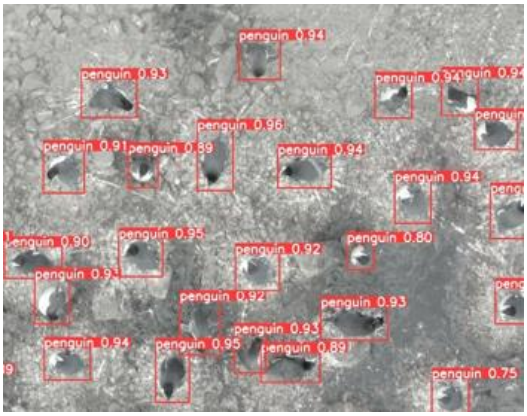

Figure 6. The detection probability annotations of more than 0,8 signifies the model's high accuracy

3. FUTURE RESEARCH

In our future related research, we plan to enhance our methodology for penguin counting using UAV images. We have identified several strategies that could contribute to this improvement:

1) Pre-processing the input images would help to increase the object detection accuracy. Some effective image preprocessing methods, such as adaptive contrast enhancement and image sharpening, can help achieve this goal. This approach would enable us to detect penguins not only during their nesting period but also address other challenges related to image quality.

2) Identifying small objects like penguins within large images, such as orthomosaics, poses a considerable challenge. One potential solution to address this issue is to employ the subsequent algorithm (See Figure 7) to reprocess an orthomosaic where it is fed to an already trained network to detect and count the penguins within it, while preserving the location information for each pixel.

4. CONCLUSION

The analyses, based on data from the 30th And 31st Bulgarian Antarctic Expeditions, showed a 97% accuracy in penguin detection by employing the YOLOv8 deep neural network architecture. It addresses challenges like distinguishing penguins from rocks and detecting them from large orthomosaic images. Future work aims to refine the methodology, particularly in preprocessing and orthomosaic reprocessing, to improve penguin detection beyond breeding season.

Overall, this study represents a significant advancement in penguin monitoring, with potential applications in broader biodiversity and ecological research.

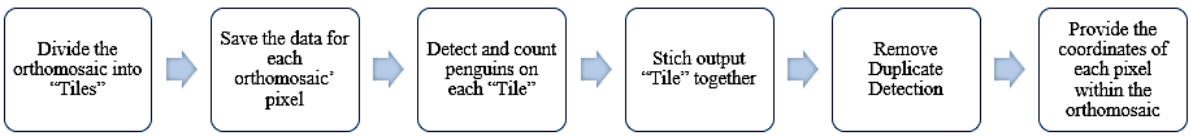

Figure 7. Proposed algorithm for preserving orthomosaic information, while counting penguins with deep neural network

5. ACKNOWLEDGMENTS

The present study has been carried out within the project "Remote multi-parametric monitoring of representative elements of biodiversity on Livingston Island, Antarctica" funded by the Bulgarian Ministry of Education and Science through the National Centre for Polar Studies and Sofia University "St. Kliment Ohridski" in the frame of the National Programme for Polar Studies 2017- 2021, grant No. 80-25- 67/03.08.2021

References

[1] C Witharana, H Lynch, "An Object-Based Image Analysis Approach for Detecting Penguin Guano in Very High Spatial Resolution Satellite Images. Remote Sens", Vol. 8(5). (2016).

[2] G. P. Rush, L. E. Clarke, M. Stone, and M. J. Wood, "Can drones count gulls? Minimal disturbance and semiautomated image processing with an unmanned aerial vehicle for colony-nesting seabirds," Ecology and evolution, vol. 8, no. 24, pp. 12 322–12 334, (2018).

[3] C.M. Waluda, M.J.Dunn, M.L. Curtis, et al. "Assessing penguin colony size and distribution using digital mapping and satellite remote sensing", Polar Biol 37, pp 1849–1855, (2014).

[4] H. J. Lynch, R. Naveen, P. N. Trathan, W. F. Fagan, "Spatially integrated assessment reveals widespread changes in penguin populations on the Antarctic Peninsula", Ecology 93, pp1367–1377, (2012).

[5] J. Linchant, J. Lisein, J. Semeki, P. Lejeune, C. Vermeulen, "Are unmanned aerial systems the future of wildlife monitoring? A review of accomplishments and challenges", Mammal Rev. 45, pp 239–252, (2015).

[6] J. C. Hodgson, R. Mott, S. M. Baylis, T. T. Pham, S. Wotherspoon, A. D. Kilpatrick, R. R. Segaran, I. Reid, A. Terauds, L. P. Koh, "Drones count wildlife more accurately and precisely than humans", Methods Ecol. Evol. 9, pp1160–1167, (2018).

[7] C. Arteta, V. S. Lempitsky, A.Zisserman, "Counting in the Wild", ECCV (7), pp 483-498, (2016).

[8] Y Qian, GRW Humphries, PN Trathan, A Lowther, CR Donovan, "Counting animals in aerial images with a density map estimation model", Ecol Evol (2023).

[9] T. -Y. Lin, P. Goyal, R. Girshick, K. He and P. Dollár, "Focal Loss for Dense Object Detection", IEEE Transactions on Pattern Analysis and Machine Intelligence, vol. 42, no. 2, pp. 318-327, (2020).

[10] K. He, X. Zhang, Sh. Ren, J. Sun ,"Deep Residual Learning for Image Recognition." IEEE Conference on Computer Vision and Pattern Recognition (CVPR), pp 770-778. (2016).

[11] Y. Liu, V.Shah, A.Borowocz et al, "Towards Efficient Machine Learning Methods for Penguin Counting in Unmanned Aerial System Imagery", IEEE/OES Autonomous Underwater Vehicles Symposium (AUV), St. Johns, NL, Canada, pp 1-7, (2020).

[12] B.Xu, W. Wang, G. Falzon, P. Kwan, L. Guo, G. Chen, A. Tait, D. Schneider, "Automated cattle counting using Mask R-CNN in quadcopter vision system," Comput. Electron. Agric., vol. 171, no. 105300, pp. 1–12, (2020).

[13] J. Peng, D. Wang, X. Liao, Q. Shao, Z. Sun, H. Yue, H. Ye, "Wild animal survey using UAS imagery and deep learning: modifed Faster R-CNN for kiang detection in Tibetan Plateau", ISPRS J. Photogramm. Remote Sens. 169, pp 364–376 (2020).

[14] C.J. Torney, D.J. Lloyd-Jones, M. Chevallier, D.C. Moyer, H.T. Maliti, M. Mwita, E.M. Kohi, G.C. Hopcraft, "A comparison of deep learning and citizen science techniques for counting wildlife in aerial survey images", Methods in Ecology and Evolution, 10(6), pp. 779-787, (2019).

[15] J Wu, W. Xu, J. He, M. Lan, "YOLO for Penguin Detection and Counting Based on Remote Sensing Images", Remote Sens., no. 10, (2023).

[16] T. Badhe, J. Borde, B. Waghmare, V. Thakur, A. Chaudhari, "Study of Deep Learning Algorithms to Identify and Detect Endangered Species of Animals", INTERNATIONAL JOURNAL OF ENGINEERING RESEARCH & TECHNOLOGY (IJERT) Volume 11, Issue 01 (2022).

[17] M. Ponika, K. Jahnavi, P. S. V. S. Sridhar, K. Veena, "Developing a YOLO based Object Detection Application using OpenCV," 7th International Conference on Computing Methodologies and Communication (ICCMC), Erode, India, 2023, pp. 662-668,(2023).

[18] MT Pham, L Courtrai, C Friguet, S Lefèvre, A Baussard,"YOLO-Fine: One-Stage Detector of Small Objects Under Various Backgrounds in Remote Sensing Images", Remote Sensing, 12 (15), pp.2501; (2020).

ARCHITECTURAL DESIGN OF A SMART HOME: IMPROVING COMFORT, SAFETY AND ENERGY EFFICIENCY FOR PEOPLE WITH DISABILITIES

Grebnev Y.V.

St. Petersburg State University
yaroslav.grebnev@gmail.com

I. Soloviev

Saint-Petersburg State University
i.soloviev@spbu.ru

Abstract

This paper is devoted to the development of scientific methods for monitoring human behavior in a smart home system and its adaptation for residents with disabilities.

The paper discusses the key components and functionalities of smart home architecture, including sensor systems, actuators, data processing, and user interfaces. The study concludes by highlighting the importance of user-centered technologies and continuous research in developing robust and scalable architectures for smart homes.

1. INTRODUCTION

With the development of technology and the emergence of new data collection methods, it has become possible to create effective behavioral monitoring systems. In this article we look at two main approaches: video-based behavioral monitoring and sensor-based behavioral monitoring. Each approach has its own advantages and limitations.

Video-based behavioral monitoring is based on the use of video cameras for observation and analyzing the object behavior. Video data can be processed by various computer algorithms and machine learning techniques to recognize and analyze different aspects of behavior.

This approach can be applied to analyse the behavior of people, animals, vehicles and other objects. In addition, video monitoring can provide detailed behavioral information such as movements, postures, gestures and facial expressions.

At the same time, it requires cameras and the infrastructure for recording and storage video data. Note that the effectiveness of this approach may be reduced in environments with limited lighting or interference.

The second approach is behavioral monitoring using portable devices. Portable devices such as accelerometers and gyroscopes, electrocardiographs provide real-time behavioral monitoring capabilities. Tracking the current state of an individual within the home allows monitoring the duration of each activity, and thus maintaining a healthy rhythm of life (by personal choice or doctor's recommendation). One may track heart rate, level of mobility, circadian rhythms [4] and help lonely people to monitor their current state, calling emergency services if necessary.

Location-based behavioral monitoring uses global positioning systems (GPS) and other technologies to track an object's movements and its interaction with the environment.

Behavioral monitoring based on non-intrusive sensors such as thermal imaging cameras, microphones and light sensors can track behavior without direct contact with the subject. They can be used to analyze motional state, sleep, noise levels and other aspects of the environment.

Developing a methodology for creating smart home systems for people with disabilities is an urgent scientific and practical challenge.

2. EXISTING SOLUTIONS

Over the last decade, domestic and foreign researchers have made significant efforts to improve activity recognition methods in various habitats [1-7].

Existing works mainly focus on the technical details of human activity recognition both from stationary sensors, including video recognition, and wearable

sensors, smart watches and fitness bracelets. In the works [8-11] appropriate data collection methods are described and compared. Machine learning algorithms and the most appropriate activity recognition metrics are applied.

Stationary and CCTV sensors may be inconvenient and violating privacy [12]. When non-violating sensors are used, accuracy of single resident activity recognition is not high enough. The research of algorithms for multiple resident activity recognition is at an early stage, and research of anomalous activity recognition is still rare [13].

In [14] the authors developed approaches to human health monitoring, analyzed statistics of the change in the number of requests for help depending on age, and made assumptions about the possible applicability of electronic tags on clothes.

The increased attention to the task of tracking human activity and life support also indicates the need to implement systems for monitoring human activity in the environment in real time, accompanied by control of the duration of actions. Such a solution allows combining results of technical activity detection with practical applications of population monitoring.

In the field of video-based behavioural monitoring the application of deep learning and neural networks allows achieving higher accuracy in the recognition and classification of actions and object behaviour. One of the active research areas is real-time analysis of human behaviour for security, anomaly detection and event prediction.

The field of sensor-based behaviour monitoring use smart watches, fitness bracelets and other wearable technologies. These devices are becoming increasingly accurate and multifunctional. Research is also focused both on developing new types of sensors with higher accuracy and reliability, and integrating different types of sensors to provide better information about the behaviour of objects.

A key area for improving Smart Home technologies is the combined use of video-based behavioural monitoring and portable wearable sensors. Integrating data from different sources can provide more complete and accurate information about the behaviour of objects.

Thus, this issue has been investigated by the scientific community in a fragmentary way and currently there is no methodology for designing a system of smart home for sedentary citizens and additional and in-depth analysis of their activity.

3. METHODS FOR MONITORING AND RECOGNITION OF ACTIVITY

Currently, there are various approaches to solve behavioural monitoring tasks of Smart Home occupants. In [15-18], five types of home activities registered by a wrist fitness bracelet were recognized: sitting, standing, doing household chores, low-activity exercise and high-activity exercise. The classification accuracy of the random forest and support vector methods were 89.2% and 85.6%, respectively. Interestingly, the inclusion of heart rate data improved the accuracy of recognizing the activity level of exercise on the exercise bike by 8%.

In the study [19] the authors applied a hierarchical approach with a modified support vector method to data obtained from a smart watch equipped with a heart rate sensor and accelerometer. The classifier consisted of two levels: the top level defined the general state (static or in motion) and the next level refined the obtained value (sitting or standing, walking or running). The accuracy of predicting the type of human activity using data from 5 to 50 hertz was more than 99%.

The study [20] used naive Bayesian classifiers and K-nearest neighbours method to identify 13 human activities such as walking, sitting, standing, running, cycling, climbing stairs, descending stairs, typing, writing, drinking beverages, talking, smoking and eating. The authors obtained high classification accuracy with an F-measure approaching 1 for the recognized activities. To improve the recognition process and divide the activity types into two categories, a hierarchical classifier was used. The authors suggest that activity type recognition could be used to limit unhealthy activity and warn of insufficient physical activity or skipping meals.

The accuracy of activity recognition using wearable devices can vary depending on the set of sensors, the number of classes to be recognized and the purpose of using the obtained human activity information.

4. ALGORITHMS FOR ACTIVITY RECOGNITION

Behavior recognition is an important task in computer vision and natural language processing. In recent years, many machine learning, logical rea-

soning and ontology techniques have been applied to this task.

4.1. Machine learning methods

Machine learning methods allow us to extract information from datasets automatically and build models capable of classifying and predicting behaviour. One of the most common is multilayer neural network.

This model, also known as a multilayer perseptron classifier [21], uses a set of programmable neurons organized into input and output layers and one or more hidden layers, to perform classification tasks.

Each neuron is activated using an activation function and linked to neurons of the next layer with a certain weight. The link weights are optimized over several training iterations by applying a special algorithm called decision function.

Error back propagation algorithm, which is one of the popular methods for training multilayer neural networks, is also widely used [22].

Advantages of multilayer neural networks are the possibility of application to a variety of tasks regardless of data structure and high classification rate after the training is complete.

However, multilayer neural networks require high computational resource when training the model. Optimal classification results can be achieved with a properly selected data structure.

4.2. Typical static classification method

It is based on using various features extracted from the data and building a model that can classify new examples based on these features. Examples of such features could be statistical motion characteristics, distribution of colour features or texture features.

4.3. Support vector method

The support vector method [23] uses hyperplanes to optimally divide the sample into classes and maximize the distance between classes. The hyperplane defined by the equation $(w, x) - b = 0$ is the solution of the problem. For each training sample element, the indentation value from the hyperplane is used and adjusted to minimize classification errors, especially in the case of linearly non-separable samples.

When dealing with more than two classes, the support vector method offers two approaches:

"One-vs-rest": p classifiers are constructed where each class is separated from the others. Then, for each feature, the classifier that gives the best value of the target function for that feature is determined.

"One versus one": for each pair of classes, a different classifier is trained (p(p-1)/2 combinations). The class membership of an object is determined by a majority vote of the classifiers.

The support vector method is sensitive to outliers, as they can become support elements and affect the construction of the hyperplane. In addition, this method does not automatically select the most important features, which may reduce the classification quality [24]. However, when maximizing the width of the separating band, the support vector method can provide more confident classification with good data separability compared to other machine learning algorithms [25].

4.4. K nearest neighbours method

The K nearest neighbors method [26] is used for classification based on the representation of the training sample as points in a metric space. The classification of an object is determined by the class to which most of its nearest neighbours belong. In weighted neighbour selection, the distance of the training sample points from the recognized object is also considered and the points are ordered by decreasing distance.

To optimize the search k-dimensional trees [27], or thinning the training sample space and removing similar objects are used.

Increasing K reduces the effect of noise on the classification result. The advantage of the method is that there is no need for a model training phase, which allows adding new instances to the training sample without a complete redesign of the model.

However, in some cases the application of this method can be difficult due to the choice of an appropriate metric. Euclidean metric is not always sufficient to compute distances in some problems. Incorrect choice of metric can increase sensitivity to irrelevant parameters and degrade the quality of recognition [28].

4.5. Hidden Markov model

A Hidden Markov Model (HMM) is a statistical model that is used to analyze time sequences. It **is a** network of states in which each state represents a probability distribution over the observed data.

HMM can be used for modeling various aspects of human or object behavior. Each state corresponds to a particular type of behavior, and the features extracted from the data are represented as observations for each state. This allows the transitions between states to be modelled, as well as the probabilities of generating the observed features for each state.

HMM is thus a powerful tool for analyzing complex temporal sequences.

4.6. Conditional random field

Conditional Random Field (CRF) is a statistical model used to model dependencies between labels in a sequence of data. CRF can be applied to model dependencies between classes of behaviour and features extracted from the data. CRF allows contextual information to be taken into account when deciding how to classify behaviour.

It is a probabilistic graphical model for labelling and segmentation of sequential data. We propose to apply CRF and its extended models to improve activity recognition algorithms in smart homes in AMI environments, where such application of CRF is rare.

In [29], an activity recognition system incorporating the linear chain conditional random field (LCRF) approach is developed. The LCRF is improved by combining features that consider state changes of multiple sensors associated with the same type of activity as a single object of observation. Experiments show that compared to Naive Bayes (NB) and Hidden Markov Model (HMM) LCRF provides higher recognition accuracy for most activities.

To model the relationships between activities and their subspecies latent-dynamic conditional random field (LDCRF) approach is proposed. Multiclassification metrics are used to evaluate the validity of LDCRF and are compared with SVM), HMM, LCRF and related HCRFs. Experimental results show that the LDCRF-based activity recognition method outperforms other methods.

A two-stage hidden Markov model (TSM-HMM) and a two-stage LCRF (TSM-LCRF) are also introduced, which define a combined set of labels and states to represent fixed a priori knowledge in a multi-residue environment. Experiments with multi-resident activity data demonstrate the superiority of the two-stage method over existing multi-resident activity recognition methods.

HCRF and LCRF based approaches are proposed to recognize three types of abnormal activity typical for smart nursing homes: "forgotten", "new activity" and "slow activity". It is shown that the HCRF-based method outperforms the feature vector-based method for "forgotten" and "new activity", while the LCRF-based one demonstrates accurate recognition of "slow activity".

4.7. Clustering method

It can be used in behaviour recognition tasks to group similar examples of data into clusters, for example, to identify different driving styles or to classify different types of animal behavior. Once the data have been grouped, more detailed analysis can be performed on each cluster to provide more detailed information about the behavior.

4.8. Naive Bayesian classifier method

It is based on Bayes' theorem and the assumption about data independence [29]. The classifier uses small training samples and has high classification accuracy and speed compared to more sophisticated methods [30]. However, it assumes pairwise independence of the parameters, which may be inconvenient restriction.

4.9. AdaBoost method

AdaBoost is an adaptive machine learning algorithm that uses the boosting method [31]. In the process, it creates copies of the base classifiers with weight adjustments, focusing on elements that were incorrectly classified by previous classifiers.

The algorithm is sensitive to noise, especially when limiting the number of base classifiers. The lack of limitation may lead to increasing the memory used and classification time [32]. The advantages are versatility, the ability to significantly improve the quality of the underlying algorithms with a large amount of training data and a small number of adjustable parameters.

4.10. Hierarchical classification

Hierarchical classification [33] extends basic machine learning methods by organizing recognition classes into a hierarchical structure, such as a tree or a directed oriented graph.

Main models of hierarchical classification are:

- local classifiers for each vertex. They are binary classifiers that recognize individual classes.

- local classifiers for parent nodes. They recognize derived classes for each parent node. The first layers recognize the basic properties of an object, which are successively refined in subsequent layers.
- local layer classifiers. implement classifiers for one or more layers of the graph. This approach is used in tasks where an object may be assigned multiple classes at each layer.
- global classifier (Big-Bang method). A single classifier that recognizes all classes. This method is applied in the tasks where the result of recognition can be a label not only in the final, but also in the parent vertex. This method gives better memory utilization and faster classification compared to hierarchical classification methods that use sets of classifiers.

4.11. Random forest

A random forest [34] is the algorithm that combines multiple decision trees. In classification tasks, each tree assigns a class label to an object in the leaves or indicates the probability of belonging to multiple classes.

Each decision tree is constructed independently on randomly generated subsamples from the training data. When classifying an object, the decision to assign a class label to the object is made by majority vote of the trees. In [35] it is shown that optimal recognition quality, classification speed and efficient memory usage are achieved when the number of trees ranges from 64 to 128.

Random forest may be applied in various subject areas. They have low sensitivity to outliers in the training sample, low risk of model overfitting [36], the ability of parallel computing of recognition by using individual decision trees, and performance with a large number of features and classes.

However, the random forest algorithm has drawbacks. In particular, it requires a significant amount of memory to store all trees, recognition time can increase significantly when the number of trees or tree depth increases, and the algorithm can be sensitive to categorical variables [37].

5. CONCLUSION

Research in behavior recognition algorithms continues to evolve and the combination of machine learning, logical reasoning and ontology techniques represents a promising approach.

Further research in this area will contribute to the development of more intelligent and adaptive systems that can analyze and understand human behavior with greater accuracy and efficiency. These models can then be integrated with logical rules to account for contextual constraints and additional knowledge about behavior. The use of ontologies can help formalize and structure knowledge about typical behavioral scenarios and enable more flexible and scalable behavioral modelling.

In addition, deep learning methods have recently been actively explored for automatically learning hierarchical feature representations and processing large amounts of data.

However, despite significant advances in research on behavior recognition algorithms, there are still some challenges.

1.Handling temporal data and modelling the dynamics of object behavior. This requires the development of algorithms that can account for changes over time and predict future actions.

2. Ethical and privacy issues associated with behavioral analysis need to be considered.

The combination of machine learning, logical reasoning and ontology techniques in behavior recognition algorithm research represents a promising direction for creating more accurate and adaptive systems.

References

[1] Ruchkin V.N., Gromov A.V., Gromov A.A., Kuznetsov A.N., Maslikhov D.A. Control structure of hardware and software "smart home" // Informatics and Applied Mathematics: interuniversity collection of scientific papers. 2017. № 23. C. 103-109

[2] Harke, V. Smart House. Networking of household appliances and communication systems in the living space / W. Harke. - Moscow: Technosphere, 2006. - 288c.

[3] Gaskarov, D.V. Intellectual information systems / D.V. Gaskarov. - Moscow: Vysshaya shkola, 2003. - 432c. - ISBN 5-06-004611-7.

[4] Bogdanov, S.V. Smart house / S.V. Bogdanov. - Saint-Petersburg: Nauka i tekhnika 2005. - 208c.

[5] Concept of the system "Smart House" - [Electronic Resource] - Mode of access. - URL: http://www.ascentis.ru/smart/smtheory/39-smtheorycon.

[6] Gaskarov, D.V. Intellectual information systems / D.V. Gaskarov. - Moscow: Higher School, 2003. - 432c. - ISBN 5-06-004611-7.

[7] Harke, W. Smart House. Networking of household appliances and communication systems in the living space / W. Kharke. - Moscow: Technosphere, 2006. - 288c

[8] Nebogatikov, I. Yu. P. Recognition of human activity by wearable sensors in the task of smart home control // Proceedings of the conference "Information Technologies in Management" - St. Petersburg: JSC "Concern "TsNII "Elektropribor", 2020. - C. 221-224

[9] Tao Tang, Lingxiang Zheng, Shaolin Weng, Ao Peng and Huiru Zheng. Human Activity Recognition with Smart Watch based on H-SVM. International Conference on Frontier Computing. 2018. P. 179-186.

[10] Tao Tang, Lingxiang Zheng, Shaolin Weng, Ao Peng and Huiru Zheng. Human Activity Recognition with Smart Watch based on H-SVM. International Conference on Frontier Computing. 2018. P. 179-186.

[11] Weng S, Xiang L, Tang W, et al. A low power and high accuracy MEMS sensor based activity recognition algorithm[C]//Bioinformatics and Biomedicine (BIBM), 2014 IEEE International Conference on. IEEE, 2014: 33-38.

[12] Anguita D, Ghio A, Oneto L, et al. Human activity recognition on smartphones using a multiclass hardware-friendly support vector machine[M]//Ambient assisted living and home care. Springer Berlin Heidelberg, 2012: 216-223

[13] Nebogatikov I. Y., Soloviev I. P. System for controlling the duration of the occupant's actions in the smart home environment //Modern technologies in the theory and practice of programming. - 2021. - C. 47-48.

[14] Bennett J., Rokas O., Chen L. Healthcare in the smart home: A study of past, present and future //Sustainability. - 2017. - T. 9. - №. 5. - C. 840.

[15] Bannikova, A. S. "Smart House" in Russia: prospects for the development of technological system / A. S. Bannikova, A. S. Krasnoukhov // Young Scientist. - 2016. - №9 - C. 479-482.

[16] Averin, A. I. Intellectual house management "Smart House": / A. I. Averin // European science. -2015. - № 4. - c. 32.

[17] Valiev, S.S. Automation systems of a residential complex / S.S. Valiev, S.V. Krivonogov // Vestnik NSTEI. - 2015 - № 4. - c. 26-29.

[18] Soldatova, O. P. P. Application of convolutional neural network for handwritten digits recognition / O. P. Soldatova, A. A. Garshin // Computer Optics. - 2010. - № 2. - C. 10-26.

[19] Choi S., Kim E., Oh S. Human behaviour prediction for smart homes using deep learning // RO-MAN, 2013 IEEE. 2013. C. 173-179.

[20] Kulkarni S.R., Lugosi G., Venkatesh S.S. Learning pattern classification-a survey // IEEE Transactions on Information Theory. 1998. T. 44. № 6. C. 2178-2206.

[21] Langley P., Simon H.A. Applications of machine learning and rule induction //Communications of the ACM. 1995. T. 38. № 11. C. 54-64

[22] Lin, T. Deep Learning for IoT / T. Lin // Proc. of the 39th International Performance Computing and Communications Conference. - Austin : IEEE, 2020. - P. 1-4. 10.1109/IPCCC50635.2020.9391558.

[23] Chuma, E. L. Internet of Things (IoT) Privacy-Protected, Fall-Detection System for the Elderly Using the Radar Sensors and Deep Learning / E. L. L. Chuma, L. L. B. Roger, G. G. de Oliveira // Proc. Of the International Smart Cities Conference. - Piscataway : IEEE, 2020. P. 1-4. 10. 1109/ISC251055.2020.9239074.

[24] Pirmagomedov, R. Y. About application of neural network methods for prediction of reliability indices of physical channel of passive optical networks / R. Y. Pirmagomedov // Reliability of functioning and information security of telecommunication systems of railway transport : mat-l. of All-Russian scientific and technical internet-conf. - Omsk : Omsk State University of Railway Transport, 2013. - C. 209-216/

[25] Saeed Mehrang, Julia Pietila, Johanna Tolonen, Elina Helander, Holly Jimison, Misha Pavel, Ilkka Korhonen. Human Activity Recognition Using A Single Optical Heart Rate Monitoring Wristband Equipped with Triaxial Accelerometer. EMBEC & NBC 2017. 2017. P. 587-590

[26] Paul Panek, L. Wolfgang, Zagler, Christian Beck, Gottfried Seisenbacher: "Smart Home Applications for the Disabled - Experiences and Perspectives" [Text] // Reprint from EIB Event 2001-Proceedings (2001), PP. [Text] // Reprint from EIB Event 2001-Proceedings (2001), PP. 71-80

[27] Z. Zhao, Q. Zheng, P. Xu, S. T and X. Wu, Object detection with deep learning: A review // IEEE transactions on neural networks and learning systems, vol. 30, no. 11, c. 3212-3232, 2019.

[28] S.V. Bukharin, A.V. Melnikov, D.N. Chernikov. Preliminary clustering of video surveillance means on the basis of non-linear and fuzzy-multiple quality indicators // Bulletin of the Voronezh Institute of the Ministry of Internal Affairs of Russia. - 2018. - № 3. - C. 23-34.

[29] A.A. Gavrishev, V.A. Burmistrov, D.L. Osipov. Assessment of wireless alarm system security from unauthorised access based on the concepts of fuzzy logic // Applied Informatics. - 2015. - T. 10, № 4. - C. 62-69.

[30] Ponce, P Meier, A Méndez, Ji Lawrence Berkeley National Laboratory // Journal Of Cleaner Production. - 2020.P.40

[31] Rychkova, V.A. Reliability of the System "Smart House" as the main criterion of the object functioning efficiency // Vestnik nauki i obrazovanie. - 2019. - № 4-2. - C. 31-34.

[32] Eremenko V.T. Informatics, Computers and Management. - 2017. C. 146-151.

[33] Application of the theory of fuzzy sets to the problem of project portfolio formation.

[34] Berchuk D.Yu., Zhuravlev D.V. Application of fuzzy logic for scenario management of the system "Smart House" // XIX International Scientific and Practical Conference "Modern Engineering and Technology". Section 7: Informatics and management in technical systems. - C. 254-255

[35] A.E. Ermilov, P.V. Misevich. Application of frame model and fuzzy logic in the basis of building tools for automated monitoring systems // Proceedings of R.E. Alekseev NSTU. - 2015. - № 1 (108). - C. 71-76.

AN UNCERTAINTY AND MUTUAL INFORMATION OF ACOUSTIC SIGNALS WITH HIGH DYNAMICS

I. Simeonov

Vasil Levski National Military University, Veliko Tarnovo, Bulgaria
76, Bulgaria Blvd., 5000, Veliko Tarnovo, Bulgaria
Tel. +359 62 618724, Fax. +359 62 618899, E-mail: ivanov_ivan@nvu.bg

Abstract

Estimation of entropy and mutual information associated with a given set of signals is a useful problem in many applications and computationally efficient technics for estimating the level of entropy is needed. In this work some possible ways for signal entropy calculating technics, are outlined.

In the case of the datasets consisting of the raw data and metadata from bell ringing, gunfire and noise recordings the idea of application of entropy-encoding compression algorithms for this purpose was exploited. It was shown that this is useful experimental tool for the recording's entropy and mutual information estimation. The results can be used in various areas of acoustic signal processing.

1. INTRODUCTION

Over the years, many acoustic data, from field experiments, such as noise of natural phenomena, battlefield acoustic, ringing of bells have been collected from team work on interdisciplinary projects. Signal processing of high dynamic range acoustic data in presence of noise was discussed in recent works [1,2,3,4].

An examples of spectral and wavelet analysis of these experimental data and scalogram transformations was regarded in work [1].

One possible direction to apply data mining methods for retrieving useful information using these experimental data are outlined in work [2].

One signal statistics analysis technique for retrieving useful information, based on Shannon entropy and wavelet processing was presented in paper [3]

The ideas of entropy of the signal or signal uncertainty and its measure (bits per signal units) was defined in communication theory.

Brief survey of the literature on the empirical estimation of entropy can be found in Verdú, 2019, see [5]. Entropy and mutual information are useful metrics for quantitative analyses of various signals across the sciences including neuroscience.

2. MUTUAL INFORMATION AND ENTROPY PROPERTIES

Mutual information rigorously quantifies, how much information the value of one variable reveals about the value of another. This has important and well-known consequences in information theory [6].

The mutual information quantifies in „bits“ between two random variables $\boldsymbol{X}$ and $\boldsymbol{Y}$ is defined in terms of their joint probability distribution as $p(\boldsymbol{X},\boldsymbol{Y})$

$$I(\boldsymbol{X},\boldsymbol{Y}) == \int dxdy\, p(x,y) \log_2 \left(\frac{p(x,y)}{p(x)p(y)} \right)$$

and she is intimately connected to the statistical problem of detecting dependencies. [6].

The mutual information I_{XY} measures the statistical dependence by the distance to the independent situation (Cover and Thomas, 2006) given by

$$I_{XY} = \sum_{i,j} p(x_i, y_j) \log_2 \left(\frac{p(x_i, y_j)}{p(x_i)p(y_j)} \right)$$

In case of independency of $\boldsymbol{X}$ and $\boldsymbol{Y}$ $\frac{p(x_i,y_j)}{p(x_i)p(y_j)} = 1$ and then $I_{XY} = 0$, [7]

In other words the mutual information $\mathrm{I}(X;Y)$ or I_{XY} can be written as difference of the entropy $\mathrm{H}(\boldsymbol{X})$ and conditional entropy $\mathrm{H}(\boldsymbol{X}|\boldsymbol{Y})$:

$$I_{XY} = \mathrm{H}(\boldsymbol{X}) - \mathrm{H}(\boldsymbol{X}|\boldsymbol{Y})$$

where

$$\mathrm{H}(\boldsymbol{X}|\boldsymbol{Y}) = \\ = -\sum_j p(y_j) \sum_i p(x_i|y_j) \log_2 p(x_i|y_j)$$

Entropy is a thermodynamics concept that measures the molecular disorder in a closed system. Entropy is an interesting tool for analyzing time series, as it does not consider any constraints on the probability distribution [8].

Shannon entropy is one of the basic measures used for evaluating entropy.

In other side Shannon entropy can be defined with Kullback–Leibler divergence. Some useful properties of Kullback–Leibler divergence was demonstrated in R. Angelova-Slavova's work [9].

For evaluating the complexity of time series other entropy measures have been introduced. For example, the approximate entropy measure introduced by Pincus [10], is widely used in applications.

3. SPECTRAL ENTROPY OF EXPERIMENTAL ACOUSTIC DATA AND APPROXIMATE ENTROPY

The sound picture and noise level is change depending on the local parameters as temperature, wind speed and direction, air pressure and humidity etc. In the next it was made the analysis of a set of experimental data and it was found their spectral entropies.

The raw data – time signals from the blasts from 122 mm 2S1 howitzer and hailstone dropping strikes, [1,3] was exported in MatLab and were analyzed spectral entropy correspondingly.

In the figures 1a), b), c) was shown some time signals from the blasts from 122 mm 2S1 howitzer ("Gvozdika"), together with their spectral entropies.

The signal in Fig. 1 a) with duration of 309sec., includes totally of four "salvo" shots or eight pulses. The second signal, 61sec., is a part from the first and contains two blasts, or four shots (pulses). The third signal is a 2 seconds part clipped from the second, contain only one burst of two pulses.

For all this, the spectral entropies are illustrated on the corresponding figure.

The spectral entropies (in upper part of figure, in red color) was calculated in MatLab as described in [11], i.e.

$$Entropy = \frac{-1}{\log_2(b_2-b_1)} \sum_{k=b_1}^{b_2} s_k \log(s_k) \ ,$$

– s_k is the spectral value at bin k.

– b_1 and b_2 are the band edges, in bins, over which to calculate the spectral entropy.

It can be seen that the presence of a strong energy and noise-like component does not significantly change the spectral entropy picture.

And when we regard the records of noise (in red) of hailstone dropping strikes plus noise of auto alarms, in concrete urban environment May 2013, see [4], see Fig.2a), and zoomed part in Fig.2b), it can see that spectral entropy (in upper part of figure, in blue color) not significantly vary, too.

Approximate entropy

The approximate entropy measure, or Measure of regularity of nonlinear time series was introduced by Pincus [10,13]. In MatLab it is the function Approximate entropy.

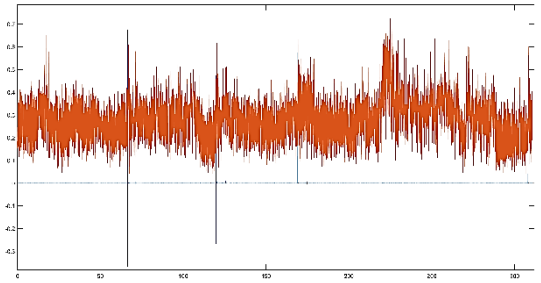

a) 20,3.10^6 samples, fs = 65536 Hz

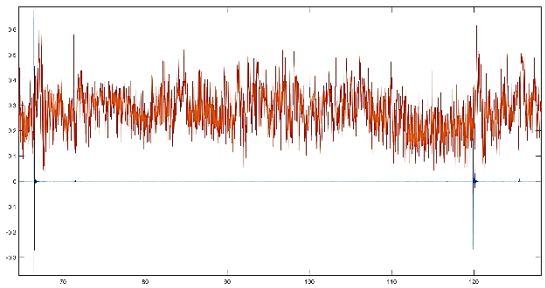

b) 4.10^6 samples

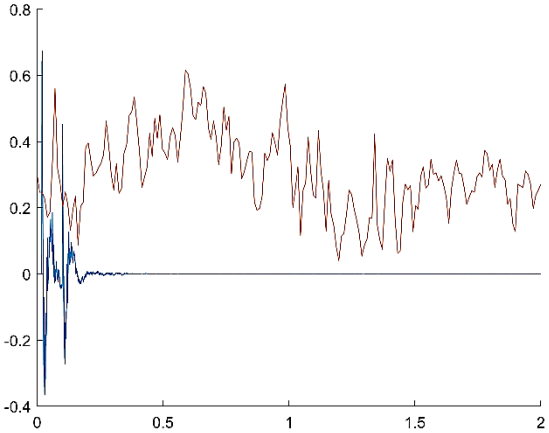

c) 1,31.10^3 samples

Figure 1. Parts from time signal and spectral entropy from the blasts from 2S1 howitzer, a) four blasts 309sec.; b) two blasts 61sec. part from a), see first and second pulse; c) only second blast 0.25sec. of a).

Time series Approximate entropy is a a scalar that measure statistic for the unpredictability of its fluctuations.

The likelihood that similar patterns of observations are not followed by additional similar observations corresponds to a higher value of approximate entropy.

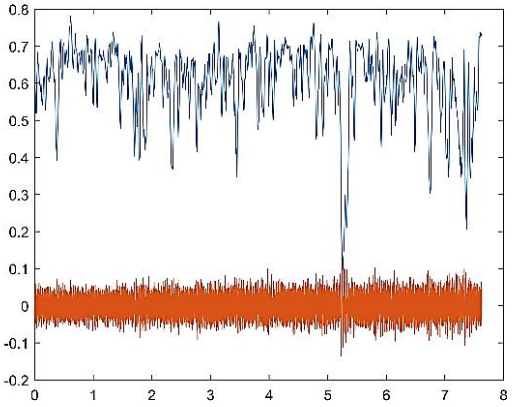

a)

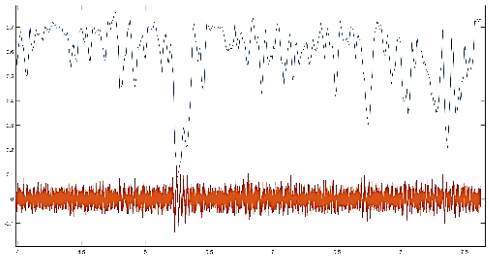

b)

Figure 2. a) Part signal waveform and spectral entropy in time from hail strikes, in V. Tarnovo, BG, urban environments, May 2013,
b) Zoom part of a), Fs=65536Hz. Signal amplitude in red was amplified, 30 dB.

For example, in engineering, the ability to distinguish levels of complexity within data sets is useful to estimate problematic component by studying their vibration and acoustic signals.

Approximate entropy in MatLab is computed as follows:

This function first generates a delayed reconstruction $Y_{1:N}$ for N data points with embedding dimension m, and lag τ . The software then calculates the number of within range points, at point i, given by,

$$N_i = \sum_{i=1, i\neq k}^{N} 1(\|Y_i - Y_k\|_\infty < R)$$

where 1 is the indicator function, and R is the radius of similarity and then calculated as

$$approxEnt = \Phi_m - \Phi_{m+1}$$

where,

$$\Phi_m = (N-m+1)^{-1} \sum_{i=1}^{N-m+1} \log(N_i).$$

The approximate entropies for concrete blast signals, totally 4 examples were calculated and results are shown in Table 1.

One interesting approach used in the field of compressed sensing and that is based on the Shannon's Source Coding Theorem was presented in Zbili and Rama's work in 2021, [12].

Essentially the idea of algorithm that was demonstrate is to saving the examined data i.e. 2D figure as a Portable Network Graphics - PNG, file.

This strategy provides a useful tool for a fast and computationally efficient estimation of how entropy changes through different conditions.

The main limitation of this approach is that the method allows only a relative entropy. It is simple, unbiased and computationally efficient tool and it is a powerful tool to estimation of entropy's and mutual information's levels.

In our case we found the zip rate (saving the examined data in zip), see Table 2 of the same wav files from Table 1.

Table 1

signal name	Samples	waveform	Approximate Entropy
Rec9__2	16384	Fig.1 c) first 1/8 samples	0,16707
Rec9__1	32768	Fig.1 c) first 1/4 samples	0,09554
Rec9__16	65536	Fig.1 c) first 1/2 samples	0,05537
Rec9__	131072	Fig.1 c)	0,03016
Rec9_	4000001	Fig.1 b)	…
Rec9	20367600	Fig.1 a)	…

Table 2

signal name	Samples	waveform	Zip rate
Rec9__2	16384	Fig.1 c) first 1/8 samples	0,2075
Rec9__1	32768	Fig.1 c) first 1/4 samples	0,1343
Rec9__16	65536	Fig.1 c) first 1/2 samples	0,1094
Rec9__	131072	Fig.1 c)	0,0936
Rec9_	4000001	Fig.1 b)	0,11102
Rec9	20367600	Fig.1 a)	0,11696

4. CONCLUSION AND FUTURE RESEARCH

Using spectral entropy can improve the detection of components containing relatively distinct harmonics.

However, for powerful noise pulses this is not so good and will not lead to success. The presence of a strong energy and noise-like component does not significantly change the spectral entropy picture. Or if we were looking for a parameter to recognize this component, energy should be evaluated in addition to entropy.

One interesting approach for relative entropy estimation used in the field of compressed sensing was demonstrated.

ACKNOWLEDGEMENTS

I would also like to thank prof. Tihomir Trifonov from Vasil Levski National Military University for his advice in acoustic signal processing.

I would also like to extend my thanks to doctor Georgi Dimkov from the Institute of mathematics, Bulgarian academy of sciences for their collaboration in projects and for providing the hardware PULSE.

References

[1] Trifonov T., I. Simeonov, N. K. Yordanov Advanced Signal Processing Methods for Analysis of High Dynamic Range Acoustic Phenomena, *Proc. 13th Conference on 'Communications, Electromagnetics and Medical Applications' (CEMA'18)*, Sofia, Bulgaria, 18-20 Oct. 2018, pp. 52-56, ISSN: 1109-1606

[2] Simeonov, T.Trifonov, T. Georgieva-Trifonova, Signal Processing and Storing of High Dynamic Range Acoustic Data for Knowledge Discovery, *Proc. of 14th International Conference on Communications, Electromagnetics and Medical Applications CEMA'19*, Sofia, Bulgaria, October 17th-19th, 2019, pp. 58-62, ISSN: 1314-2100.

[3] Simeonov I., An Analysis of Uncertainty and Statistics of High Dynamic Range Acoustic Signals*, Proc. of 15th International Conference on Communications, Electromagnetics and Medical Applications CEMA'21*, Athens, Greece, October 21st, 2021, pp. 10-14, ISSN: 1314-2100

[4] Ivanov I.S., Hajnal É. Characteristics of Hail Dropping Noise in Urban Environment Journal *"Mathematics, Computer Science and Education"* Vol. 1, No. 1, 2018, pp. 37–43, "St. Cyril and St. Methodius" University of V. Tarnovo, Bulgaria, ISSN: 2603-4670 (Print)

[5] *Verdú*, *S. Empirical estimation of information measures: a literature guide*. *Entropy 2019*, *21*, 720. https://doi.org/10.3390/e210.

[6] Kinney, J. B., & Atwal, G. S. (2014). Equitability, mutual information, and the maximal information coefficient. *Proceedings of the National Academy of Sciences of the United States of America*, 111(9), 3354–3359. https://doi.org/10.1073/pnas.1309933111

[7] Thomas M. Cover and Joy A. Thomas*, Elements of Information Theory*. John Wiley & Sons, Second edition, 2006.

[8] Velichko, A.; Heidari, H. A Method for Estimating the Entropy of Time Series Using Artificial Neural Networks. Entropy 2021, 23, 1432. https://doi.org/10.3390/e23111432

[9] Angelova-Slavova, R.L. *Convergence and applications of the Metropolis - Hastings Algorithm.* Plovdiv: Astarta, 2020. ISBN 978-954-350-284-4 (in Bulgarian)

[10] Pincus, Steven M. Approximate entropy as a measure of system complexity. *Proceedings of the National Academy of Sciences*. 1991 88 (6) 2297-2301; doi:10.1073/pnas.88.6.2297.

[11] Misra, H., S. Ikbal, H. Bourlard, and H. Hermansky. "Spectral Entropy Based Feature for Robust ASR." 2004 *IEEE International Conference on Acoustics, Speech, and Signal Processing.*

[12] Zbili M and Rama S (2021) A Quick and Easy Way to Estimate Entropy and Mutual Information for Neuroscience. Front. Neuroinform. 15:596443. doi: 10.3389/fninf.2021.596443.

[13] Kedadouche M., M. Thomas, A. Tahan, R. Guilbault, Nonlinear Parameters for Monitoring Gear: Comparison Between Lempel-Ziv, Approximate Entropy, and Sample Entropy Complexity, *Shock and Vibration*, vol. 2015, Article ID 959380, 12 pages, 2015. https://doi.org/10.1155/2015/959380

ON THE APPLICATION OF THE GRASSBERGER-PROCACCIA ALGORITHM TO CLASSIFICATION OF QUADCOPTER SOUNDS

Andrei Kadomskii

St. Petersburg State university
st099001@student.spbu.ru

Abstract

Time series are records of various types of signals. They may be investigated by nonlinear dynamics methods – reconstruction of the attractor of the system generating the series. Such an approach allows one to calculate correlation dimension of the attractor of the system under study or to establish that the system does not have any attractor. In this work we apply this method to solve a practical problem of identification a quadcopter according to its acoustic signals.

1. INTRODUCTION

Many applied problems deal with results of observations or measurement. Records of measurement are represented as time series of various type: scalar or vector in dimension, and equidistant and non-equidistant on the length of time interval. Along with traditional methods of time series analysis ([1,2])

the Takens method won wide recognition [5,6]. This method of nonlinear dynamics is based on the topological fact that any smoot manifold with dimension N may be embedded in a Euclid space with dimension 2N+1. Takens proposed the procedure for the reconstruction of attractor using series of observation only for one variable, and proved that the map from initial space to the constructed one is embedding almost always.

The Grassberger-Procaccia algorithm [4], implementing the Takens method, calculates the correlation dimension of the attractor, which is the same for the attractor in the initial space and the space of embedding. It is a time delay method in which from a given scalar time series we form state vectors with a given time delay.

To estimate the embedding dimension, the algorithm sequentially increases the length of state vectors (m), calculate correlation integral and then correlation dimension. The value m (corresponding to 2N+1) beginning from which the stabilization takes place is the dimension of embedding. In other case we cannot interpret the time series as a result of functioning of a dynamical system.

Thus, the Takens method allows one to restore the attractor of the original system in a space of a larger dimension, being we can use observations of changes only in one variable.

It was successfully applied mainly to the analysis of EEG records.[3]

The goal of our work is to implement the Takens method for identification of acoustic signal of quadcopters.

Most of the articles on detecting quadcopters focus on finding them in a videorecord or image. But due to small size of devices, different weather conditions, and the limited camera view, this method not always may be useful.

At the same time, works that focus on sound detection are associated with the creation of spectrograms and training a neural network to detect quadcopters using them. [7]. The main disadvantage of this method is the need for a large amount of data and neural network training, which can have quite high requirements for the device.

2. MAIN NOTIONS

2.1. Data desciption and experimental results

In experiments records with length 1 seconds and the frequency 192000 hz were used; for each quadcopter one record was analyzed.

Each recording was divided into 100 segments, 0.01 seconds each, all parts of the audio recording were analyzed using an algorithm, dimensions were obtained, as well as attractors for each recording.

The experiments involved recordings of three different quadcopters and one small.

CX10:

- Low-power engine.
- Compact size.
- Limited maneuverability and speed.

- Can only be used indoors. Is not a professional quadcopter.

DJI Phantom 3 (P3):

- Powerful motors and the ability to carry a camera.
- Good stability and handling.
- Professional photography and videography.

FPV 250:

- Very powerful and high-speed motors.
- Compact size with an emphasis on aerodynamics and speed.
- Very high maneuverability and speed.

DJI Mavic Pro:

- Same as DJI Phantom 3
- Folds up to a compact appearance

Data were taken from the website hissandroar.com, the recordings were made by professional equipment in close to ideal conditions for flight.

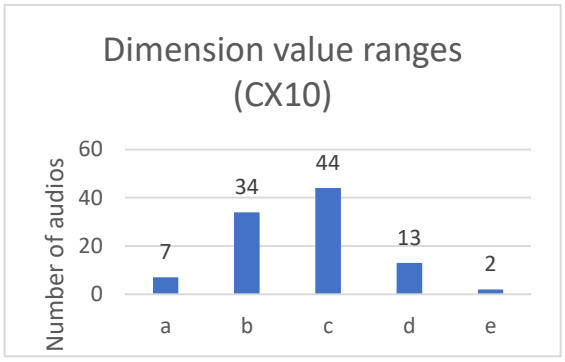

Figure 1. Distribution of obtained dimensions for CX10. a – [0.1,0.2), b – [0.2,0.3), c – [0.3,0.4), d – [0.4,0.5), e – [0.5,0.6]

The CX 10 turned out to have very low dimensions, the main part lies in the range 0.2 – 0.3. (This is a toy quadcopter that was launched from the palm of your hand indoors).

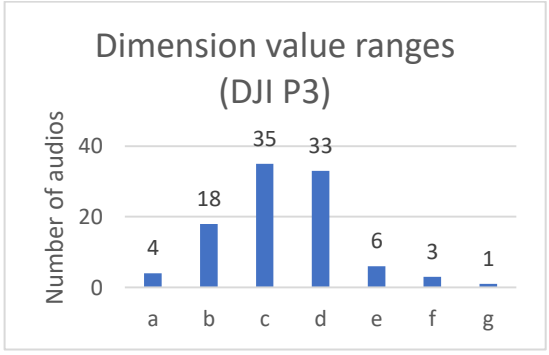

Figure 2. Distribution of obtained dimensions for DJI P3. a – [0.4, 2), b – [2.0,2.1), c – [2.1,2.2), d – [2.2,2.3), e – [2.3,2.4), f – [2.4,2.5), g – [2.5,2.6]

On DJI P3, most of the dimensions turned out to be higher than 2, the main part lies in the range from 2 to 2.3.

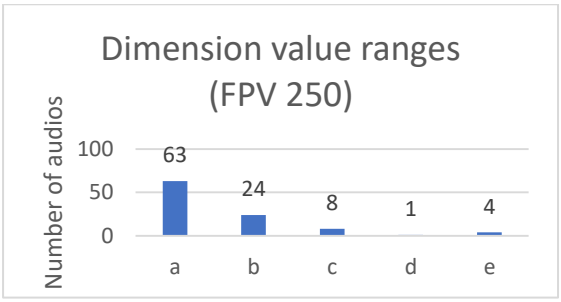

Figure 3. Distribution of obtained dimensions for FPV 250. a – [0.1,1), b – [2.1,2.2), c – [2.2,2.3), d – [2.3,2.4), e – [2.4,2.5)

On the FPV 250, more than half of the values (63) were less than one, but the rest were higher than 2.1.

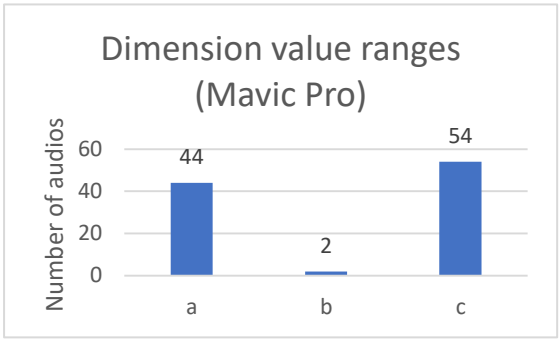

Figure 4. Distribution of obtained dimensions for Mavic Pro. a – [0.1,1), b – [1.0,2.0), c – [2.0,2.1]

On Mavic Pro, most of the values were above 2, although a large number of values were less than 1.

The results of calculation are given in the table 1.

Table 1. Distribution of dimensions

Type of quadcopter	Common interval	Main interval
CX10	[0.1,0.6]	[0.2,0.4]
DJI P3	[0.4,2.6]	[2.1,2.3]
FPV 250	[0.1,1]∪[2.1,2.5]	[0.1,1]
DJI Mavic Pro	[0.1,2.1]	[0.1,1]∪[2,2.1]

Below the examples of images of restored attractors for each quadcopter are given. All attractors are shown in the projection on the plane in axes x(t), x(t+τ), where τ is time delay. In all the experiments this parameter is 1.

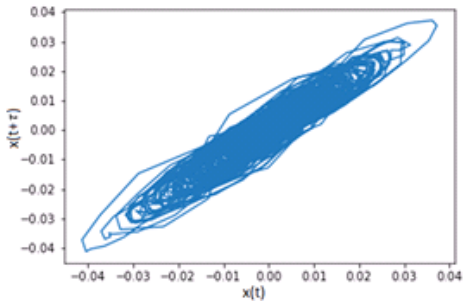

Figure 5. Restored attractor for audio recording with a length of 0.01 s for CX10. Dimension – 0.353

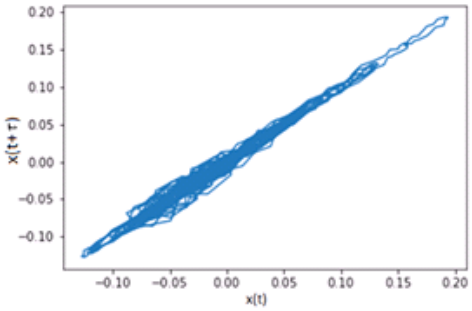

Figure 6. Restored attractor for audio recording with a length of 0.01 s for DJI P3 quadcopter. Dimension – 2.151

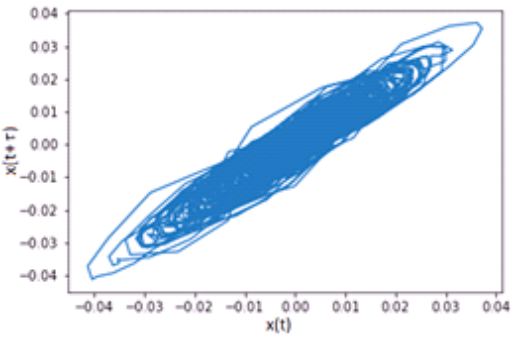

Figure 7. Restored attractor for audio recording with a length of 0.01 s for FPV 250. Dimension – 2.19

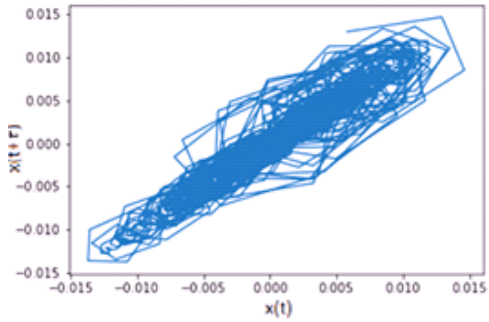

Figure 8. Restored attractor for audio recording with a length of 0.01 s for Mavic Pro. Dimension – 2.019

In the first case the dimension is practically zero, hence we may assume that the system has a point attractor.

For each type of quadcopters we obtained a histogram showing the distribution of correlation dimensions. That means that during 0.01s the process generating the signal may be modeled by different systems, and value of the period of stationarity may be less than 0.01.

3. CONCLUSION

Thus, the application of the Grassberger-Procaccia algorithm for classifying acoustic signals of quadcopters leads to interesting results and can be used for identifying quadcopter models.

Attractors can be used, for example, to train a neural network that will classify quadcopters

This can be proved crucial in various areas, including military, civilian and entertainment spheres, in which the accurate identification of quadcopter models is required.

References

[1] Bezruchko B.P., Smirnov D.A., Mathematical modeling and chaotic time series, 2005 ,izd. GosUNZ "College", Saratov.(in Russian)

[2] Chumak O.V., "Entropies and fractals in data analysis", https://www.researchgate.net/publication/235247584,2022-04-05 (in Russian)

[3] Frank, G.W., Lookman, T., Nerengerg, M.A.H., Essex, C., Lemieux, J. and Blume, W. "Chaotic time series analyses of epileptic seizures". Physica D, 1990, 46: 427-438.

[4] Grassberger P., Procaccia I. "Measuring the strangeness of strange attractors.", Physica D. №1, v.9, 1983. P. 189-208.

[5] Malinezkii G.G.,Potapov A.B., Modern problems of nonlinear dynamics,2002, URSS, Moskva (in Russian)

[6] Takens F., "On the numerical determination of the dimension of an attractor", In: Dynamical systems and bifurcations (Eds. B.L.J. Braaksma, H.W.Broer and F. Takens). Lect. Notes in Math. 1125, Springer, Heidelberg. 1985.

[7] Harini Kolamunna, Thilini Dahanayaka, Junye Li, Suranga Seneviratne, Kanchana Thilakaratne, Albert Y. Zomaya, and Aruna Seneviratne. 2021. DronePrint: Acoustic Signatures for Open-set Drone Detection and Identification with Online Data. Proc. ACM Interact. Mob. Wearable Ubiquitous Technol. 5, 1, Article 20 (March 2021), 31 pages. https://doi.org/10.1145/3448115.

AN APPROACH TO COMPUTING THE GRADIENTS IN FPGA BASED EDGE DETECTION FOCUSED ON ULTIMATE EXECUTION SPEED AND EXACTNESS OF DETECTED CONTOURS

Dimitre Kromichev

Department of Marketing and International Economic Relations, University of Plovdiv
24 Tzar Asen Str, Plovdiv 4000, Bulgaria
dkromichev@yahoo.com

Abstract

Computing the gradients is a critical issue for FPGA based gradient edge detection in terms execution speed and exactness of detected contours. Proposed in this paper a technology for computating the gradients guaranteeing ultimate execution speed on the basis of the detected contours' exact localization and elimination of false positives and false negatives. The experiments conducted in ten Intel (Altera) FPGA families show that the proposed technology of computing the gradients which encompasses all possible three pixel combinations in the detected contours takes only four clock cycles to execute with its accurate mathematics at clock frequencies much higher than the maximum operating frequency of the embedded memory under all test conditions.

1. INTRODUCTION

In FPGA based gradient edge detection, gradients are critical to the localization the detected contours and the quantity of false positives and negatives. Therefore, for demanding applications, needed is a technology focused on detected contours' exactness in terms of their localization and elimination of false positives and negatives. Real time use of FPGA based gradient edge detection requires the solving of the problem of ultimate execution speed with respect to two factors: 1) the maximum operating frequency of embedded memory as the upper limit of clock frequency in FPGA gradient edge detection; 2) the smallest possible number of clock cycles needed to compute the x- and y- gradients by using accurate mathematics, which impacts pipeling efficiency of the entire FPGA gradient edge detection.

There are several groups of approaches to the computation of gradients in FPGA. It is pointed out that traditional Sobel cannot satisfy the demand for accuracy [3][15]. Because Sobel uses a single threshold, most often the result is a discontinuous contour [16][9]. The minimization of false positives and negatives focuses on: four [10][17] and eight directional Sobel [20][21], eight directional Sobel which combines 5x5 mask and a new grey relevancy method [18], weighted least squares method [12], Freichen algorithm [2] improved morphological gradient [19]. The ultimate execution speed in the stages proceeding and following the computation of gradients in FPGA gradient edge detection is addressed by proposing three integer arithmetic algorithms: division [4], square root [5], inverse tangent [6] and by investigating speed capabilities of different adders in FPGA [7][8]. FPGA based Sobel's speed is increased by pipelining in Spartan 3 [11][14] and Spartan 6 [13][1]. All these approaches are based on approcimations. The achieved maximum frequency in Spartan 6 is 63.84 MHz.

This paper proposes an organization of the computation of gradients in FPGA based edge detection focused on ultimate execution speed and exactness of detected contours in terms of localization and elimination of false positives and negatives. The task is to investigate the proposed technology for maximum operating frequency and minimum number of clock cycles in ten Intel (Altera) FPGA families by using the tools Scilab, VHDL Intel (Altera) Quartus, TimeQuest Timing Analyzer, ModelSim. The analyses and conclusions are relevant for gray scale images.

2. THE PROPOSED TECHNOLOGY FOR COMPUTING THE GRADIENTS

The proposed technology set as a general goal to define a number of masks used for computing the x- and y-gradients which must encompass all possible arrangments defined by three consecutive pixels in any object boundary in a digital image contour. According to this, the essentials of the proposed technology are: each of the x- and y-gradients is computed on the basis of 19 3x3 masks with each mask being characterized by different

positioning of the positive and negative coefficients. The final values of the x- gradient and the y-gradient are obtained by comparing the values computed with each of the 19 masks as real numbers or zero. The sign of the greatest value is retained as a separate entity and sent to the next module of the corresponding FPGA gradient based edge detection method for further processing.

3. THE ORGANIZATION OF FPGA BASED COMPUTATION OF THE GRADIENTS FOCUSED ON ULTIMATE EXECUTION SPEED

Computing the gradients is a square neighbourhood operation which provides values for the next stages in an FPGA based gradient edge detection method. Hence, the organization of computations must define:

- Maximum operating frequency of gradients computations $F_{max}(Grad)$ must be related to the maximum operating frequency of embedded memory $F_{max}(embeddedMem)$ by the inequality

$$F_{max}(Grad) > F_{max}(embeddedMem) \quad (1)$$

- Minimum number of clock cycles of gradients computations $nTclk_{min}(Grad)$ must be equal to 4 under all test conditions.
- Technology of dealing with the negative integers must satisfy

for $n \in N, m \in N, n < m$

$$n - m = |Rsub| \in N = m - n = Rsub \in N \quad +(-)$$
$$m - n = Rsub \in N = n - m = |Rsub| \in N \quad +(+). \quad (2)$$

where

$Rsub$ denotes the subtraction result,

$(-)$ denotes that the sign of $Rsub$ is negative,

$(+)$ denotes that the sign of $Rsub$ is positive.

The integer arithmetic of gradients computation includes:

- Division. The dividend is within $[0,2^{10}-4]$. The divider is a constant: 2^2. To divide, right shift $>> 2$ is emulated by using bit slicing. The quotient's maximum value is 2^8-1.
- Multiplication. The multiplicand is within $[0,2^8-1]$. The multiplier is 2. To multiply in FPGA using the hardware description language, operation $<< 1$ is emulated.
- Addition. There are two consecutive additions. They must be executed within two separate clock cycles. On that basis, addition #1 uses addends which are within $[0,2^8-1]$. The sum resulting from addition #1 and the product resulting from << 1 operation are the addends in addition #2. Thus, both inputs of adder #2 are within $[0,2^9-2]$.
- Subtraction. Both the minuend and the subtrahend are within $[0,2^{10}-4]$. This is the arithmetic which produces the deepest logic in gradients computations.
- Comparison: $>0/=0$. Comparison follows the addition of positive and negative integers. Thus, on the basis of subtraction results, $Rsub>0$ and $Rsub = 0$ require only checking for equality to 0 and the sign bit of the differences.

Gradients computation is based on the following requirements:

- All the square neighbourhood pixels must be accessible within a single clock cycle
- All identical computations for x-and y-gradients with all 19 masks must be executed in parallel. Therefore, it is a must that

$$nTclk(x) = nTclk(y) \quad (3)$$

where

$nTclk(x)$ denotes the number of clock cycles taken by the x-gradient,

$nTclk(y)$ denotes the number of clock cycles taken by the y-gradient.

This concept is presented in Figure 1. The separate operations by clock cycles are given in Table 1. Stage III in Table 1 is critical to defining $F_{max}(Grad)$ It is required that

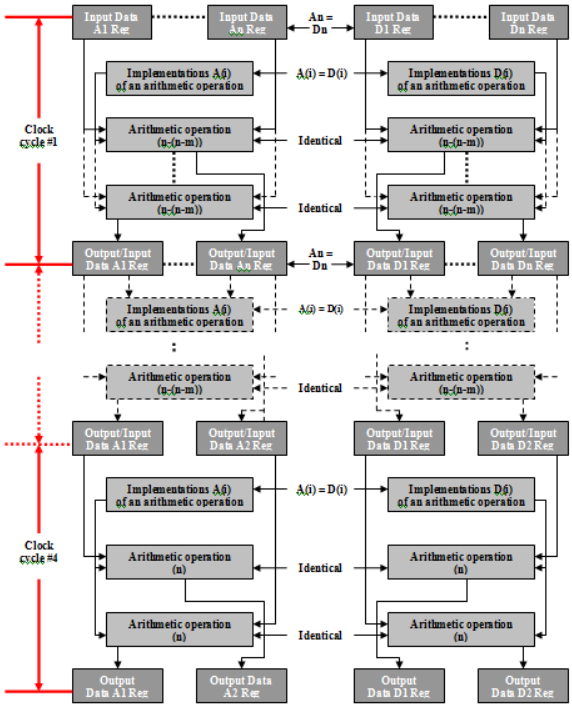

Figure 1. The model of parallel execution of operations

Table 1. Separate arithmetic operations by clock cycles

Stage	x-gradient						y-gradient					
	>> 2	< 1	Add	Sub	>0/ =0	Sign	>> 2	< 1	Add	Sub	>0/ =0	Sign
	Input values ∈ N / =0	Input values ∈ N / =0	Input values ∈ N / =0	Input values ∈ N / =0	Input ∈ Z	+ - 0	Input values ∈ N /=0	Input values ∈ N /=0	Input values ∈ N / =0	Input values ∈ N /=0	Input ∈ Z	+ - 0
I		2	2					2	2			
II			2						2			
III				3	3	1				3	3	1
IV	1						1					

$$Tsub + T > 0/=0 < \frac{1}{F_{max}(Grad)} \qquad (4)$$

where

Tsub denotes the propagation delay of subtractor,

$T > 0/=0$ denotes the propagation delay of comparator.

Negative coefficients have fixed locations: the left column of x-gradient, and the upper row of y-gradient. The negative sign is replaced with the position of negative coefficients. Now all arithmatic operations in Stage I and Stage II are executed using only positive coefficients. When only positive coefficients are used (Figure 10) the sum of results is replaced with subtraction. Hence, all possible variants are based on alternating parallel subtractions. Thus, in Stage III calculated is the dividend for the operation division executed in Stage IV. It can only be a positive integer or 0. Also, in Stage III defined is the sign of the gradients. The information (+)/(-)/(0) is sent to the gradient direction module.

4. FPGA IMPLEMENTATION: FUNCTIONALITY AND RTL DESIGN

Figure 2 presents the functional model in FPGA.

In the 4th clock cycle the accurate values of x- and y-gradients are calculated and the information on the sign of the gradients is sent to gradient magnitude and direction module. Minimum number of clock cycles required to compute a gradient using each of the 19 masks $nTclk_{min}(Grad)$ is 4.

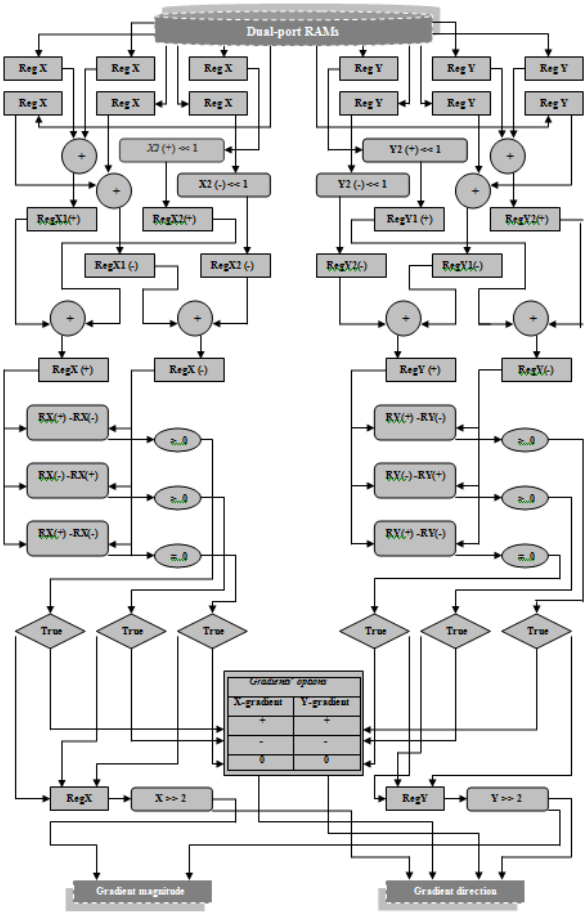

Figure 2. The functional model of gradients computation in FPGA

The RTL design is in Figure 3.

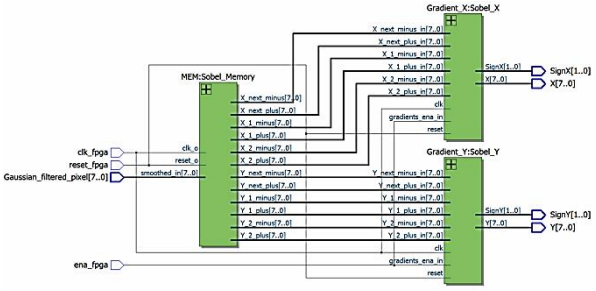

Figure 3. RTL design of gradients computations (Source: (Intel (Altera) Quartus RTL Viewer)

Resource utilization is shown in Table 2.

Table 2. Resource utilization of gradients computation

FPGA family	Logic utilization (in LEs/ ALUTs/ALMs)	Total registers	Total memory bits	Total DSP blocks	Embedded multiplier 9 bit elements
Cyclone	595 (LEs)	-	81920	-	-
Cyclone II	559 (LEs)	315	81920	-	0
Cyclone III	493 (LEs)	362	81920	-	0
Cyclone IV	493 (LEs)	362	81920	-	0
Cyclone V	194 (ALMs)	370	81920	0	-
Stratix	442 (LEs)	412	81920	0	-
Stratix II	348 (ALUTs)	388	81920	0	-
Stratix III	352 (ALUTs)	374	81920	0	-
Stratix IV	358 (ALUTs)	374	81920	0	-
Stratix V	188 (ALMs)	382	81920	0	-

5. INVESTIGATING THE ULTIMATE EXECUTION SPEED OF GRADIENTS COMPUTATIONS IN FPGA

Methodology: the experiments are conducted by using all values which can be inputs to the gradients computation module of FPGA based gradient edge detection. The obtained investigation results for the ultimate execution speed are presented in Table 3.

Table 3. Obtained results for the ultimate execution speed of the gradients computation

FPGA family	Ultimate execution speed speed of the designed organization of gradients computation	
	$F_{max}(Grad)$ (in MHz)	$nTclk_{min}(Grad)$
Cyclone	232	4
Cyclone II	319	4
Cyclone III	367	4
Cyclone iV	370	4
Cyclone V	388	4
Stratix	331	4
Stratix II	464	4
Stratix III	589	4
Stratix IV	637	4
Stratix V	685	4

Analysis of the data for $F_{max}(Grad)$ from Table 3 proves that $F_{max}(Grad) > F_{max}(embeddedMem)$ for all possible values in gradients computations. Therefore, the inequality (1) is satisfied.

The data for $nTclk_{min}(Grad)$ proves that $nTclk_{min}(Grad)$ is equal to 4 under all test conditions. The key to this achivement is the new way of handling the negative coefficients and the use of parallelism.

6. CONCLUSION

The proposed organization of gradients computation which uses 19 3x3 masks with different positioning of the positive and negative coefficients for each of the two gradients is investigated in ten Intel (Altera) FPGA families for maximum operating frequency and minimum number of clock cycles. The obtained experimental data proves that the maximum operating frequency of the proposed technology exceeds the maximum operating frequency of embedded memory for all possible values in gradients computations. The data for minimum number of clock cycles proves that 4 clock cycles are taken to compute the gradients under all test conditions due to the new way of handling the negative coefficients and the use of parallelism.

References

[1] Abidha Abdul Karim Rawther and Leena Mary, "The design of lowpower Sobel edge detection in FPGA", AIP Conference Proceedings, Volume 2222, Issue 1, April 2020, pp. 472-479

[2] Artyom Grigoryan and Sos Agaian, "Two General Models for Gradient Operators", IS&T 2018 International Symposium on Electronic Imaging, Image Processing: Algorithms and Systems XVI, 2018, pp. 568-576

[3] Charu, P. Kumar and K. Singh, "Hardware Model for Efficient Edge Detection in Images", 2020 IEEE International Conference on Computing, Power and Communication Technologies (GUCON) 2020, pp. 798-802

[4] D. Kromichev, "FPGA Based Edge Detection: Integer Division Algorithm with a Constant Divisor", 2022 13th National Conference with International Participation (ELECTRONICA), Sofia, Bulgaria, 2022, pp. 1-4

[5] Dimitre Kromichev, "FPGA Based Edge Detection: Integer Square Root Algorithm", Proceedings of 16th International Engineering Conference on Communications, Electromagnetics and Medical Applications (CEMA'22), 2022, pp. 25-29

[6] Dimitre Kromichev "FPGA Based Edge Detection: Integer Inverse Tangent Algorithm", Proceedings of16th International Engineering Conference on 'Communications, Electromagnetics and Medical Applications' (CEMA'22), 2022, pp. 30-34

[7] Dimitre Kromichev, "Study of Different Adders Focused on Ultimate Execution Speed in FPGA Based Edge Detection", Journal of the Technical University - Sofia, Plovdiv Branch "Fundamental Sciences and Applications", vol. 28(1), 2022

[8] Dimitre Kromichev, "Ultimate Execution Speed of FPGA based Edge Detection: Parallel Addition", Journal of the Technical University - Sofia, Plovdiv Branch "Fundamental Sciences and Applications", vol. 28(1), 2022

[9] Liu bo feng, Gao lipeng. "Based on FPGA's Sobel image edge detection algorithm", Journal of Application technology, 2016, 43(6), pp. 59-61

[10] Parth V. Parikh, Bhinjan A. Dalwadi, Ghanshyam D. Zambare, "Sobel Edge Detection Using FPGA-Artix®-7", International Journal of Scientific & Technology Research, Vol. 5(6), 2016, pp. 250-253

[11] Priscilla Whitin, V. Jayasankar, "Real Time Sobel Edge Detection Based on Reconfigurable Computing", International Journal of Recent Technology and Engineering (IJRTE), Volume-8 Issue-5, January 2020, pp. 2466-2468

[12] Qin, X, "A modified Canny edge detector based on weighted least squares", Comput Stat 36, 2021, pp. 641–659

[13] R. Menakaa, K. Deebac, "FPGA implementation of low power and high speed image edge detection algorithm", Microprocessors and Microsystems, Volume 75, June 2020, pp. 675-679

[14] Sanka Neelavathi, K.Chanra Sekhar, "FPGA Implementation of Approximate Sobel Edge Detection using Approximate Circuits", Journal of Information and Computational Science Volume 10, Issue 9, 2020, pp. 676-684

[15] S. Siddhartha Raman, Rahul Gottipati, "A Robust, Efficient FPGA based implementation of edge detection using Sobel Mask", Asian Journal of Convergence in Technology, Volume IV, Issue III, 2018, pp. 1-8

[16] Wang xiaojuan, Zhai chenry, "Design and implementation of real-time image edge detection system based on FPGA combined Sobel algorithm", Journal of Computer measurement and control, 25(1), 2017, pp. 34-37

[17] Xiaokang Yu, Zhiwen Wang, Yuhang Wang, Canlong Zhang, "Edge Detection of Agricultural Products Based on Morphologically Improved Canny Algorithm", Mathematical Problems in Engineering, vol.14, 2021, pp. 41-48

[18] Yang, Y. and Wei, L., "Grey Relevancy Degree and Improved Eight-Direction Sobel Operator Edge Detection", Journal of Signal and Information Processing, 12, 2021, pp. 43-55

[19] Yi-Bin He, Ya-Jun Zeng, Han-Xin Chen, San-Xia Xiao, "Research on improved edge extraction algorithm of rectangular piece", International Journal of Modern Physics, Vol. 29, No. 01, 2018, pp. 212-220

[20] Zou Xiangxi, Zhang Yonghui, Zhang Shuaiyan, Zhang Jian, "FPGA implementation of edge detection for Sobel operator in eight directions", IEEE Asia Pacific Conference on Circuits and Systems. Chengdu, 2018, pp. 520-523

[21] Z. Xiangxi, Z. Yonghui, Z. Shuaiyan and Z. Jian, "FPGA implementation of edge detection for Sobel operator in eight directions", 2018 IEEE Asia Pacific Conference on Circuits and Systems (APCCAS), 2018, pp. 520-523.

GRADIENT BASED EDGE DETECTION: INVESTIGATING THE PROBLEM OF FALSE NEGATIVES IN TERMS OF EDGE THINNING

Dimitre Kromichev

Department of Marketing and International Economic Relations, University of Plovdiv
24 Tzar Asen Str, Plovdiv 4000, Bulgaria
dkromichev@yahoo.com

Abstract

The problem of false negatives is essential for gradient based edge detection which uses edge thinning. This problem is exacerbated by the mathematics of the generally accepted and applied standard procedure for edge thinning which does not provide a comprehensive set of conditions to reliably define whether a gradient magnitude pixel should retain its value or be reduced to zero. The paper studies the false negatives in gradient based edge detection and proposes a different approach to edge thinning mathematics aimed at eliminating the induced false negatives by applying adaptable test parameters in the conducted experiments.

1. INTRODUCTION

The two important focuses in edge detection are: the quality of detected contours and the execution speed of the edge detection method. The latter is addressed generally by the FPGA hardware implementation [5] with the integer arithmetic algorithms [7] being the most studied factor for increasing speed [4][6] [8]. In terms of increasing the quality of detected contours the problem of false negatives stands out as essential. When a multistage edge detection method is analyzed and assessed with respect to the quality of the edges it produces it is of capital impotrance to know the individual contribution of each stage and the degree to which this stage impacts the final contour detected image.

The standard computational technique of applying edge thinning is defined in [2]. It is based on the following:

$M(x,y) = M(x,y)$ only for

$[M(x,y) > M\_1(x1,y1) \& M(x,y) > M\_2(x2,y2)]$

$M(x,y) = 0$ in all the other cases, (1)

where

$M(x,y)$ is a possible edge pixel,

$M\_1(x1,y1)$, $M\_2(x2,y2)$ are the magnitudes of the two adjacent pixels positioned along the gradient direction.

So far, this approach has been generally accepted and literally applied in the gradient based edge detection [10] without taking into account that this leads to false negatives depending on the edge type and direction. In all methods, the searching for local maximum at each image point is essentially defined by applying Laplacian in one direction. Thus, the deficiencies of Laplacian directly impact the edge thinning results [3]. On the other hand, the definition of edge thinning and its application focus mainly on step edges without considering the specifics of the other four edge types [1]. Another aspect of the standard approach to edge thinning is that it does not address the relations between the edge thinness and the detected contours' belonging to the object or to the background [9].

The goal of this paper is to thoroughly investigate the problem of false negatives in gradient based edge detection in terms of edge thinning. The tasks are: 1) analyze the impact of the existing standard edge thinning approach on the problem of false negatives; 2) propose a different approach to edge thinning mathematics so that the false negatives introduced by the standard approach can be eliminated and the experimental results of the edge detection methods which use edge thinning can be properly analyzed and assessed. Scilab Image and Video Processing Toolbox, Scilab Image Processing Design Toolbox are the tools used to conduct the experiments throughout this work. The analyses performed and the conclusions drawn in this work are relevant for gray-scale images.

2. POSING THE PROBLEM OF FALSE NEGATIVES WITH RESPECT TO THE EXISTING STANDARD APPROACH TO EDGE THINNING

In the existing standard approach, the essence of edge thinning is: an image matrix value is retained unchanged only if it is greater than both its immediate neighbours along the gradient direction. Otherwise, it is replaced by zero. Applying that rule literally, it turns out that if there are two or more gradients of equal magnitudes positioned continuously along any of the four directions, they must all be reduced to zero as graphically illustrated (Figure 1, Figure 2, Figure 3, Figure 4)).

1) Gradient direction 0

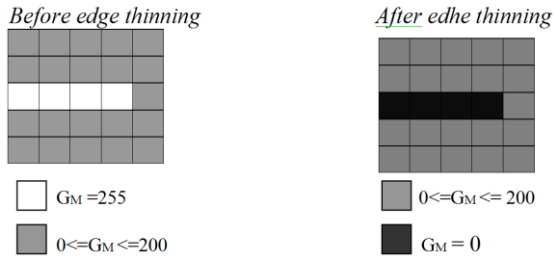

Figure 1. False negatives induced by the standard approach for gradient direction 0

2) Gradient direction 45

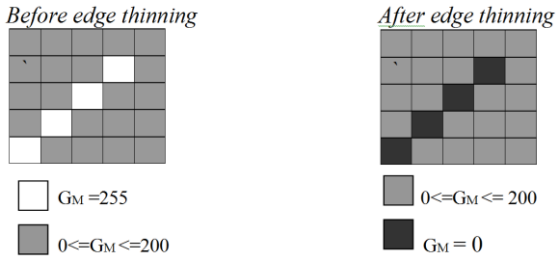

Figure 2. False negatives induced by the standard approach for gradient direction 45

3) Gradient direction 90

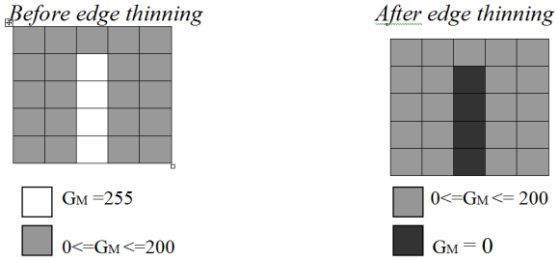

Figure 3. False negatives induced by the standard approach for gradient direction 90

4) Gradient direction 135

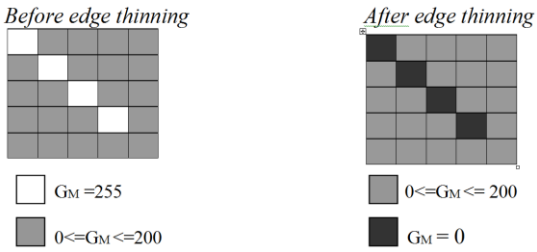

Figure 4. False negatives induced by the standard approach for gradient direction 135

The problem of false negatives induced by applying the standard approach to edge thinning is demonstrated graphically in Figure 5. In this figure, edge thinning is the fourth stage in a gradient based edge detection method.

The analysis proves that applying certain approximation approaches can result in consecutive values equal to 255. Although they are 100% contour pixels they all will be defined as zeroes after executing the edge thinning. The occurrence of a succession of equal values different from zero depends on the concrete image statistics and is quite a regular option when applying accurate mathematics in the x- and y-gradients, gradient magnitude and gradient direction computations. There is no means by which such a succession of equal values different from zero can be predicted and avoided correspondingly. Therefore, using the expressions in (1) in all cases as a rule for defining a single pixel thin contour can lead to wrong results.

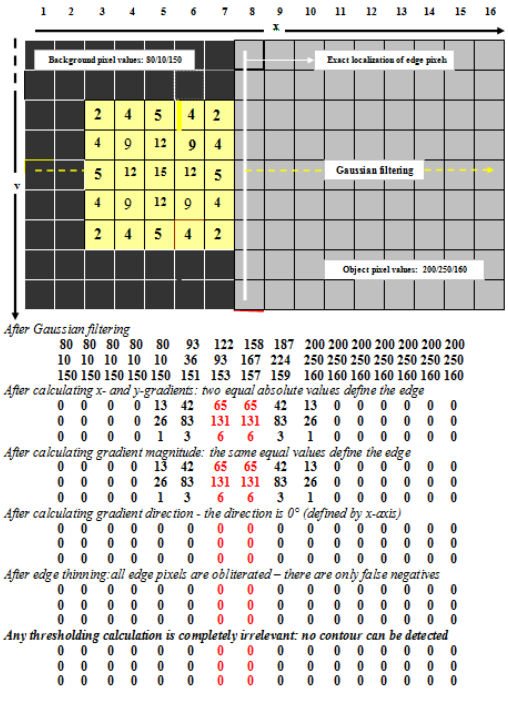

Figure 5. The problem of false negatives induced by the standard approach for a gradient based edge detection method with edge thinning as the fourth stage

3. EXPERIMENTAL INVESTIGATION OF THE FALSE NEGATIVES INDUCED BY THE STANDARD APPROACH TO EDGE THINNING

The experiments to ascertain the false negatives induced by the standard approach to edge thinning are conducted using programs written in Scilab. In the Scilab program snippet below presented is the standard approach implementation (Figure 6). The following denotations are used: X_Y_M(i,j) is the matrix containg the gradient magnitudes; X_Y_D(i,j) is the matrix containg the gradient directions; XY-ET(i,j) is the matrix containing the pixel values after executing the edge thinning operation. The original image matrix of a synthetic image presenting a rectangle is (Figure 6). The result of applying literally (1) by using the program snippet in Figure 7 is shown in the contour detected image matrix in Figure 8.

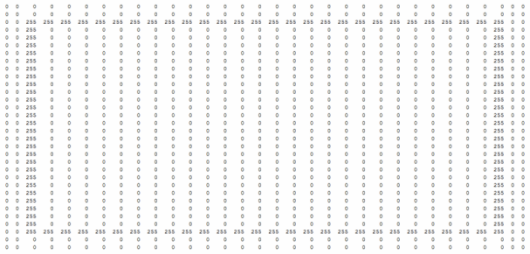

Figure 6. The original matrix of a rectangle in a synthetic image

```
for i = 2: row-1
  for j =2: col-1
D = X_Y_D(i,j);
Mm = 0;
if D == 0
  if (X_Y_M(i,j) > X_Y_M(i,j-1)) & (X_Y_M(i,j) > X_Y_M(i,j+1))
      Mm = X_Y_M(i,j);
    else
      Mm = 0;
end
end
if D == 45
  if (X_Y_M(i,j) > X_Y_M(i+1,j-1)) & (X_Y_M(i,j) > X_Y_M(i-1,j+1))
    Mm = X_Y_M(i,j);
    else
    Mm = 0;
end
end
if D == 90
  if (X_Y_M(i,j) > X_Y_M(i-1,j)) & (X_Y_M(i,j) > X_Y_M(i+1,j))
    Mm = X_Y_M(i,j);
    else
    Mm = 0;
end
end
if D == 135
  if (X_Y_M(i,j) > X_Y_M(i-1,j-1)) & (X_Y_M(i,j) > X_Y_M(i+1,j+1))
      Mm = X_Y_M(i,j);
  else
      Mm = 0;
end
end
XYET(i,j) = Mm;
   end
 end
```

Figure 7. Scilab program snippet for edge thinning by applying the standard approach

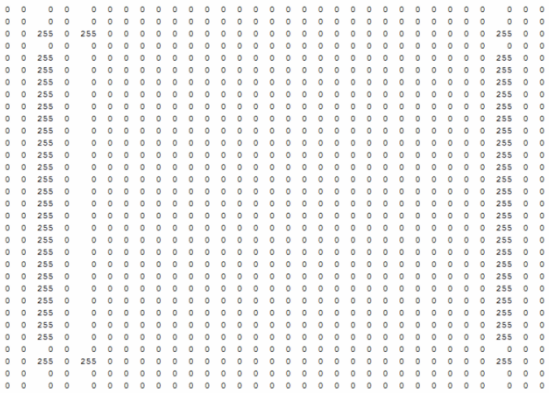

Figure 8. The resultant contour matrix for the program snippet in Figure 7

The assessment results show that the resultant contour detected image has 50% false negatives.

4. A DIFFERENT APPROACH TO EDGE THINNING MATHEMATICS AIMED AT REDUCING THE FALSE NEGATIVES

Reduction of the false negatives induced by the standard approach to edge thinning can be achieved by:

- Technique #1. Replace ''>='' with ''>'' in Figure 7 only with respect to the left hand neighbouring pixel along the gradient direction, thus leaving ''>='' comparison with the right hand neighbouring pixel unchanged. The obtained image matrix is shown in Figure 9.

Figure 9. The resultant contour matrix for technique #1

The assessment results show that the resultant contour detected image has 46% false nagatives.

- Technique #2. Replace ''>='' with ''>'' in Figure 7 only with respect to the right hand neighbouring pixel along the gradient direction, thus leaving ''>='' comparison with the left hand neighbouring pixel unchaged. The obtained image matrix is shown in Figure 10.

The assessment results show that the resultant contour detected image has 46% false nagatives. Therefore, the experimental data prove that the mathematics of (1) produces false negatives.

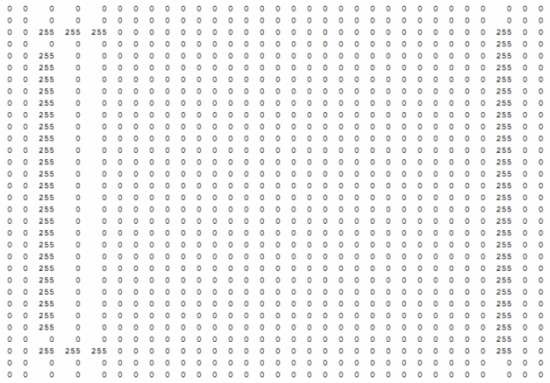

Figure 10. The resultant contour matrix for technique #2

5. ELIMINATING THE FALSE NEGATIVES INDUCED BY THE STANDARD APPROACH TO EDGE THINNING

The way to eliminate false negatives induced by the standard approach to edge thinning is presented in the Scilab program snippet below (Figure 11). The denotations are the same as in Figure 7.

```
for i = 2: row-1
  for j =2: col-1
D = X_Y_D(i,j);
Mm = 0;
if== 0
  if (X_Y_M(i,j) >= X_Y_M(i,j-1)) & (X_Y_M(i,j) >= X_Y_M(i,j+1))
      Mm = X_Y_M(i,j);
    else
      Mm = 0;
end
end
if D == 45
  if (X_Y_M(i,j) >= X_Y_M(i+1,j-1)) & (X_Y_M(i,j) >= X_Y_M(i-1,j+1))
    Mm = X_Y_M(i,j);
    else
    Mm = 0;
end
end
if D == 90
  if (X_Y_M(i,j) >= X_Y_M(i-1,j)) & (X_Y_M(i,j) >= a_new_X_Y_M(i+1,j))
    Mm = X_Y_M(i,j);
    else
    Mm = 0;
end
end
if D == 135
  if (X_Y_M(i,j) >= X_Y_M(i-1,j-1)) & (X_Y_M(i,j) >= X_Y_M(i+1,j+1))
      Mm = X_Y_M(i,j);
  else
      Mm = 0;
end
end
XYET(i,j) = Mm;
   end
 end
```

Figure 11. Scilab program snippet for edge thinning aimed at eliminating the false negatives induced by the standard approach

The resultant detected contour image matrix is the same as the original matrix in Figure 6 – the number of false negatives is 0. Therefore, the required change in mathematics to achieve 0% of false negatives in this case is replacing ''>'' in the Scilab program snippet in Figure 7 with ''>='' as it is experimentally proved by the results obtained with the program snippet in Figure 11.

Therefore, the experiments and analyses to ascertain the capabilities of a gradient based edge detection method must be conducted on the basis of four settings with respect to the problem of false negatives and edge thinning. When comparing three consecutive values in the image matrix along the computed direction to ascertain whether the central one is an edge pixel or it must be replaced with 0 it must be tested:

- left hand pixel < central pixel > right hand pixel
- left hand pixel <= central pixel >= right hand pixel
- left hand pixel < central pixel >= right hand pixel
- left hand pixel <= central pixel > right hand pixel.

The setting which defines the least percentage of false negatives provides the required information on the optimal application of edge thinning mathematics for the particular image statistics.

6. CONCLUSION

Experimentally investigated and analyzed in this paper is the impact of the standard approach to edge thinning on the false negatives in gradient based edge detection. It is ascertained that the standard approach can lead to up to 50% of false negatives in comparison with the original true object boundaries. Proposed is a new implementation of edge thinning mathematics to eliminate the false negatives. Presented are all the aspects required to conduct experiments and assess the capabilities of a gradient based edge detection method.

References

[1] B. Kumar Shah, V. Kedia, R. Raut, S. Ansari, A. Shroff, "Evaluation and Comparative Study of Edge Detection Techniques", IOSR Journal of Computer Engineering, Vol. 22(5), 2020, pp. 6-15

[2] Canny J., "A Computational Approach to Edge Detection", IEEE Transaction on Pattern Analysis and Machine intelligence, No. 6, 1986, pp. 679-698

[3] Cesar Bustacara-Medina, Leonardo Florez-Valencia, Luis Carlos Diaz, "Improved Canny Edge Detector Using Principal Curvatures", Journal of Electrical & Electronic Engineering. Vol. 8, No. 4, 2020, pp. 109-116

[4] Dimitre Kromichev, "Investigation of Different Multipliers Focused on Ultimate Execution Speed in FPGA Based Edge Detection", Computer Science and Technologies, ISSN 1312- 3335, Vol. 1, 2022, pp. 6-14

[5] Dimitre Kromichev, "Ultimate Execution Speed in FPGA Based Edge Detection: Technology of Accurate Rounding in Integer Division with a Variable Divisor", Computer Science and Technologies, ISSN 1312- 3335, Vol. 1, 2022, pp. 15-24

[6] Dimitre Kromichev, "Ultimate Execution Speed in FPGA Based Edge Detection: Investigating the Speed Parameters of Iterative Integer Division", Computer Science and Technologies, ISSN 1312- 3335, Vol. 1, 2022, pp. 25-35

[7] Dimitre Kromichev, "Multiplication in FPGA Based Edge Detection: Maximum operating Frequency", Автоматизация на дискретното производство, ISSN 2682-9584, 2022 (4), pp. 227-232

[8] Dimitre Kromichev, "FPGA Based Edge Detection: Maximum operating Frequency of Integer Division with a Variable Divisor and Division by Multiplying with the Reciprocal of Divisor", Автоматизация на дискретното производство, ISSN 2682-9584, 2022 (4), pp. 233-237

[9] Song, R., Zhang, Z. & Liu, H., "Edge connection based Canny edge detection algorithm", Pattern Recognition and Image Analysis, 27, 2017, pp. 740–747

[10] Veeranagoudapatil, Chitra Prabhu, "Distributed Canny Edge Detector: Algorithm & FPGA Implementation", International Journal for Research in Applied Science & Engineering Technology, Vol. 3 (5), 2015, pp. 586-588.

AUTHOR INDEX